A Szilikátipari Tudományos Egyesület lapja

építőanyag

Journal of Silicate Based and Composite Materials

A TARTALOMBÓL:

- Copolymer electrode self-modified with fullerene C_{60}
- Silylated functionalized montmorillonite clay for nanocomposite preparation
- Comparative Analysis of Flexible Stabilization Devices Based on Polymeric and Composite Materials for Degenerative Disorders: Finite Element Analysis
- Characteristics of cement pastes incorporating different amounts of waste cellular concrete powder
- Effect of combined use of crushed sand and Algerian desert dune sand on fresh properties and strength of self-compacting concrete
- The localization of plastic deformation in bimetal

2018/5


TUNGSRAM
Innovation is our heritage
EST.1896
INNOVATUNGSRAM
Tungsram returns to the market as an innovative, premium brand with design, development and manufacturing in Europe and a commitment to continue and expand its outreach.
tungsram.com

építőanyag

Journal of Silicate Based and Composite Materials

2018/5

TARTALOM

134 C_{60}-fullerénnel módosított kopolimer elektróda
Muhammed Mizher RADHI ▪ Emad Abbas Jaffar AL-MULLA

140 Szilanizált funkcionális montmorillonit agyag nanokompozit előállításához
David P. PENALOZA Jr. ▪ Thomas AP SEERY

146 Degeneratív elváltozások polimer és kompozit anyagú rugalmas stabilizáló szerkezeteinek összehasonlító vizsgálata: Végeselemes analízis
Moustafa MOSBAH ▪ Mohammed BENDOUKHA

151 Hulladék pórusbeton por kiegészítő anyagot tartalmazó cementpépek jellemzői
Mohammed ABED ▪ Rita NEMES

155 Zúzott homok és algériai sivatagi dűne homok kombinált alkalmazásának hatása öntömörödő beton frissbeton tulajdonságaira és szilárdságára
Benchaa BENABED

168 Képlékeny alakváltozás lokalizálása bimetálban
Yulia V. LI ▪ Svetlana A. BARANNIKOVA ▪ Lev B. ZUEV

CONTENT

134 Copolymer electrode self-modified with fullerene C_{60}
Muhammed Mizher RADHI ▪ Emad Abbas Jaffar AL-MULLA

140 Silylated functionalized montmorillonite clay for nanocomposite preparation
David P. PENALOZA Jr. ▪ Thomas AP SEERY

146 Comparative Analysis of Flexible Stabilization Devices Based on Polymeric and Composite Materials for Degenerative Disorders: Finite Element Analysis
Moustafa MOSBAH ▪ Mohammed BENDOUKHA

151 Characteristics of cement pastes incorporating different amounts of waste cellular concrete powder
Mohammed ABED ▪ Rita NEMES

155 Effect of combined use of crushed sand and Algerian desert dune sand on fresh properties and strength of self-compacting concrete
Benchaa BENABED

168 The localization of plastic deformation in bimetal
Yulia V. LI ▪ Svetlana A. BARANNIKOVA ▪ Lev B. ZUEV

A finomkerámia-, üveg-, cement-, mész-, beton-, tégla- és cserép-, kő- és kavics-, tűzállóanyag-, szigetelőanyag-iparágak szakmai lapja
Scientific journal of ceramics, glass, cement, concrete, clay products, stone and gravel, insulating and fireproof materials and composites

A folyóiratot referálja · The journal is referred by:
Cambridge Scientific Abstracts ProQuest

A folyóiratban lektorált cikkek jelennek meg.
All published papers are peer-reviewed.
Kiadó · Publisher: Szilikátipari Tudományos Egyesület (SZTE)
Elnök · President: ASZTALOS István
1034 Budapest, Bécsi út 122–124.
Tel.: +36-1/201-9360 ▪ E-mail: epitoanyag@szte.org.hu
Tördelő szerkesztő · Layout editor: NÉMETH Hajnalka

Címlapfotó · Cover photo: KÓSA Luca Kornélia

WWW.EPITOANYAG.ORG.HU
EN.EPITOANYAG.ORG.HU

Online ISSN: 2064-4477
Print ISSN: 0013-970x
INDEX: 2 52 50 ▪ 70 (2018) 133–172

Vol. 70, No. 5

Copolymer electrode self-modified with fullerene C_{60}

Muhammed Mizher RADHI ▪ Radiologic Technical Department, Health and Medical Technology college-Baghdad, Middle Technical University (MTU), Iraq ▪ mmradhi@yahoo.com

Emad Abbas Jaffar AL-MULLA ▪ College of Health and Medical Techniques, Al-Furat Al-Awsat Technical University, 54003 Al-Kufa, Iraq ▪ almullaemad@gmail.com

Érkezett: 2018. 05. 01. ▪ Received: 01. 05. 2018. ▪ https://doi.org/10.14382/epitoanyag-jsbcm.2018.25

Abstract

A copolymer of polystyrene-acrylonitrile was modified with fullerene C_{60} using gamma irradiation technique to produce a new copolymer with high quality in physical and chemical properties and using to fabrication a working electrode alternative for the modification of commercial working electrode in cyclic voltammetric technique (such as glassy carbon electrode, Pt, Au electrode). The new copolymer electrode self-modified with C_{60} ($CESMC_{60}$) was characterized electrochemically by cyclic voltammetric method using a standard solution of 0.3 mM $K_4[Fe(CN)_6]$ in 1 M KCl to evaluate the redox current peaks of Fe(II)/Fe(III). The electrochemical and physical properties of the new fabrication electrode has good hardness, insoluble in aqueous and non-aqueous solvent, electrochemical stability, resistance to high temperatures and different pH. It was found that 0.3 mM of $K_4[Fe(CN)_6]$ in 1 M KCl of the new electrode at different concentration using reagent, scan rate, pH, temperature, electrolytes, stability and reliability. The new electrode was given encouraging properties for using in high-precision analysis and resuscitates commercial electrodes such as glassy carbon electrode, platinum electrode, gold electrode, and so on.

Keywords: cyclic voltammetry, copolymer electrode modified C_{60}, $K_4[Fe(CN)_6]$, redox process

Kulcsszavak: ciklikus voltammetria, C_{60} módosított kopolimer electróda, $K_4[Fe(CN)_6]$, redox eljárás

Muhammed Mizher RADHI
Professor, Department of Radiological Techniques, Health and Medical Technology College-Baghdad, Middle Technical University, Baghdad, Iraq. He received his PhD from University Putra of Malaysia (UPM) in 2010 in Electrochemistry, Nanotechnology. Research topics: conductivity of grafted polymer with nano-deposit and fabrication of sensors by nanomaterials to study drugs in blood medium by electrochemical analysis.

Emad Abbas Jaffar AL-MULLA
is an Asst. Prof., College of Health and Medical Techniques, Al-Furat Al-Awsat Technical University, Iraq; He has received his PhD from University Putra Malaysia, Malaysia in 2010, He was a Post Doctoral researcher at the same University from April 2012 to April 2013; main fields of interest: bioorganic synthesis, nanomaterials, biopolymer nano-composites; He has more than 50 papers in Scopus and ISI journals; his H-Index = 14 according to Scopus database.

1. Introduction

Some scientists were manufactured high quality electrodes from conductive polymer which were used in the device of cyclic voltammetry and pH meter [1-3] and reference electrode [4].

IUPAC was upheld the modification of electrodes with conductive and semiconductive polymers to enhancement of the redox current peaks in cyclic voltammetric technique [5,6]. The modification of electrode in cyclic voltammetry was performed as chemical sensors and biosensors [7].

Fullerene C_{60} film as single wall on gold electrode was studied in cyclic voltammetric technique which characterization in this method [8,9]. Some polymer synthesis with nanoparticles like poly(methyl methacrylate) complex with Fullerene C_{60} using as organic solar cell [10-12].

The use of C_{60} with the polymer composition has been gotten a polymer with different recipes for the polymer and that irradiation under vacuum pressure and at 300 °C to produce different spectral of conductive polymer [13]. C_{60} and carbon nanotubes (CNT) were deposed with the polymer to production of new recipes on the polymer where the polymer gave the new specification in photovoltaic cells manufacturing [14].

Some of researches were studied an application of important biosensors using fullerene C_{60}, the new biosensor electrode with nanomaterials which has a functionalization in electrochemical applications [15,16].

Polymer-fullerene was synthesized and characterized by cyclic voltammetric technique to observation of energetic offsets which has up to value of 150 meV, this energy contribute for improving performance of the polymer solar cells [17].

New electrochemical sensors were used in detection of ions in voltammetric analysis by modification of electrode with metalloporphyrin dimer – fullerene C_{60} [18].

Cyclic voltammetry was studied the modification glassy carbon electrode with single wall carbon nanotube and chitosan as a sensor to determination of acetaminophen, uric acid and ascorbic acid in human serum and urine medium with satisfactory results [19].

Cyclic voltammetry and differential pulse voltammetry were studied the modification gold electrode with fullerene-pyrrolidine to analysis the electrochemical characterized of the synthesized fullerene derivatives [20].

A thin film of C_{60} with nano-TiO_2 on the electrode was determined the photocurrent efficiency photoactive of the polycrystalline TiO_2 and decreases the recombination effect [21].

In this work, a new fabrication of copolymer electrode self-modified with C_{60} as alternative working electrode using in cyclic voltammetric technique was characterized.

2. Experimental

2.1. Synthesis of copolymer modified with fullerene C_{60}

The copolymer was manufactured process of polystyrene – acrylonitrile modified with Fullerene C_{60} using gamma-irradiation by ferrous ammonium sulfite (FAS) as a catalyst. The minimization of the copolymer production was the following:

- 0.25% (w/w) of the catalyst FAS
- 80% (w/w) of monomer (acrylonitrile)
- 1.5 MRD dose of gamma-irradiation
- 2 g of polymer (polystyrene)
- 1 mg of Fullerene C_{60}

Fig. 1 shows the mechanism reaction as a suggestion [22].

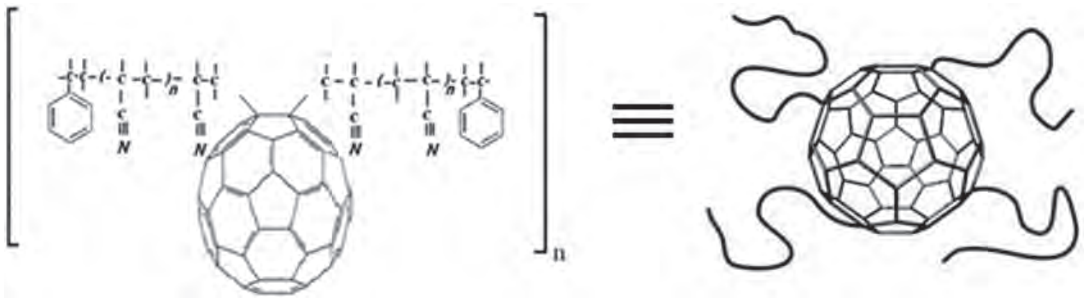

Fig. 1 Suggested reaction mechanism of copolymer modified with fullerene C_{60}
1. ábra Kopolimer módosítása C_{60} fullerénnel – javasolt reakció mechanizmus

2.2. Fabrication of copolymer electrode self-modified with fullerene C_{60} ($CESMC_{60}$)

The new fabrication working electrode ($CESMC_{60}$) has been fabricated by a diameter of 5 mm of the material of copolymer manufacturer, and entered into a hole works in the center of the piece of the copolymer restaurant and prove to the wire of platinum 1 cm length where it executes a very small part of the other party, and the other part links with copper wire and all parts covered with glass tube and prove with epoxy adhesive, as shown in *Fig. 2*.

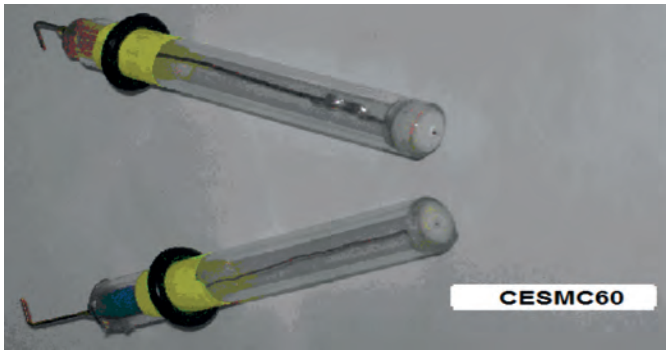

Fig. 2 Copolymer electrode self-modified with fullerene C_{60}
2. ábra C_{60} fullerénnel módosított kopolimer elektróda

2.3 Instrument and electrochemical analysis methods

EZstat series (potentiostat/galvanostat) NuVant Systems Inc. pioneering electrochemical technologies USA were used in this study. An Ag/AgCl (3 M NaCl) and platinum wire (1 mm diameter) were used as a reference and counter electrodes, respectively. The new fabrication working electrode $CESMC_{60}$ was used in this study.

Cyclic voltammetric cell was used in this technique by adding 10 ml of electrolyte in the quartz cell and immerse three electrodes in the supporting electrolyte, then all the electrodes was connected with potentiostat to finding the results of analysis by the cyclic voltammogram using personal computer as a soft ware of the analysis results.

2.4 Reagents

The following reagents were used: KCl powder purity from SCRC (China), potassium hexacyanoferrate II $K_4[Fe(CN)_6]\cdot 3H_2O$ from Fluka AG Chem. (Fabrik CH-9470 Buchs Germmany) and other chemicals in high purity from the manufactures. All reagents were prepared by deionized distilled water. All experimental analysis in cyclic voltammetry cell was dissolved oxygen remove with pure nitrogen gas bobbling for 10 to 15 min to avoid the peroxide producing from the oxidation of oxygen in the water of the solution in the cyclic voltammetric cell.

2.5. Scanning Electron Microscopy

Scanning Electron Microscopy (SEM) was used to examine the morphology of the copolymer of polystyrene-acrylonitrile and the copolymer modification with fullerene C_{60} as shown in *Fig. 3a* and *3b*, respectively.

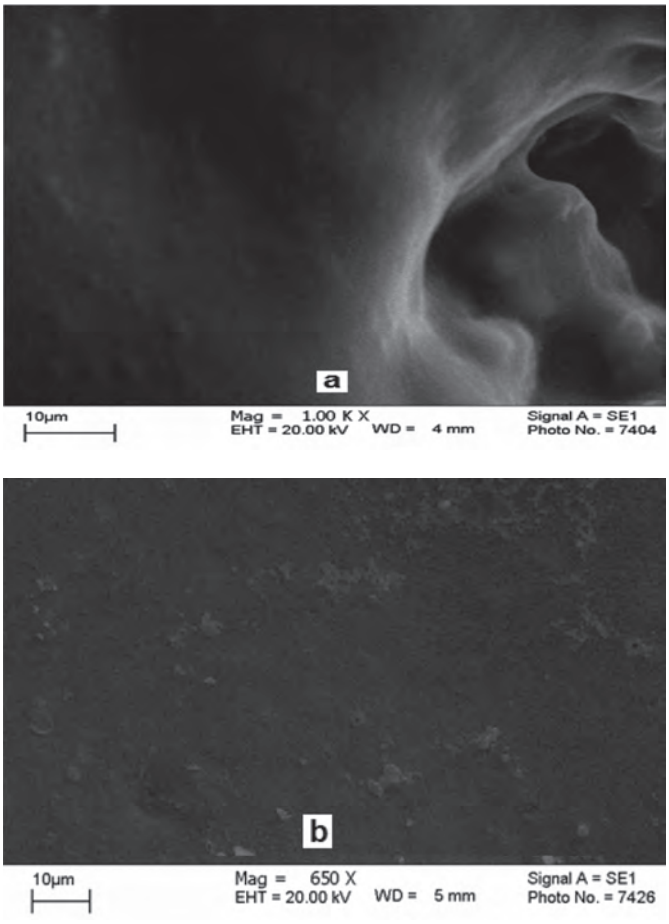

Fig 3. Scanning Electron Microscopy (SEM) of (a) the copolymer of polystyrene-acrylonitrile only (b) the copolymer of polystyrene-acrylonitrile modification with C_{60}
3. ábra Pásztázó elektronmikroszkópos (SEM) felvételek (a) polisztirén-akrilnitril kopolimer (b) C_{60} fullerénnel módosított polisztirén-akrilnitril kopolimer

3. Results and discussion

3.1. Electrochemical properties of the copolymer electrode self-modified with fullerene C_{60}

3.1.1. Effective of potential area

It can be compared to the potential area that are in commercial working electrode such as glassy carbon electrode (GCE), Platinum electrode (Pt-electrode), gold electrode (Au-electrode) with a new fabrication copolymer working electrode in 0.1 KCl electrolyte. It was noted that the new average potential area of the $CESMC_{60}$ is larger than GCE where the average potential area of $CESMC_{60}$ covers -1.8 to +2.0 V while the average potential area of GCE covers -1.5 to +1.8 V. It can also note that the presence of redox current peaks at commercial electrodes compared with flat area at $CESMC_{60}$.

3.1.2. Effect of $CESMC_{60}$ on the current and potential for redox current peaks in $K_4[Fe(CN)_6]$

Commonly it was used a compound of 1mM $K_4[Fe(CN)_6]$ in the calibration of the cyclic voltammetric technique, when using in aqueous solutions. Good redox current peaks Fe(III)/Fe(II) were found to the $CESMC_{60}$. Where it was noted that the separation potential between redox peaks value ΔEpc-a = 200 mV in aqueous solution 0.1M KCl and this is that the electrode used in the reaction is almost reversible type of interaction of Fe(II)/Fe(III) which is an acceptable value. As for the ratio of the cathode to the anode (Ipa/Ipc) it was approximately equal to 1, which represents the value of the reversible electrode as shown in *Fig. 3*.

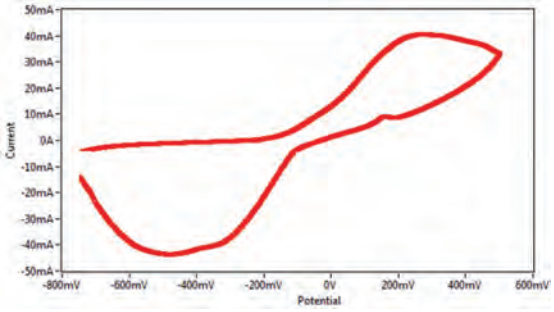

Fig. 4 cyclic voltammogram of 0.3mM $K_4[Fe(CN)_6]$ in 1M KCl as a supporting electrolyte using $CESMC_{60}$ as working electrode verses Ag/AgCl as reference electrode at scan rate 100 mVs-1

4. ábra Ciklikus voltammogram: $CESMC_{60}$ munkaelektróda 0.3mM $K_4[Fe(CN)_6]$ 1M KCl oldatban, Ag/AgCl referencia elektródával; mintavételi sebesség 100 mVs-1

3.2. Effect of scan rate on the $CESMC_{60}$

The different scan rates (0.01 – 0.1 Vs^{-1}) was studied for the $CESMC_{60}$ in a solution of 1M KCl as a supported electrolyte and 0.3 mM $K_4[Fe(CN)_6]$. It has been observed that the redox current peaks of Fe(II)/Fe(III) increased with increasing the scan rate which get heterogeneous kinetics phenomenon as shown in *Table 1* [23].

A rational linear relationship between Log(Ipa) and Log(SR) of the $CESMC_{60}$ 0.3 mM $K_4[Fe(CN)_6]$ which described by the equation: y=0.4835X – 2.1379, R^2 =0.9976.

The slope of graph in *Fig. 5* is 0.48 which is destination compatible with theoretical slope of 0.5 for diffusion controlled process [24].

Fig. 6 shows the relationship between oxidative potential and scan rate of Fe(II)/Fe(III) at the new fabrication working electrode, the oxidation current peak of 63mV at low scan rate (10mV/sec) was increased linearly to 279mV at high scan rate (100mV/sec) as described in the equation: Y=2338.3X+63.013 (R^2=0.9476).

From *Fig. 6* the intercepts at zero current or scan rate produces zero current potential (E0, 1) of 63mV for the process of Fe(II)/Fe(III) at $CESMC_{60}$ [25].

Scan rate (Vsec-1)	Epc (V)	Epa (V)	Ipc (A)	Ipa (A)	ΔE= Epa-Epc (V)	Ratio Ipa/Ipc	Df (Cm-2sec-1)
0.01	-0.274	0.052	-0.0194	0.144	0.222	0.74	1.59x10-10
0.02	-0.338	0.111	-0.0269	0.212	0.227	0.79	1.72x10-10
0.03	-0.384	0.141	-0.0320	0.259	0.243	0.81	1.71x10-10
0.04	-0.419	0.170	-0.0361	0.298	0.249	0.83	1.70x10-10
0.05	-0.447	0.198	-0.0394	0.327	0.249	0.83	1.64x10-10
0.06	-0.471	0.217	-0.0424	0.356	0.254	0.84	1.62x10-10
0.07	-0.498	0.238	-0.0447	0.381	0.260	0.85	1.59x10-10
0.08	-0.509	0.247	-0.0472	0.406	0.262	0.86	1.58x10-10
0.09	-0.534	0.263	-0.0493	0.427	0.271	0.87	1.55x10-10
0.10	-0.542	0.279	-0.0515	0.446	0.263	0.87	1.52x10-10

Table 1. Scan rate, potential, current, peak potential separation, peak current ratio and diffusion coefficient (D_f) for Fe(II)/Fe(III) in KCl solution using $CESMC_{60}$

1. táblázat Mintavételi sebesség, potenciál, áramerősség, elválasztó csúcspotenciál, csúcs áramerősség arány és diffúziós tényező (D_f); Fe(II)/Fe(III) KCl oldatban $CESMC_{60}$ elektródával

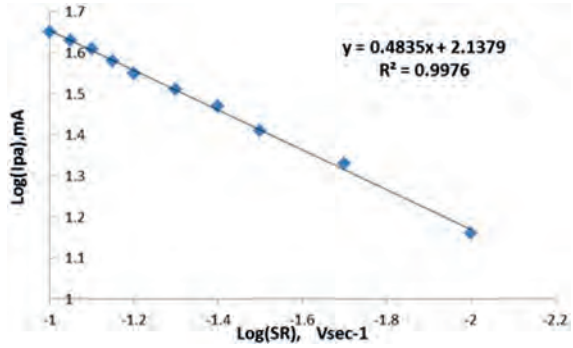

Fig. 5 Plot of Log (anodic current peak) of 0.3 mM $K_4[Fe(CN)_6]$ in 1M KCl at fabrication working electrode $CESMC_{60}$ versus Ag/AgCl and different SR (0.01- 1 Vs-1)

5. ábra Anódos csúcs áramerősség logaritmikus ábrázolása: $CESMC_{60}$ munkaelektróda 0.3mM $K_4[Fe(CN)_6]$ 1M KCl oldatban, Ag/AgCl referencia elektródával; mintavételi sebesség 0.01- 1 Vs-1

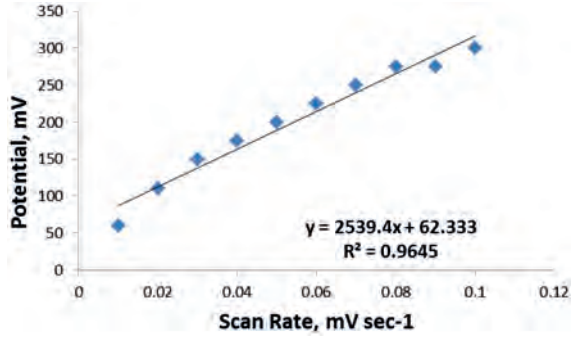

Fig. 6 Plot of anodic potential peak of 0.3 mM $K_4[Fe(CN)_6]$ in 1M KCl at fabrication working electrode $CESMC_{60}$ versus Ag/AgCl and different SR (0.01- 1 Vs-1)

6. ábra Anódos csúcs potenciál logaritmikus ábrázolása: $CESMC_{60}$ munkaelektróda 0.3mM $K_4[Fe(CN)_6]$ 1M KCl oldatban, Ag/AgCl referencia elektródával; mintavételi sebesség 0.01- 1 Vs-1

3.3. Calculation of diffusion coefficient (D_f)

The diffusion coefficient of the oxidation reaction for ferric ions to ferrous ions through cyclic voltammetry at the $CESMC_{60}$ can be calculated by Eq. (1) and from the data in *Table 1* and Eq. (1) [26,27]:

$$Ipa = 2.69x10^5(n)^{3/2}AC_o(D_f)^{1/2}(v)^{1/2} \quad (1)$$

Where:

Ipa is oxidative current peak, A is the area of the electrode, F is Faraday, C_o is the concentration, v is the scan rate and D_f is the diffusion coefficient of the reacting species.

It was found that the D_f values of Fe(II)/Fe(III) in the 0.1M KCl as supporting electrolyte has average value of the $D_f = 1.622\times10^{-10}$ cm^2sec^{-1} of the oxidative current peak of $K_4[Fe(CN)_6]$ when used the new fabrication working electrode $CESMC_{60}$ that means the heterogeneous transfer of electron through the electrolyte by nanomaterials fullerene C_{60}in the modified working electrode which acts as electro-catalyst for the enhancement of the processing the Fe(II)/Fe(III) in the electrolyte by increasing of scan rate against to the diffusion coefficient values as shown in *Table 1* [28,29].

3.4. The influence of different temperatures on the $CESMC_{60}$

The influence of different temperatures on the new fabrication electrode was used the redox current peaks value of output potential using $K_4[Fe(CN)_6]$ and increasing the temperature from 10 °C to 80 °C. The logarithm of current versus inverse temperature depends on the Arrhenius equations [24]:

$$\sigma = \sigma^o \, Exp\,(-E^* / RT) \quad (2)$$

$$D = D^o \, Exp\,(-E^* / RT) \quad (3)$$

Where:

σ / D - is the quotient of connectivity

σ° / D° -is the quotient of the standard connectivity

E* - is the activation energy

R - is the ideal gas constant

T - is the temperature in Kelvin

The activation energy which needed to oxidizing the Fe(II) to Fe(III) was found as $E^*=1.05$ $kJmol^{-1}K^{-1}$ with less value than using other electrodes such as grafted polymer electrode in the same operation as $E^*=1.75kJmol^{-1}K^{-1}$ [30]. Also, the stability of GPE at high temperature has high resistance than other working electrodes [31-38].

3.5. Sensitivity of $CESMC_{60}$ in low detection limit at different concentrations

The new fabrication working electrode $CESMC_{60}$ of the polarization of high sensitivity in the detection of low concentrations of solutions of $K_4[Fe(CN)_6]$ in 0.1M KCl solution as a supporting electrolyte, where it can be seen as a good sensor for low concentrations of chemical compounds with high sensitivity (R^2=0.9822 for anodic current peak and R^2=0.9834 for cathodic current peak) of the $CESMC_{60}$ for both oxidation-reduction current peaks as shown in *Figs. 7* and *8* respectively.

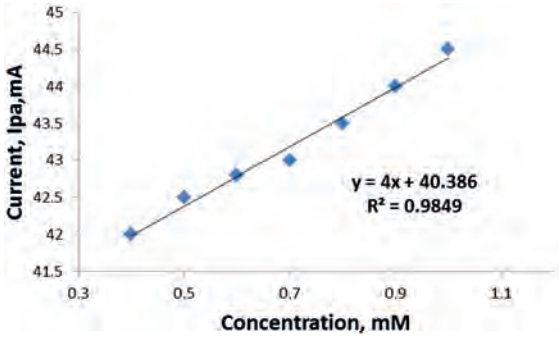

Fig. 7 Plot of anodic current peak of different concentrations (0.3-1mM) $K_4[Fe(CN)_6]$ in 1M KCl at fabrication working electrode $CESMC_{60}$ versus Ag/AgCl and SR 100 mVs-1

7. ábra Anódos csúcs potenciál különböző koncentrációk esetén: $CESMC_{60}$ munkaelektróda 0.3mM $K_4[Fe(CN)_6]$ 1M KCl oldatban, Ag/AgCl referencia elektródával; mintavételi sebesség 100 mVs-1

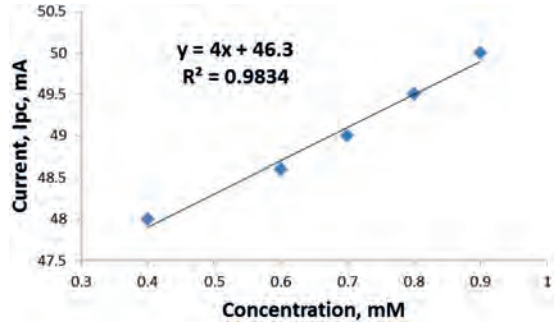

Fig. 8 Plot of cathodic current peak of different concentrations (0.3-1mM) $K_4[Fe(CN)_6]$ in 1M KCl at fabrication working electrode $CESMC_{60}$ versus Ag/AgCl and SR 100 mVs-1

8. ábra Katódos csúcs áramerősség különböző koncentrációk esetén: $CESMC_{60}$ munkaelektróda 0.3mM $K_4[Fe(CN)_6]$ 1M KCl oldatban, Ag/AgCl referencia elektródával; mintavételi sebesség 100 mVs-1

3.6. Stability and reliability of $CESMC_{60}$

The potential cycling of the redox current peaks of the modified working electrode $CESMC_{60}$ in 0.3 mM $K_4[Fe(CN)_6]$ with 1M KCl was carried out during cyclic voltammetry. Continuous potential cycling did not seem to affect the redox current peak of the new working electrode, since the faradic activity appears reliable even after ten times, and the relative standard deviation (RSD) of the cathodic current peak of the new fabrication electrode is ±4.16 % as shown in *Table 2*. *Table 3* shows the reliability of $CESMC_{60}$ as working electrode at SR is 100 mV s^{-1} for anodic current peak 0f 0.3 mM $K_4[Fe(CN)_6]$ in 0.3 M KCl and the RSD is ±3.34 %.

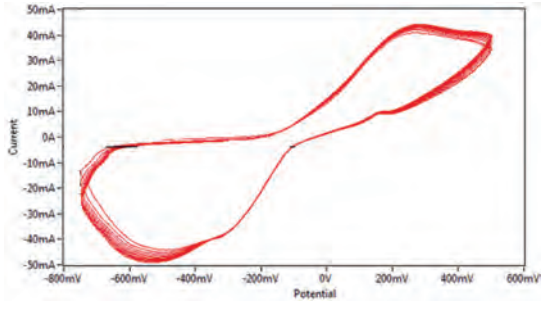

Fig. 9 Cyclic voltammogram of ten times for redox current peaks of $CESMC_{60}$ in 0.3 mM $K_4[Fe(CN)_6]$ with 1 M KCl at SR 100mVs-1

9. ábra Tíz ciklusos ciklikus voltammogram: $CESMC_{60}$ munkaelektróda 0.3mM $K_4[Fe(CN)_6]$ 1M KCl oldatban, mintavételi sebesség 100 mVs-1

Fig. 9 shows the cyclic voltammogram of redox current peaks of 0.3 mM $K_4[Fe(CN)_6]$ in 1M KCl for ten times of Fe((II)/Fe(III) which illustrate the good stability of the cyclic voltammogram of the new fabrication working electrode by overlapping the lines.

Numbers	Ipc (uA)	Mean	RSD
1	-49.0		
2	-48.9		
3	-47.9		
4	-47.5		
5	-46.9		
6	-45.5		
7	-45.8		
8	-44.8		
9	-44.4		
10	-43.4	-46.41	±4.16%

Table 2. Reliability of $CESMC_{60}$ as working electrode at SR is 100 mVs-1 for cathodic current peak of 0.3 mM $K_4[Fe(CN)_6]$ in 1 M KCl
2. táblázat $CESMC_{60}$ munkaelektróda megbízhatósága katódos csúcs áramerősségre; 0.3mM $K_4[Fe(CN)_6]$ 1M KCl oldatban, mintavételi sebesség 100 mVs-1

Numbers	Ipa (uA)	Mean	RSD
1	40.9		
2	41.0		
3	42.2		
4	42.5		
5	42.7		
6	43.4		
7	43.7		
8	44.5		
9	44.7		
10	44.8	43.02	±3.34%

Table 3. Reliability of $CESMC_{60}$ as working electrode at SR is 100 mVs-1 for anodic current peak 0.3mM $K_4[Fe(CN)_6]$ in 1 M KCl
3. táblázat $CESMC_{60}$ munkaelektróda megbízhatósága anódos csúcs áramerősségre; 0.3mM $K_4[Fe(CN)_6]$ 1M KCl oldatban, mintavételi sebesség 100 mVs-1

3.6. Study the $CESMC_{60}$ at different pH

The new fabrication $CESMC_{60}$ was studied at different pH in aqueous solution for both acidic and alkaline medium as shown in *Table 4*. It was observed that the fabrication electrode properties of the redox current peaks for Fe(II)/Fe(III) in 0.3 mM $K_4[Fe(CN)_6]$ with 1M KCl as a supporting electrolyte have the same affective against to the acidic and alkaline medium by increasing the current peak against to increasing of acidity and the same phenomena increasing the current peak versus ton increasing the alkaline medium as shown in *Table 4* and *Figs. 10* and *11*.

pH	Epc V	Epa V	Ipc mA	Ipa mA
3	-544	263	-47.2	41.3
4	-531	228	-50.4	41.9
5	-553	238	-49	41.3
6	-574	279	-51.2	41.9
7	-534	247	-49.4	40
8	-506	347	-55.4	48.1
11	-580	317	-48.6	42.3

Table 4. Relationship between pH and redox current and potential peaks of 0.3 mM $K_4[Fe(CN)_6]$ with 1 M KCl at $CESMC_{60}$
4. táblázat Kapcsolat a pH érték, a redox csúcs áramerősség és csúcs potenciál között; $CESMC_{60}$ munkaelektróda 0.3mM $K_4[Fe(CN)_6]$ 1M KCl oldatban

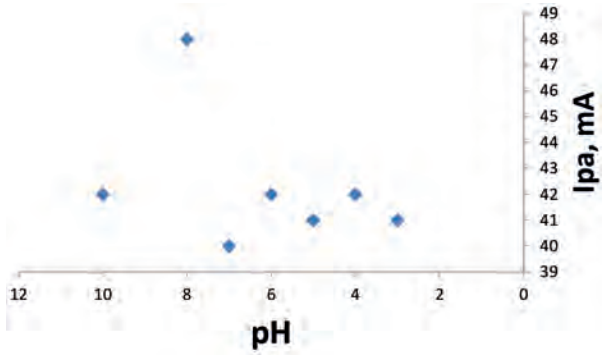

Fig. 10 Plot of anodic current peak of 0.3 mM $K_4[Fe(CN)_6]$ in 1M KCl at fabrication working electrode $CESMC_{60}$ against to pH using Ag/AgCl as reference electrode and SR 0.1 Vs-1
10. ábra Anódos csúcs áramerősség ábrázolása: $CESMC_{60}$ munkaelektróda 0.3mM $K_4[Fe(CN)_6]$ 1M KCl oldatban, Ag/AgCl referencia elektródával; mintavételi sebesség 0.01 Vs-1

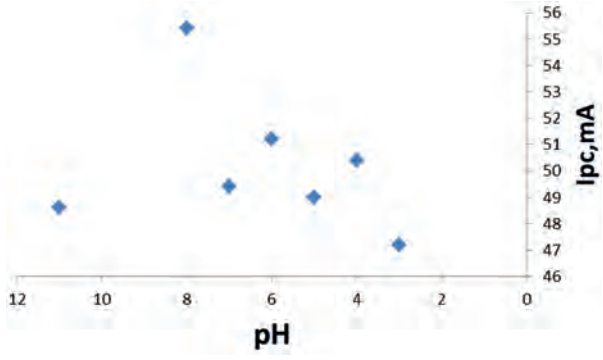

Fig. 11 Plot of cathodic current peak of 0.3 mM $K_4[Fe(CN)_6]$ in 1M KCl at fabrication working electrode $CESMC_{60}$ against to pH using Ag/AgCl as reference electrode and SR 0.1 Vs-1
11. ábra Katódos csúcs áramerősség ábrázolása: $CESMC_{60}$ munkaelektróda 0.3mM $K_4[Fe(CN)_6]$ 1M KCl oldatban, Ag/AgCl referencia elektródával; mintavételi sebesség 0.01 Vs-1

4. Conclusions

A new fabrication working electrode $CESMC_{60}$ was manufactured and characterized electrochemically in the laboratory of cyclic voltammetry. All chemical and physical properties was studied using 0.3 mM $K_4[Fe(CN)_6]$ in 1M KCl for redox current peaks of reversible reaction of Fe(II)/Fe(III). It was found an enhancement current peak of the $CESMC_{60}$ for redox process of Fe(II)/Fe(III) was observed compared to the GCE about ten times, also extended potential area working region between 2.0 to -2.0 V for the new electrode. The sensitivity of the fabrication electrode has high detection analysis using cyclic voltammetry significantly depend on the different concentration, pH, temperature, scan rates, and Stability and reliability. It was determined the diffusion coefficient (D_f) of the $CESMC_{60}$ in the 0.3 mM $K_4[Fe(CN)_6]$ in 1M KCl which has average value $1.6x10^{-10}$ cm^2sec^{-1}.

References

[1] Radhi, M. M. – Al-Mulla, E. A. J. (2015): Voltammetric characterization of grafted polymer electrode self-modification with carbon nanotubes (GPESMCNT), *Quarterly Adjudicated Journal for Natural and Engineering Research and Studies*, 2015, 1: 35-44.
[2] Radhi, M. M. – Tan, Wee Tee – Rahman, M. Z. (2012): Synthesis and characterization of grafted acrylonitrile on polystyrene modified with

activated carbon using gamma-radiation, *Scientific Research and Essays*, 2012, 7(7):790-795.

[3] Radhi, M. M. – Al-Mulla, E. A. J. – Tan, W. T. (2012): Electrochemical characterization of the redox couple of Fe(III)/Fe(II) mediated by grafted polymer electrode, *Research on Chemical Intermediates*, 2012, 38 https://doi.org/10.1007/s11164-012-0954-6

[4] Radhi, M. M. (2013): Electrochemical characterization of the redox couple of Fe(III)/Fe(II) mediated by grafted polymer reference electrode (GPRE) *Research on Chemical Intermediates*, 2013, 39: 9-15. https://doi.org/10.1007/s11164-013-1095-2

[5] Rad, A. S. – Mirabi, A. – Binaian, E. – Tayebi, H. (2011): A Review on Glucose and Hydrogen Peroxide Biosensor Based on Modified Electrode Included Silver Nanoparticles. *Int. J. Electrochem*. Sci. 2011, 8, 3671–3683.

[6] Radhi, Muhammed M. – Tan, Wee T. – Ab Rahman, Mohamad Z. B. – Kassim, Anuar Bin (2010): Electrochemical Characterization of the Redox Couple of $[Fe(CN)_6]^{-3}/[Fe(CN)_6]^{-4}$ Mediated by a Grafted Polymer Modified Glassy Carbon Electrode, *Journal of Chemical Engineering of Japan*, Vol. 43, No. 11, pp. 927–931. https://doi.org/10.1252/jcej.10we150

[7] Desimoni, Elio – Brunetti, Barbara (2015): X-Ray Photoelectron Spectroscopic Characterization of Chemically Modified Electrodes Used as Chemical Sensors and Biosensors. *Chemosensors*, 2015, 3, 70-117. https://doi.org/10.3390/chemosensors3020070

[8] Cecchet, Francesca – Rapino, Stefania – Margotti, Massimo – Ros, Tatiana Da – Prato, Maurizio – Paolucci, Francesco – Rudolf, Petra (2006): Structural and electrochemical characterization of fullerene-based surfaces of C60 mono- or bis-adducts grafted onto self-assembled monolayers, *Carbon 44* (2006) 3014–3021. https://doi.org/10.1016/j.carbon.2006.05.024

[9] Pilehvar, Sanaz – De Wael, Karolien (2015): Recent Advances in Electrochemical Biosensors Based on Fullerene-C60 Nano-Structured Platforms. *Biosensors*. 2015 Dec; 5(4): 712–735. https://doi.org/10.3390/bios5040712

[10] Ren, Jing M. – Subbiah, Jegadesan – Zhang, Bolong – Ishitake, Kenji – Satoh, Kotaro – Kamigaito, Masami – Qiao, Greg G. – Wong, Edgar H. H. – Wong, Wallace W. H. (2016): Fullerene peapod nanoparticles as an organic semiconductor–electrode interface layer Chemical Communications, 2016, 52, 3356-3359. https://doi.org/10.1039/C5CC10444K

[11] Saxena, Amit – Singh, Pramod Kumar – Bhattacharya, Bhaskar (2014): Structural and electrical studies of fullerene (C_{60}) dispersed polymer electrolytes, *Materiali in tehnologije / Materials and technology*, MTAEC9, 48(4)485(2014).

[12] Tasaki, Ken – Venkatesan, Arun – Pugazhendhi, Perumal – Raouf, O. Loutfy (2004): Fullerene-based PEM for dry operation of polymer electrolyte fuel cell. *American Chemical Society, Division of Fuel Chemistry.* 2004, 49(2), 531.

[13] Kazachenko, Viktor (2009): Structure of C_{60} polymer coatings deposited via electron-beam dispersion of fullerite, *Physics of the Solid State 51* (2009) 870-875. https://doi.org/10.1134/S1063783409040416

[14] Li, Cheng – Chen, Yuhong – Wang, Yubing – Iqbal, Zafar – Chhowalla, Manish – Mitra, Somenath (2007): A fullerene–single wall carbon nanotube complex for polymer bulk heterojunction photovoltaic cells, *Journal of Materials Chemistry*, (2007) https://doi.org/10.1039/b618518e

[15] Pilehvar, Sanaz – De Wael, Karolien (2015): Recent Advances in Electrochemical Biosensors Based on Fullerene-C60 Nano-Structured Platforms, *Biosensors*, 2015, 5, 712-735. https://doi.org/10.3390/bios5040712

[16] Harrod, John F. – Laine, Richard M. (1994): Applications of Organometallic Chemistry in the Preparation and Processing of advanced materials, *Springer Science*, Business media, B.V., 1994, France.

[17] Sweetnam, Sean – Graham, Kenneth R. – Ndjawa, Guy O. Ngongang – Heumüller, Thomas – Bartelt, Jonathan A. – Burke, Timothy M. – Li, Wentao – You, Wei – Amassian, Aram – McGehee, Michael D. (2014): Characterization of the Polymer Energy Landscape in Polymer:Fullerene Bulk Heterojunctions with Pure and Mixed Phases, *Journal of the American Chemical Society*. 2014, 136, 14078–14088. https://doi.org/10.1021/ja505463r

[18] D'Souza, Francis (2016): Porphyrin and Fullerene Modified Electrodes for Electrochemical Catalytic and Sensor Applications, CPhI Istanbul 2016, The Leading Pharma Fair in Eurasia. 1-3 June 2016.

[19] Afrasiabia, Mohammad – Kianipoura, Shokat – Babaeib, Ali – Nasimic, Ali Asghar – Shabanian, Meisam (2013): A new sensor based on glassy carbon electrode modified with nanocomposite for simultaneous determination of acetaminophen, ascorbic acid and uric acid, *Journal of Saudi Chemical Society*, https://doi.org/10.1016/j.jscs.2013.02.002

[20] Piotrowski, P. – Pawłowska, J. – Pawłowski, J. – Czerwonka, A. M. – Bilewicza, R. – Kaim, A. (2015): Self-assembly of thioether functionalized fullerenes on gold and their activity in electropolymerization of styrene, *RSC Advances*, 2015, 5, 86771-86778. https://doi.org/10.1039/C5RA14318G

[21] Bustos, Erika – Rocha, Juan Manríquez – Echegoyen, Luis – Chapman, Thomas W. – Godínez, Luis A. (2007): Synthesis and Characterization of Multilayer Films of Dendrimer Assembled C_{60} Materials on Nanocrystalline TiO_2 Electrodes, *Journal of the Mexican Chemical Society*, 2007, 51(2), 72-80.

[22] Manas, C. (2006): Introduction to polymer science and chemistry: a problem solving approach, USA: *CRC press*; 315-320 (2006)

[23] Tan, Wee Tee – Yusri, Farhan – Zainal, Zulkarnain (2009): Electrochemical Reduction of Potassium Ferricyanide Mediated by Magnesium Diboride Modified Carbon Electrode, *Sensors & Transducers Journal*, 104, 5, 2009, 119-127.

[24] Tan, W. T. – Lim, E. – Bond, A. (2003): Voltammetric studies on microcrystalline C_{60} adhered to an electrode surface by solvent casting and mechanical transfer methods. *Journal of Solid State Electrochemistry*, 7: 134-140. https://doi.org/10.1007/s10008-002-0295-2

[25] Bard, A. J. – Faulkner, L. R. (2001): Electrochemical Methods: Fundamentals and Applications, 2nd Ed. *Wiley*, New York.

[26] Bhatti, Naheed Kaukab – Subhani, M. Sadiq – Khan, Ather Yaseen – Qureshi, Rumana – Rahman, Abdur (2006): Heterogeneous electron transfer rate constants of viologen monocations at a platinum disk electrode, *Turkish Chemical Journal*. 30 (2006), 165-180.

[27] Perrin, D. D. – Armarego, W. L. F. – Perrin, D. R. (1966): Purication of Laboratory Chemicals, pp. 143, *Paragon*, London, 1966.

[28] E. L. (1997): Diffusion: Mass Transfer in Fluid Systems (2nd ed.). New York: *Cambridge University Press*.

[29] Grathwohl, P. (1998): Diffusion in natural porous media: Contaminant transport, sorption / desorption and dissolution kinetics. *Kluwer Academic*.

[30] Radhi, M. M. – Al-Mulla, Emad A. Jaffar – Tan, W. T. (2014): Electrochemical characterization of the redox couple of Fe(III)/Fe(II) mediated by grafted polymer electrode, *Research on Chemical Intermediates*, January 2014, Volume 40, Issue 1, pp. 179–192. https://doi.org/10.1007/s11164-012-0954-6

[31] Jacob, S. R. – Hong, Q. – Coles, B. A. – Compton, R. G. (1999): Variable-Temperature Microelectrode Voltammetry: Application to Diffusion Coefficients and Electrode Reaction Mechanisms. *Journal of Physical Chemistry*. 103, 2963 https://doi.org/10.1021/jp990024w

[32] Radhi, Muhammed Mizher (2016): Fabrication and characterization of grafted polymer electrode self-modification with activated carbon, *International Journal of Industrial Chemistry*, (2016) 7:103–108. https://doi.org/10.1007/s40090-015-0058-4

[33] Al-Mulla, E. A. J. – Al-Mosawy, M. G. – Mohamad, M. J. (2017): New biopolymer nanocomposites-based epoxidized palm oil/polybutylene succinate modified clay: Preparation and characterization. *Rendiconti Lincei*, 2017, 28(4): 721-730. https://doi.org/10.1007/s12210-017-0646-7

[34] Al-Mulla, E. A. J. (2018): Nanoparticles of TiO_2-ZnO Modified Polystyrene-Acrylonitrile Characterization Using Glassy Carbon Electrode, 2018, *Nano Biomedical Engineering* 10 (1), 34-39. https://doi.org/10.5101/nbe.v10i1.p34-39

[35] Al-Mosawy, M. G. – Mohamad, M. J. (2017): Bentonite-based organoclays using chalcone and azo dye as organophilic reagents, *Építőanyag-Journal of Silicate Based and Composite Materials*, 2017, 69(2): 49-54. https://doi.org/10.14382/epitoanyag-jsbcm.2017.9

[36] Jabbar, F. H. – Kadhim, Z. J. – Abdullah, A. A. – Wadday, A. G. (2017): Epoxidized Palm Oil Plasticized Polycaprolactone Nanocomposites Preparation. *Nano Biomedical Engineering 9* (3), 214-220. https://doi.org/10.5101/nbe.v9i3.p214-220

[37] Al Mutoki, S. M. M. – Al-Ghzawi, B. A. H. K. – Amohsin, S. M. A. (2017): Raman shift of silicon rubber-nano titania PMNC, *Építőanyag-Journal of Silicate Based and Composite Materials*, 2017, 69(1): 20-23. https://doi.org/10.14382/epitoanyag-jsbcm.2017.4

Ref.:

Radhi, Muhammed Mizher – **Al-Mulla**, Emad Abbas Jaffar: *Copolymer electrode self-modified with fullerene C_{60}*
Építőanyag – Journal of Silicate Based and Composite Materials, Vol. 70, No. 5 (2018), 134–139. p.
https://doi.org/10.14382/epitoanyag-jsbcm.2018.25

Silylated functionalized montmorillonite clay for nanocomposite preparation

David P. PENALOZA Jr.
is an associate professor in the Chemistry Department, College of Science, De La Salle University. His research interests focus on self-assembled systems and nanostructured materials.

Thomas AP SEERY
is an associate professor in the Chemistry Department and the Polymer Program, Institute of Materials Science (IMS), University of Connecticut. He previously served as the Polymer Program director at IMS. His research interests include polymer synthesis at surfaces and physical chemistry of polymers in solution.

David P. PENALOZA Jr. ▪ Chemistry Department, College of Science, De La Salle University, Manila, Philippines ▪ david.penaloza.jr@dlsu.edu.ph
Thomas AP SEERY ▪ Chemistry Department and Polymer Program, Institute of Materials Science, University of Connecticut, Connecticut, USA ▪ Email: thomas.seery@uconn.edu

Érkezett: 2018. 05. 24. ▪ Received: 24. 05. 2018. ▪ https://doi.org/10.14382/epitoanyag-jsbcm.2018.26

Abstract
Hydrothermal silylation reaction between a norbornenyl-bearing chlorosilane coupling agent and the silanol groups of the montmorillonite (MMT) clay results in a functionalized organoclay. To do this, the clay samples were previously modified using different alkyl ammonium surfactants prior to silylation. Apparently, the different surfactant modifiers used led to different clay morphologies for the silylated functionalized clay templates as confirmed by x-ray diffraction and elemental micro-analysis.
Keywords: silylation, surface modification, silicate clay, nanocomposite, organoclay
Kulcsszavak: szilanizálás, felület modifikálás, szilikát agyag, nanokompozit, szerves agyag

1. Introduction

A polymer-clay nanocomposite represents a new class of hybrid materials composed of an organic polymer matrix with an inorganic clay acting as a filler material having at least one dimension in the nanometer range. A fully exfoliated, individual clay platelet is about a nanometer in thickness. At this length scale, the presence of these individual nanometer thin platelets dispersed in the polymer matrix even at a low amount of the silicate filler (<10% by wt) can impact the resulting hybrid organic-inorganic material to exhibit greatly enhanced and new properties relative to the neat polymer [1-5]. These new and enhanced properties observed for these nanomaterials have found numerous applications and have attracted the attention of both the academe and the industries.

Among the clay fillers, the montmorillonite (MMT) clay is the usual choice in preparing most polymer-clay nanocomposites because of its individual nanometer-"thick" platelets, extremely large surface areas [2], rich intercalation and surface chemistry [6-7]. Further, this type of clay is universally abundant in nature and can be obtained in pure form at a low cost.

An MMT clay, being hydrophilic in nature, obviously would only be miscible with hydrophilic polymers like poly(ethylene oxide), poly(vinyl alcohol), etc.. Generally, it would be very difficult to mix this clay with hydrophobic polymers because of its pristine hydrophilic nature. One way of increasing the favorable interaction between organic molecules and clay surfaces is by introducing some hydrophobic groups onto the layer surfaces [8]. This method of clay modification can be possible with the reaction of silanes with the silanol groups found in the clay layered structure [6, 9-12]. The introduced technique makes use of the existing silanol groups found in the clay structure to react with organosilane agents. Silanol groups (Si-OH) are located on the clay edges due to broken edges and crystalline defects [13-18]. Using a chloro- or alkoxysilanes as modifying agents, several functionalities can be introduced to the clay [19]. Unlike the ion-exchanged clays, the covalently modified clays achieved through the hydrosilylation of the silanol groups are more thermally stable [9,15]. More importantly, the characteristics of the modified clays can be easily fine-tuned through the introduction of various end groups of the silane modifiers [14, 20-23].

2. Experimental

2.1 Materials

Hexanes (98.5%) were purchased from Acros Organics. Tetrahydrofuran (THF) (99%) and methanol (absolute) were purchased from J.T. Baker Inc. Decyltrimethylammonium bromide (DTAB) was obtained from Aldrich. [(Bicycloheptenyl) ethyl] dimethylchlorosilane was obtained from Gelest Inc.

Cloisite15A clay and sodium montmorillonite clay were obtained from Southern Clay Products, Inc.

2.2 Preparation of MMT_C10 clay via ion-exchange reaction

Montmorillonite clay (MMT) was reacted first with an alkyl ammonium halide to hydrophobize the clay. This was accomplished by an ion exchange reaction between clay and decyltrimethylammoniumbromide, $CH_3(CH_2)_8CH_2N^+(CH_3)_3Br^-$ (DTAB). A 5.0 g MMT was added to 500 mL of deionized water, stirred for 2 hours and sonicated for 3 hours. 1.5 g of DTAB was then added and stirred for 24 hours. The ion exchanged clay (MMT_C10) was separated by centrifuge, washed several times with de-ionized water to remove excess DTAB, air-dried prior to vacuum drying at 100 °C.

2.3 Silylation of the host silicate clays

Two MMT clay derivatives were considered for silylation: (1) commercial organoclay Cloisite15A from the Southern Clay Products, Inc. and (2) an MMT clay that we previously modified via io-exchange reaction using decyltrimethyl ammonium bromide, $CH_3(CH_2)_8CH_2N^+(CH_3)_3Br^-$.

The organoclay was vacuum-dried at 50 °C prior to silylation. A silane coupling agent having a norbornene moiety, [(bicycloheptenyl)ethyl] dimethylchlorosilane, was used to functionalize the clay. A 5.0 g sample of the organoclay was placed in an air-free three-neck round bottom flask and flushed with nitrogen for few minutes. 150 mL of dry hexane was then added to the sample and the mixture was stirred under static nitrogen for 10 minutes.

Then, 5 mL of norbornene-chlorosilane was added to the flask and the mixture was refluxed under nitrogen for 48 h. The final product (silylated organoclay) was then filtered off and repeatedly washed with hexane, before being dried at 60 °C for 24 h under vacuum.

2.4 Instrumentation

2.4.1 X-ray diffraction (XRD)

The X-ray diffraction analyses in the small-angle (2θ=0-10) region were performed using a Bruker GADDS X-ray diffractometer. The beam was Cu K_α (λ = 0.154 nm) operated at 40kV and 40 mA.

2.4.2 Transmission Electron Microscopy (TEM)

TEM was employed to observe the morphology of the organoclay. TEM micrographs were obtained using FEI Spirit Twin transmission electron microscope. Samples for TEM observation were dissolved in THF and a 5-ug aliquot was solution cast onto carbon-coated grids.

2.4.3 Carbon and Nitrogen Content Analysis

The percentage content of carbon and nitrogen of the organoclay materials before and after the silylation process was determined using Elementar CHNOS Elemental Analysis equipment.

3. Results and discussion

One of the inorganic fillers often considered to prepare polymer nanocomposites is layered silicate clay. Among the layered clays, the montmorillonite (MMT) clay is most often used. It has a layered structure made up of stacks of nanometer-"thick" silicate platelets. *Fig. 1* shows the XRD pattern and TEM micrograph of a pristine sodium montmorillonite (Na^+-MMT) clay. The unmodified clay contained sodium (Na^+) ions found in the interlayers of the MMT layered structure. Based on the XRD measurement of the clay, the Na^+-MMT clay has a d spacing (d_{001}) of 1.18 nm. The value of the d_{001} spacing is calculated using the Bragg's equation based from the 2θ position of the (001) diffraction peak (*Fig. 1.a*). Considering that one silicate platelet has a thickness of 0.96 nm and the calculated d_{001} spacing of 1.18 nm, an interlayer spacing due to the sodium ions found in the MMT galleries equal to 0.22 nm can be calculated. This value (0.22 nm) is larger than the reported value for the diameter of a sodium ion. This is because the ions originally found in the interlayers of the MMT structure most often are hydrated. The TEM micrograph (*Fig. 1.b*) of the clay shows that along the edges of the clay sample (as pointed by the arrow), the stacking of a number of silicate platelets can be clearly observed, showing the layered morphology of the MMT clay.

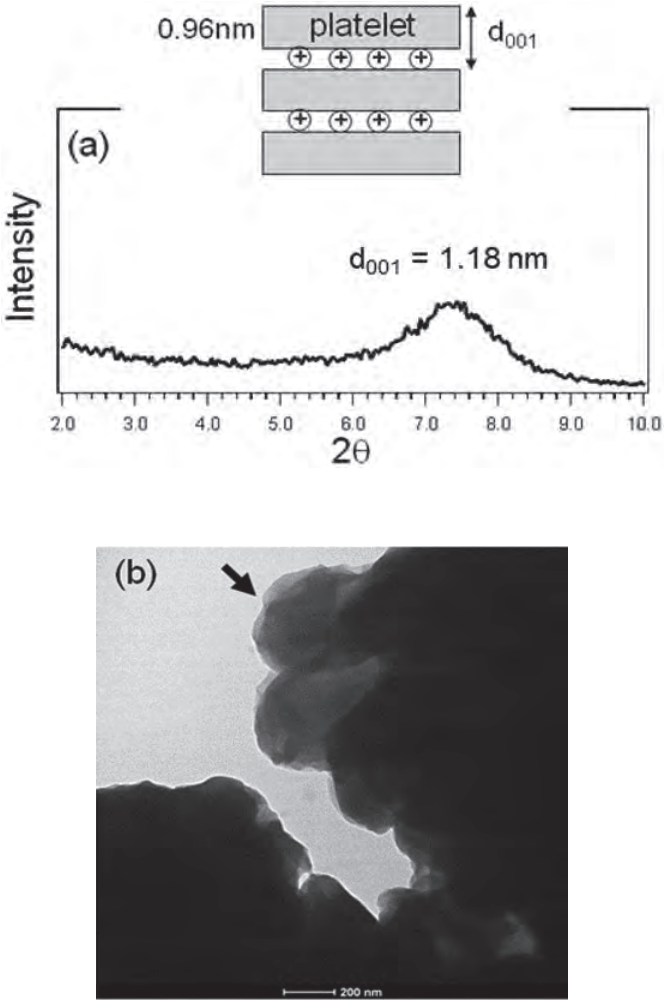

Fig. 1. (a) XRD profile and (b) TEM micrograph of a sodium montmorillonite (Na^+-MMT) clay
1. ábra Nátrium montmorillonit (Na^+-MMT) agyag (a) röntgendiffraktogramja és (b) TEM mikroszkópos képe

Our research group's interest is in the preparation of nanostructured hybrid materials with covalently tethered polymer architecture [24-27]. In our most recent work involving clay-based polymer nanocomposite preparation, norbornene-bearing silanes are attached on the surface and edge of an MMT organoclay, and the polymerization of norbornene directly from the organoclay results in the successful formation of an exfoliated silicate clay-polymer nanocomposite as confirmed by XRD and TEM. To achieve this, we initially modify Cloisite15A clay, a commercial MMT organoclay from Southern Clay Products, Inc. that was previously modified with ammonium salt bearing naturally occurring tallows. In this previously published work, we have demonstrated that norbornene-bearing initiators can be successfully grafted via covalent binding to the MMT clay as confirmed by the results of the fourier-transform infrared (FTIR), ^{29}Si solid-state nuclear magnatec resonance (^{29}Si-NMR) spectroscopic measurements and thermogravimetric analysis (TGA) [26].

There is a need, however, to evaluate if the silylation reaction between the norbornene-chlorosilane and the silanols of the MMT clay modified the surface of the clay template or only the edges (*Fig. 2*). This is important in our case since modifying the clay surface would enable us to facilitate the polymerization between the galleries of the host clay template. To do this, we have compared the XRD profiles of the MMT organoclays before and after the silylation reaction as well as their nitrogen content. The silylation reaction would change the distance between the platelets and shift the d_{001} which can be detected by XRD. The nitrogen content of the organoclays before and after the silylation reaction will help us monitor if some of the previously intercalated ammonium modifiers are lost during the silylation process.

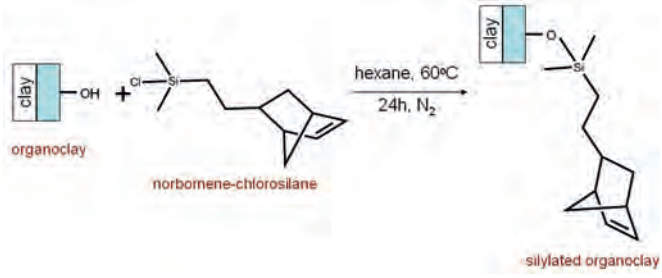

Fig. 2. Scheme of the silylation process between norbornene-chlorosilane and MMT clay
2. ábra Szilanizálás sémája norbornén-kloroszilán és MMT agyag kölcsönhatásában

3.1 X-ray diffraction

The basal spacing (d_{001}) of the clay samples was determined using Bragg's Law: $d_{001} = \lambda/(2 \sin \theta)$; where λ represents the wavelength of the X-ray (1.5418A°). An X-ray diffraction (XRD) spectrum is usually a plot of the scattering angle, 2θ, against an arbitrary intensity of a diffraction peak. *Fig. 3* represents the XRD patterns of the nonsilylated and silylated Cloisite15A clays.

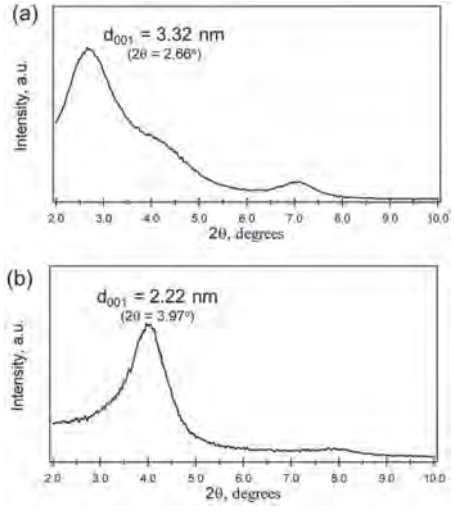

Fig. 3. XRD patterns of the (a) ion-exchanged montmorillonite clay (Cloisite15A) and (b) silylated Cloisite15A (Cloisite15A_sil)
3. ábra Röntgendiffraktogramok (a) ioncserélt montmorillonit agyag (Cloisite15A) és (b) szilanizált Cloisite15A (Cloisite15A_sil)

The XRD spectrum of the nonsilylated organoclay, Cloisite15A, shows a broad peak at around $2\theta = 2.66°$ that corresponds to a d_{001} spacing of 3.32 nm based from the calculation made using the Bragg's equation. The distributor of this organoclay, Southern Clay Products, Inc. reported the d_{001} value for Cloisite15A to be equal to 3.15 nm. The d_{001} values of this MMT derivative as determined by various authors fall in the range of 2.8 - 3.4 nm [28-31].

Pristine sodium MMT clay has 2θ value corresponding to the (001) plane lies at 8.9°, with a basal spacing of 9.80 Å calculated from the Bragg equation [32].

As expected, the (001) peak of the organo-modified MMT clay is shifted at a lower scattering angle when the long alkyl ammonium cations were used to replace the cations originally found in the native MMT clay. A shift of the MMT characteristic diffraction peak to lower angles corresponds to an increase in the gap between two silicate platelets (larger d_{001} value) and suggests that the organic surfactants were successfully intercalated in the interlayers of the host MMT clay.

Assuming a stretched configuration for the hydrogenated tallow of the ammonium modifier, the chain length was calculated based from the work of Xi et al. (2005) [33] and was estimated to have lengths between 2.4 - 3.0 nm taking into account that the tallow is a mixture of long alkyl chains (C_{14} - C_{18}). To calculate the increase in the interlayer spacing brought about by the intercalation of the organic surfactants, the net difference between the calculated d_{001} value of Cloisite15A (3.32 nm) and the reported thickness of an individual MMT platelet (0.96 nm), was considered and the distance of the interlayer gap was determined to be 2.32 nm after intercalation of the tallow surfactant. Based from this calculated value and the length of a stretched tallow, it is not possible for the layer of chains to be oriented in such a way that the chains stretch out perpendicular relative to the interlayer surfaces. Vaia et al. (1994) [34]; Hackett et al. (1998) [35]; Park et al. (2004) [36] suggested a tilted paraffinic monolayer arrangement of the intercalant for an organoclay modified with an ammonium salt containing long alkyl chains. For Cloisite15A, the inner layer surfaces of an MMT clay were treated with dimethyl dihydrogenated tallow ammonium modifiers. A hydrogenated tallow alkyl chain is found to contain about 65 wt% of C_{18}, 30 wt% of C_{16} and 5 wt% of C_{14} (Southern Clay Products, Inc.)

After silylation reaction of the organoclay, Cloisite15A, with a chlorosilane bearing a norbornene moiety, a decrease in the basal spacing was noted as the characteristic (001) diffraction peak of the organoclay shifted at a higher angle, $2\theta = 3.97°$ (d_{001} = 2.22 nm).

The same observation of decreased interlayer gaps after a silylation reaction using the same silane agent, norbornene-chlorosilane, was reported by Guino et al.(2005) [24] on a layered silicate clay previously ion exchanged with an alkyl ammonium salt, dodecyltrimethylammonium chloride (C_{12}TMACl). Magadiite, a layered silicate clay like MMT, is capable of incorporating guest species in the interlayer space due to the exchangeable cations located between its galleries [37-38]. Unlike MMT, however, there are reactive silanol groups on the interlayer surface which can be modified [11, 39]. The alkyl ammonium modifier (C_{12}TMACl), was first introduced in the clay structure to increase the basal spacing between the MMT platelets so that the norbornene-chlorosilane, can be

intercalated to modify the clay surface.

After silylation, the d_{001} peak shifts to a higher diffraction angle (2θ =3.97°) which corresponds to a basal spacing of d_{001}=2.22 nm. The decrease in the basal spacing between platelets during the silylation process is due to some alkyl ammonium salts previously intercalated between platelets of the MMT clay template being replaced by the norbornene-silane. The chain length of the silylating agent is much shorter than that of the alkyl ammonium intercalating agent, hence the smaller basal spacing observed for Cloisite15A_sil.

To establish that the loss of some amounts of ammonium modifiers is due to the result of successful silylation of the silanols on the surface of the clay template, and not on other factors (like due to stirring or reflux condition, we simulate the silylation condition without the norbornene-chlorosilane by stirring the organoclay in the same solvent (hexane) at the same condition (reflux for 48 hours under nitrogen) and getting the XRD profile of the recovered organoclay. No change in the position of the (001) diffraction peak was observed.

3.2 Nitrogen content of Cloisite15A organoclays

To verify that the change in the XRD profile of the organoclay during the silylation process is accompanied by the loss of some previously ionically anchored ammonium modifiers, we did a comparison of the nitrogen content of the two organoclays. The result obtained from the comparison of the nitrogen content of both organoclays (before and after silylation) complements the XRD measurements and confirms our observation that some of the alkyl ammonium modifiers previously used to modify the MMT surface were lost during the silylation process. In *Table 1*, the nitrogen content of the silylated clay (0.98%) is much less than those of the unsilylated clay (1.20%). The nitrogen content of both clays is due to the alkyl ammonium modifiers used to modify the MMT clay. The loss of some of the ammonium-based modifiers previously anchored in the galleries of the MMT template was due to its replacement by the protons generated during the silylation reaction between the silanol group of the host clay and the norbornene-chlorosilane [10]. The newly formed silanols further reacted with the silylating agent as evident in the results of the XRD measurements conducted on the organoclays.

Organoclays	%N	%C	C/N	d_{001} (in nm)
Cloisite15A (before silylation)	1.20%	32.0%	26.7	3.32
Cloisite15A_sil (after silylation)	0.98%	35.4%	36.1	2.22

Table 1. Elemental analysis and d_{001} spacing of the Cloisite15A organoclays
1. táblázat Elem összetétel és d_{001} távolság Cloisite15A szerves agyagokra

3.3 Silylation of MMT_C10 organoclay

The same silylation procedure was applied to another MMT clay derivative and the XRD profile and nitrogen content before and after the silylation were compared. The clay was an MMT derivative ion-exchanged with a decyltrimethyl ammonium bromide, $CH_3(CH_2)_8CH_2N^+(CH_3)_3Br^-$. This was labeled MMT_C10. The same (001) spacing of the organoclay was observed before and after the silylation (*Fig. 4*). The nitrogen content also did not change (*Table 2*). These results suggested that in the silylation reaction of this organoclay, only the silanol groups found on the edges of the MMT_C10 clay template were modified, and not the surface, unlike in the case of Cloisite15A organoclay.

Organoclays	%N	%C	C/N	d_{001} (in nm)
MMT_C10 (before silylation)	1.16%	19.3%	16.6	1.42
MMT_C10_sil (after silylation)	1.15%	19.2%	16.7	1.43

Table 2. Elemental analysis and d_{001} spacing of the MMT_C10 organoclays
2. táblázat Elem összetétel és d_{001} távolság MMT_C10 szerves agyagra

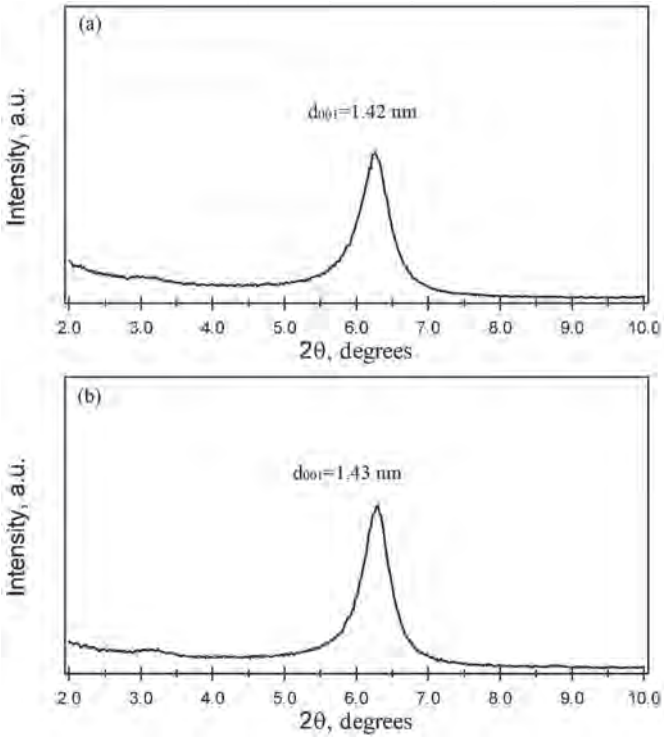

Fig. 4. XRD patterns of the (a) ion-exchanged montmorillonite clay (MMT_C10) and (b) silylated MMT_C10 (MMT_C10_sil)
4. ábra Röntgendiffraktogramok (a) ioncserélt montmorillonit agyag (MMT_C10) és (b) szilanizált MMT_C10 (MMT_C10_sil)

4. Conclusions

The silylation scheme results in silane-modified clays having different morphologies: (1) both surface- and edge-modified in the case of Cloisite15A and (2) only edge-modified for MMT_C10 clay as confirmed by XRD measurements and nitrogen content analysis of both organoclays.

Using this silylation approach, a norbornene-bearing silane can be grafted on the surfaces and/or edges of the clay template. Apparently, the silylation as a way of modifying the clay morphology is affected by the length of previously attached alkyl ammonium surfactant. The ability to covalently attach the silane coupling agent having certain functional moieties, i.e. norbornene groups as initiating sites – is an important step in preparing a special class of polymer nanocomposites.

The grafted norbornene functionalities upon the addition of a metal alkylidene can facilitate the direct polymerization on the clay surface yielding covalently bound polymer chains on an inorganic substrate.

References

[1] Xie, W. – Gao, Z. – Pan, W. P. – Hunter, D. – Singh, A. – Vaia, R. (2001): Thermal degradation chemistry of alkyl quaternary ammonium montmorillonite. *Chemistry of Materials*, Vol. 13, No. 9, pp. 2979-2990. https://doi.org/10.1021/cm010305s

[2] Alexandre, M. – Dubois, P. (2000): Polymer-layered silicate nanocomposites: preparation, properties and uses of a new class of materials. *Materials Science and Engineering*: R: Reports, Vol. 28, Nos. 1&2, pp. 1-63 (2000). https://doi.org/10.1016/S0927-796X(00)00012-7

[3] Tjong, S. C. – Meng, Y. Z. – Hay, A. S. (2001): Novel preparation and properties of polypropylene-vermiculite nanocomposites. *Chemistry of Materials*, Vol. 14, No. 1, pp. 44-51. https://doi.org/10.1021/cm010061b

[4] Kotek, J. – Kelnar, I. – Studenovský, M. – Baldrian, J. (2005): Chlorosulfonated polypropylene: preparation and its application as a coupling agent in polypropylene-clay nanocomposites. *Polymer*, Vol. 46, No. 13, pp. 4876-4881. https://doi.org/10.1016/j.polymer.2005.02.119

[5] Pramoda, K. P. – Liu, T. (2004): Effect of moisture on the dynamic mechanical relaxation of polyamide-6/clay nanocomposites. *Journal of Polymer Science* Part B: Polymer Physics, Vol. 42, No. 10, pp. 1823-1830. https://doi.org/10.1002/polb.20061

[6] Zhang, Z. H. – Li, T. S. – Yang, F. – Fu, C. G. (1998): Montmorillonite clay catalysis XI: protection and deprotection of hydroxyl group by formation and cleavage of trimethylsilyl ethers catalysed by montmorillonite K-10. *Synthetic Communications*, Vol. 28, pp. 3105-3114. https://doi.org/10.1080/00397919808004891

[7] Tyan, H. L. – Liu, Y. C. – Wei, K. H. (1999): Thermally and mechanically enhanced clay/polyimide nanocomposite via reactive organoclay. *Chemistry of Materials*, Vol. 11, No. 11, pp. 1942-1947. https://doi.org/10.1021/cm990187x

[8] Herrera, N. N. – Letoffe, J. M. – Putaux, J. L. – David, L. – Bourgeat-Lami, E. (2004): Aqueous dispersions of silane-functionalized laponite clay platelets. A first step toward the elaboration of water-based polymer/clay nanocomposites. *Langmuir*, Vol. 20, No. 5, pp. 1564-1571. https://doi.org/10.1021/la0349267

[9] He, H. P. – Duchet, J. – Galy, J. – Gerard, J. F. (2005): Grafting of swelling clay materials with 3-aminopropyltriethoxysilane. *Journal of Colloid and Interface Science*, Vol. 288, No. 1, pp. 171-176. https://doi.org/10.1016/j.jcis.2005.02.092

[10] Zhang, J. G. – Gupta, R. K. – Wilkie, C. A. (2006): Controlled silylation of montmorillonite and its polyethylene nanocomposites. *Polymer*, Vol. 47, No. 13, pp. 4537-4543. https://doi.org/10.1016/j.polymer.2006.04.057

[11] Okutomo, S. – Kuroda, K. – Ogawa, M. (1999): Preparation and characterization of silylated-magadiites. *Applied Clay Science*, Vol. 15, Nos. 1&2, pp. 253-264. https://doi.org//10.1016/S0169-1317(99)00010-1

[12] Ogawa, M. – Okutomo, S. – Kuroda, K. (1998): Control of interlayer microstructures of a layered silicate by surface modification with organochlorosilanes. *Journal of the American Chemical Society*, Vol. 120, No. 29, pp. 7361-7362. https://doi.org/10.1021/ja981055s

[13] Deuel, H. – Huber, G. – Iberg, R. (1950): Organische derivate von tonmineralien. *Helvetica Chimica Acta*, Vol. 33, No. 5, pp. 1229-1232. https://doi.org/10.1002/hlca.19500330514

[14] Herrera, N. N. – Letoffe, J.-M. – Putaux, J.-L. – David, L. – Bourgeat-Lami, E. (2004): Aqueous dispersions of silane-functionalized laponite clay platelets. A first step toward the elaboration of water-based polymer/clay nanocomposites. *Langmuir*, Vol. 20, No. 5, pp. 1564-1571. https://doi.org/10.1021/la0349267

[15] Song, K. – Sandi, G. (2001): Characterization of montmorillonite surfaces after modification by organosilane. *Clays and Clay Minerals*, Vol. 49, No. 12, pp. 119-125. https://doi.org/10.1002/app.12979

[16] Herrera, N. N. – Letoffe, J.-M. – Reymond, J.-P. – Bourgeat-Lami, E. (2005): Silylation of laponite clay particles with monofunctional and trifunctional vinyl alkoxysilanes. *Journal of Materials Chemistry*, Vol. 15, No. 8, pp. 863-871. https://doi.org/10.1039/b415618h

[17] Lee, D. C. – Jang, L. W. (1996): Preparation and characterization of PMMA-Clay hybrid composite by emulsion polymerization. *Journal of Applied Polymer Science*, Vol. 61, No. 7, pp. 1117-1122. https://doi.org/10.1002/(SICI)1097-4628(19960815)61:7<1117::AID-APP7>3.0.CO;2-P

[18] Park, M. – Shim, I.-K. – Jung, E.-Y. – Choy, J.-H. (2004): Modification of external surface of laponite by silane grafting. *Journal of Physics and Chemistry of Solids*, Vol. 65, Nos.2&3, pp. 499-501. https://doi.org/10.1016/j.jpcs.2003.10.031

[19] Romanzini, D. – Piroli, V. – Frache, A. – Zattera, A. J. – Amico, S. C. (2015): Sodium montmorillonite modified with methacryloxy and vinylsilanes: Influence of silylation on the morphology of clay/unsaturated polyester nanocomposites. *Applied Clay Science*, Vol. 114, No. 1, pp. 550-557. https://doi.org/10.1016/j.clay.2015.07.003

[20] Wheeler, P. A. – Wang, J. – Baker, J. – Mathias, L. J. (2005): Synthesis and characterization of covalently functionalized laponite clay. *Chemistry of Materials*, Vol. 17, No. 11, pp. 3012-3018. https://doi.org/10.1021/cm050306a

[21] Bee, S. L. – Abdullah, M. A. A. – Mamat, M. – Bee, S. T. – Sin, L. T., Hui, D. – Rahmat, A. R. (2017): Characterization of silylated modified clay nanoparticles and its functionality in PMMA. *Composites Part B: Engineering*, Vol. 110, pp. 83-95. https://doi.org/10.1016/j.compositesb.2016.10.084

[22] Bertuoli, P. T. – Piazza, D. – Scienza, L. C. – Zattera, A. J. (2014): Preparation and characterization of montmorillonite modified with 3-aminopropyltriethoxysilane. *Applied Clay Science*, Vol. 87, pp. 46-51. https://doi.org/10.1016/j.clay.2013.11.020

[23] Su, L. – Tao, Q. – He, H. – Zhu, J. – Yuan, P. – Zhu, R. (2013): Silylation of montmorillonite surfaces: Dependence on solvent nature. *Journal of Colloid and Interface Science*, Vol. 391, pp. 16-20, https://doi.org/10.1016/j.jcis.2012.08.077

[24] Guino, R. – Lagadic, I. L. – Seery, T. A. P. (2005): Polymer nanocomposites from silica nanowafers. *Abstracts of Papers of the American Chemical Society*, Vol. 229, No. 2, pp. 508-INOR

[25] Jordi, M. A. – Seery, T. A. P. (2005): Quantitative determination of the chemical composition of silica-poly(norbornene) nanocomposites. *Journal of the American Chemical Society*, Vol. 127, No. 12, pp. 4416-4422. https://doi.org/10.1021/ja044456i

[26] Penaloza, D. P. – Sandberg, D. J. – Giotto, M. V. – Seery, T. A. P. (2015): An exfoliated clay-poly(norbornene) nanocomposite prepared by metal-mediated surface-initiated polymerization. *Polymer Engineering & Science*, Vol. 55, No. 10, pp. 2349-2354. . https://doi.org/10.1002/pen.24123

[27] Yavuz, M. S. – Jensen, G. C. – Penaloza, D. P. – Seery, T. A. P. – Pendergraph, S. A. – Rusling, J. F. – Sotzing, G. A. (2009): Gold nanoparticles with externally controlled, reversible shifts of local surface plasmon resonance bands. *Langmuir*, Vol. 25, No. 22, pp. 13120-13124. https://doi.org/10.1021/la901779k

[28] Pozsgay, A. – Frater, T. – Szazdi, L. – Muller, P. – Sajo, I. – Pukanszky, B. (2004): Gallery structure and exfoliation of organophilized montmorillonite: effect on composite properties. *European Polymer Journal*, Vol. 40, No. 1, pp. 27-36 (2004). https://doi.org/10.1016/j.eurpolymj.2003.09.010

[29] Ton-That, M.-T. – Perrin-Sarazin, F. – Cole, K. C. – Bureau, M. N. – Denault, J. (2004): Polyolefin nanocomposites: Formulation and development. *Polymer Engineering and Science*, Vol. 44, No. 7, pp: 1212-1219 (2004). https://doi.org/10.1002/pen.20116

[30] Benetti, E. M. – Causin, V. – Marega, C. – Marigo, A. – Ferrara, G. – Ferraro, A. – Consalvi, M. – Fantinel, F. (2005): Morphological and structural characterization of polypropylene based nanocomposites. *Polymer*, Vol. 46, No. 19, pp. 8275-8285. https://doi.org/10.1016/j.polymer.2005.06.056

[31] Li, J. – Ton-That - M.-T. – Tsai, S.-J. (2006): PP-based nanocomposites with various intercalant types and intercalant coverages. *Polymer Engineering & Science*, Vol. 46, No. 8, pp. 1060-1068. https://doi.org/10.1002/pen.20552

[32] Figueras, F. (1998): Pillared clays as catalysts. *Catalysis Reviews: Science and Engineering*, Vol. 30, No. 3, pp. 457 - 499. https://doi.org/10.1080/01614948808080811

[33] Xi, Y. – Frost, R. L. – He, H. (2007): Modification of the surfaces of Wyoming montmorillonite by the cationic surfactants alkyl trimethyl, dialkyl dimethyl, and trialkyl methyl ammonium bromides. *Journal of Colloid and Interface Science*, Vol. 305, No. 1, pp. 150-158. https://doi.org/10.1016/j.jcis.2006.09.033

[34] Vaia, R. A. – Teukolsky, R. K. – Giannelis, E. P. (1994): Interlayer structure and molecular environment of alkylammonium layered silicates. *Chemistry of Materials*, Vol. 6, No. 7, pp. 1017-1022. https://doi.org/10.1021/cm00043a025

[35] Hackett, E. – Manias, E. – Giannelis, E. P. (1998): Molecular dynamics simulations of organically modified layered silicates. *Journal of Chemical Physics*, Vol. 108, No. 17, pp. 7410-7415. https://doi.org/10.1063/1.476161

[36] Park, C. I. – Kim, M. H. – Ok Park, O. (2004): Effect of heat treatment on the microstructural change of syndiotactic polystyrene/poly(styrene-co-vinyloxazolin)/clay nanocomposite. *Polymer*, Vol. 45, No. 4, pp. 1267-1273. https://doi.org/10.1016/j.polymer.2003.12.011

[37] Eugster, H. P. (1967): Hydrous sodium silicates from Lake Magadi, Kenya: Precursors of bedded chert. *Science*, Vol. 157, No. 3793 , pp. 1177-1180. https://doi.org/10.1126/science.157.3793.1177

[38] Rojo, J. M. – Ruiz-Hitzky, E. – Sanz, J. (1988): Proton-sodium exchange in magadiite. Spectroscopic study (NMR, IR) of the evolution of interlayer OH groups. *Inorganic Chemistry*, Vol. 27, No. 16 , pp.2785-2790. https://doi.org/10.1021/ic00289a009

[39] Theng, B. K. G. (1974): The Chemistry of Clay–Organic Reactions. *Adam Hilger*.

Ref.:
Penaloza Jr., David P. – **Seery**, Thomas AP: *Silylated functionalized montmorillonite clay for nanocomposite preparation*
Építőanyag – Journal of Silicate Based and Composite Materials, Vol. 70, No. 5 (2018), 140–145. p.
https://doi.org/10.14382/epitoanyag-jsbcm.2018.26

Comparative Analysis of Flexible Stabilization Devices Based on Polymeric and Composite Materials for Degenerative Disorders: Finite Element Analysis

Moustafa MOSBAH ▪ Laboratory of numerical and experimental modeling of mechanical phenomena, Department of Mechanical Engineering, University Abd El Hamid Ibn Badis of Mostaganem, Algeria

Mohammed BENDOUKHA ▪ Laboratory of numerical and experimental modeling of mechanical phenomena, Department of Mechanical Engineering, University Abd El Hamid Ibn Badis of Mostaganem, Algeria▪ bendoukham@yahoo.fr

Érkezett: 2018. 06. 01. ▪ Received: 01. 06. 2018. ▪ https://doi.org/10.14382/epitoanyag-jsbcm.2018.27

Abstract

The radiographic apparent assumed that the asymptomatic adjacent segment disease ASD is common after lumbar fusion, but this does not correlate with the functional outcomes while compensatory increased motion and stresses at the adjacent level of fusion is well-known to be associated to ASD [4,5,8]. Newly developed, hybrid and flexible stabilizations are allocated to substitute for mostly the superior level of the fusion in an attempt to reduce the number of fusion levels and likelihood of degeneration process at the adjacent levels during the fusion with pedicle screws. Nevertheless, its biomechanical efficiencies still remain unknown and the complications associated with failure of constructs such screw loosening and toggling should be elucidated [4]. In the current study, a finite element (FE) study was performed using a validated L2/S1 model subjected to a moment of 10 Nm and follower load of 100 N to assess the biomedical behavior of hybrid constructs based on dynamic topping off, semi-rigid fusion using polymeric and composite materials.

Keywords: adjacent segment disease, fusion, degeneration, finite element, hybrid constructs, dynamic topping off, semi-rigid

Moustafa MOSBAH
PhD candidate in biomechanics under the supervision of Dr. BENDOUKHA at the laboratory of numerical and experimental modeling of mechanical phenomena. Obtained the licence and Master's degree from the University of Mostaganem in Mechanics.

Mohammed BENDOUKHA
Research Professor at the University of Mostaganem. Obtained his Engineering degree in Mechanical Engineering from the University of Science and Technology of Oran (USTO). After postgraduation studies he obtained Magister at the USTO IN 1991. Obtained his PhD in tribology speciality in 2010 at the University of Mostaganem, and subsequently his habilitation to direct the research of the same university in 2011. He is active in the field of research at the laboratory of numerical and experimental modeling of mechanical phenomena.

1. Introduction

Lumbar fusion is considered as the "gold standard" surgical treatment indicated for a wide range of well-recognized painful conditions [1, 8, 11]. Which aimed to alleviate and treat the pain from disc/facet loading in the instable degenerated levels, probably cause of the abnormal load share and stresses in lumbar spine [8,12], while the surgical intervention is based on the topping off fusion stabilization, we used a validated Finite Element (FE) Model to determine the biomechanical basis exists for believing that the reduced stiffness and increased axial motion conferred by dynamic instrumentation using mobile and fixed screw implants to alter the stresses in adjacent-level discs [8,11]. Conventionally, the Posterior Dynamic Stabilization PDS constructs has been promoted to be used as a total fixation system [5] or joined to spinal fusion (topping off or bottoming off fusion) of various rigid or semi rigid fixators assumed to diminish the load on adjacent disc and the facet joint [3, 6, 9]. It will be used in treating multi-level spinal degeneration requiring surgical procedure by strengthening their arthrodesis (fusion) at one or more levels and neutral stabilization (non-fusion) at an adjacent level for common pathological condition to limit stress prophylactically at the level above or below the fusion.

2. Methods and materials

The L2/S1 spine model was adopted from the previously validated nonlinear finite element (FE) model L1/S1 [19], and computationally established to simulate instability by discectomy and quantify implant stability as a function of implant/bone quality. The mesh was developed using ANSYS version 15 (Swanson Analysis System) and Hypermesh 13.0 (Altair Engineering. Inc). Model was subjected to combined compression load to flexion, extension moment of 10 Nm, the axial compressive load of 100 N was applied as a follower load to follow the motion of the spine [10]. Utmost component geometry of the spine was originally taken from Computer Tomography images. The detailed bone anatomy of the spine: vertebrae, endplates, bone processes, and facet joints were defined using 8-node Hex element [3, 8, 18]. Generally; the IVD composed three highly specialized structures the Annulus Fibrosis (AF), The Nucleus Pulposus (NP), and the cartilage endplate that form the interface with the adjacent vertebral bodies. The Nucleus pulposus NP occupies 30~50% volume of the IVD according to Chen et al [1] and the annulus has several layers. For saving time from creating several IVDs, the annulus fiber layers are simplified to the inner and the outer laminates. The IVD boundary curve is already done in previous validation process [19]. The seven major ligaments, including anterior Longitudinal Ligament ALL; Posterior Longitudinal Ligament PLL; Intertransverse Ligament ITL; Ligamentum

Flavum LF; Capsular Ligament CL; Supraspinous Ligament SSL; and Interspinous Ligament ISL were modeled as three dimensional, 2 noded truss elements (T3D2) and allocated nonlinear hypoelastic behavior [5,11,3].

The cross section areas of ligaments are separated into several trusses for avoiding the constraint of stress. The entire model consists of approximately 115000 C3D8 element and 128000 nodes and 465516 DOF. The annulus rebar reinforced layer is meshed in isotropic quads, and each quad shell element has its local orientation axes. The isotropic mesh benefits all first axes parallel with the endplate, facilitate defining the material orientation. The collagenous fibers lamellae were defined as fiber-reinforced concentric rings including embedded bands of reinforced collagenous fibers defined as rebar element surrounded the nucleus pulpous [14]. These Fibers elements were oriented at approximately (±30) into one layer. The Nuclei Pulposi (NP) was modeled as hydrostatic fluid elements [9, 13]. The facet joints simulated by a cartilaginous layer of thickness of 0.4 mm were modeled to be multi-linear elastic in compression [8] by surfaces-to surface contact with softened contact in the normal direction with a coefficient of 0.1 [13, 14] An initial typically gap of 0.2 mm was specified as reported [8,19].

Bony structures	Young's modulus E (MPa)	Poisson's ratio υ	Reference
Concellous bone	100	0.2	
Cortical bone	12,000	0.3	[3,5,18]
Posterior Process	3,500	0.25	
Cartilaginous End plate	23.8	0.4	[15,16]
Facet cartilage	11	0.4	
Facet contact	Nonlinear soft contact		[5, 13]
Annulus Ground	incompressible fluid		[13]
Nucleus Pulposus	4.2	0.45	[2,3]
Annulus fibers	175	0.3	[3]

Major Ligaments	E (MPa)	Strain transition	Cross-Sectional Area (mm^2)	Reference
ALL	7.8 - 20	12%	63.7	
PLL	10 - 20	11%	20	
LF	15 - 19	6.2%	40	
CL	7.5 - 33	25%	30	[2,3]
ITL	10 - 59	18%	1.8	
ISL	10 - 12	14%	40	
SSL	8 - 15	20%	30	

Table.1. Material properties used in the FE-Model of lumbosacral spine L2/S1
1. táblázat Az L2/S1 lumboszakrális gerinc végeselemes modelljében használt anyagjellemzők

3. Implant placements

The instable post-operative segments was modeled using polymeric materials (PolyEtherEtherKetone PEEK, PET PolyEthylene Terephthalate, Poly

Carbonate Urethan PCU) and carbon reinforce composite material (ostaPek) in six different configurations of the model by:

Fusion model is shown in Fig. 1: two 5.5-mm PEEK rods or two 5.5-mm ostaPek rods and one PEEK spacer were added through placing them along the L3/L4 segments without distraction. All pedicle screws were rigidly fixed to the vertebrae.

The topping off fusion assembly was simulated using pedicle screw based PEEK or ostaPek Fusion with Supra adjacent level PEEK (Fig. 1) or OstaPek Rods.

Topping off fusion using Hybrid Dynesys DTO systems, DynaPEEK and DynostaPek constructs.

Implants Component	E (MPa)	Poisson's ratio υ	Pretension (N)	Reference
Pedicular screws (all models)	110.000	0.3	-	[16]
PEEK rods	3,500	0.4	-	[17]
ostaPek rods	45000	0.4	-	[21]
PCU Spacers (all models)	62.5	0.4	-	[16]
300 N Pretention Cord	1500	0.4	300	[16]

Table 2. Material properties used in the implant
2. táblázat. Az implantátumban használt anyagjellemzők

The ostaPek composite is composed of long carbon fibers (66.6%) and a PEKEKK (PolyEtherKetoneEtherKetoneKetone) matrix (33.3%) designed to stable construct, and improves the patient's possibilities to create a viable, stable and definitive fusion and provide high strength of metals combined with the biocompatibility and imaging advantages of polymers. ostaPek composite provides the necessary stiffness to achieve stabilization, combined with the desired flexibility to prevent stress shielding (Fig. 1).

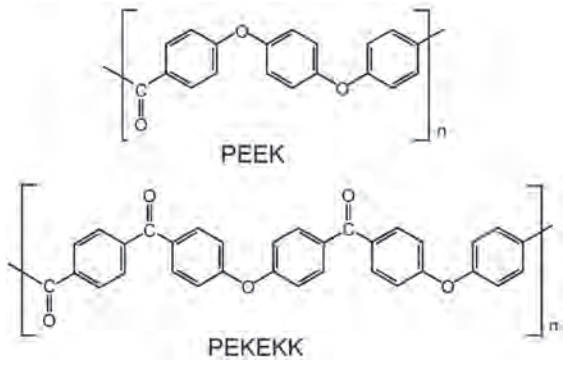

Fig.1. Chemical structure of PEEK and PEKEKK
1. ábra PEEK és PEKEKK kémiai szerkezete

The novel implant for the Dynesys + Fusion (DTO) model consisted of six titanium alloy screws (diameter: 6.4 mm, length: 45 mm) and using PEEK or OstaPek rod instead of Titanium Ti rod Moreover, two PCU spacers (Diameter: 12 mm, Length: 30 mm) and 300 N pretention PET cord, which contacted the screw in Dynesys model [16]. The intact model was modified to simulate the instability caused by a discectomy, which modeled by removing some part of the annulus from the anterior side of the disc [17] that produces natural physiological spinal motions (Fig. 2). The cage was simulated in the fused level attempting to restore the lumbar lordosis during surgery.

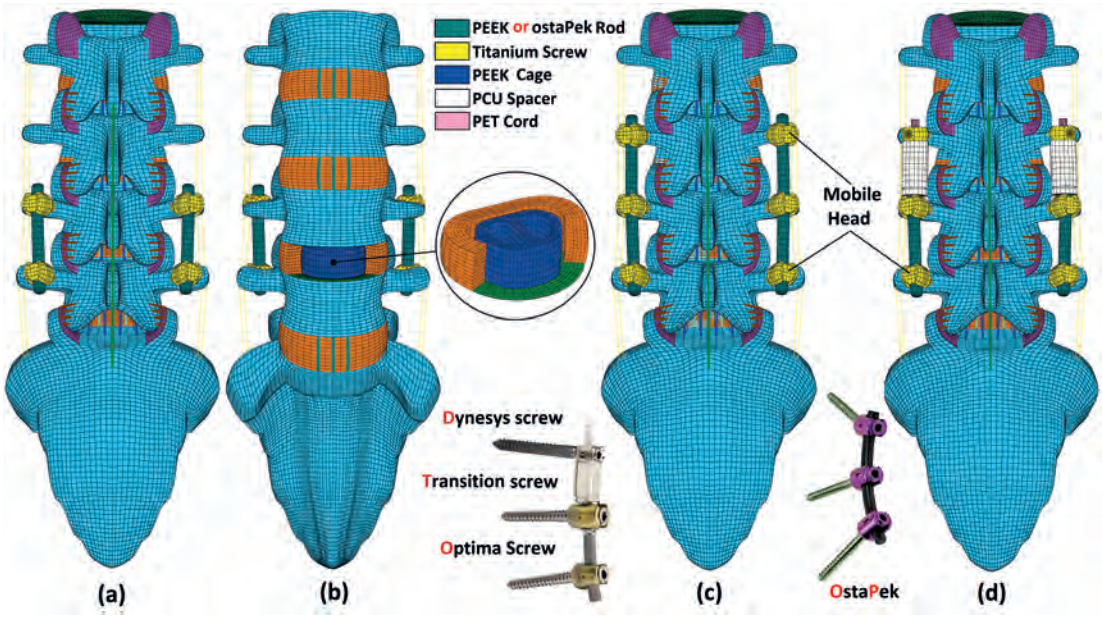

Fig. 2. FE-Model of the lumbosacral spine after posterior hybrid surgery: (a) Intact, (b) PEEK or OstaPek Fusion, (c) BiPEEK or BiostaPek, (d) DTO: DynaPEEK or DynostaPek (DTO)
2. ábra Lumboszakrális gerinc végeselemes modellje posterior hibrid műtét után: (a) ép, (b) PEEK vagy OstaPek fúzió, (c) BiPEEK vagy BiostaPek, (d) DTO: DynaPEEK vagy DynostaPek (DTO)

4. Results

4.1 Intersegmental rotation

The results indicate that the free (unfused) intervertebral level is subjected to additional stresses and acquires increasing motions overtime (Fig. 3). There have been several biomechanical studies attempting to document changes in spine due to simulated fusion. Hypermotion in flexion was predicted after PEEK or ostaPek fusion by 10~16% in L2/3 and L3/4 and about 43~55% in L2/3 and L3/4 in extension. The reduction of ROM following hybrid instrumentation is shown in Fig. 3. Following discectomy, L3/4 extension ROM decreased by 63% for PEEK and ostaPek fusion and 57% for DynaPEEK and DynostaPek. Stabilizing these segments with DTO controlled that ROM to 70% versus that of an intact segment. Adding PEEK fusion and Dynesys systems is sufficient to stabilize the corresponding L3/4 ROM while preserving more than 32~28% of its intact flexion. DTO systems allows displacement while eliminating screw loads in the topping of fusion level, a major source of the screw toggling and loosening. The OstaPek rod, due to its bending flexibility, reduces the ROM comparing to PEEK system. At the fused segment (L2/3), all hybrid implants had the same stabilizing effect by reducing the angular motion by 86% compared to the intact spine. The fusion induced increased motion at the adjacent segment (L3/4) while the bilevel stabilization BiPEEK reduced potentially the motion. While the Bilevel BiostaPek Preserve motion in the adjacent level L2/3 in flexion/extension by 95~99% of rotation and strength the arthrodesis by reducing the mobility in the topping off fusion level L3/4 by 35~39% versus that of an intact

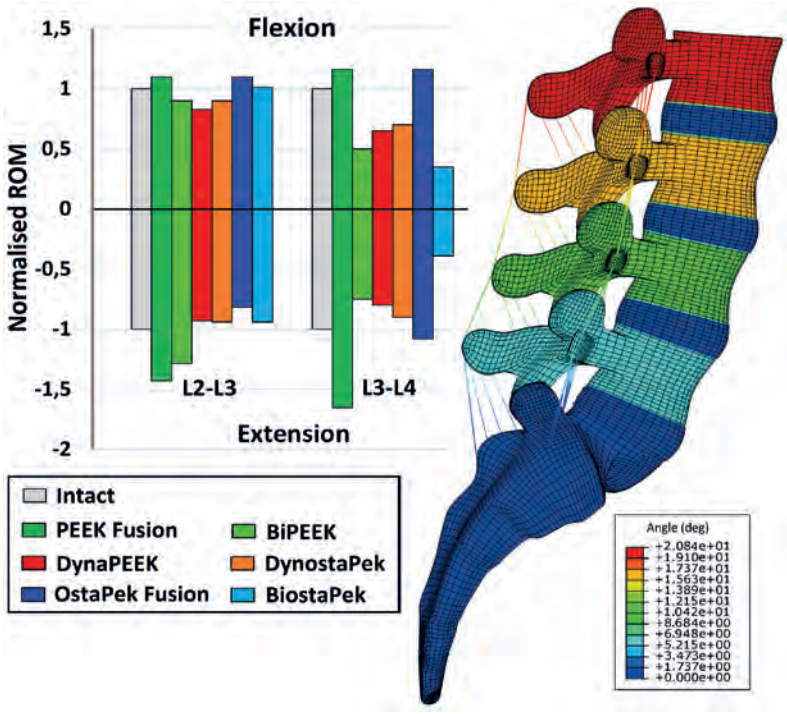

Fig. 3. ROM (deg) at the level of fusion, topping off fusion and adjacent level as compared to the intact model
3. ábra Mozgásterjedelem (fokokban) a fúzió szintjén; fúziós feltöltés és szomszédos szint összehasonlítása az ép modellel

4.2. The intradiscal pressure

At adjacent level L2/3 in the PEEK Fusion model is slightly higher than the intact model for flexion (about 328 KPa and 165 KPa) (Fig.4). In contrast, it is affected by DTO implant which is slightly lower (186 KPa).

The pressure reduction in extension is even more pronounced for hybrid solution, however the IDP of bilevel stabilization increases to a level of about 37% compared to the fusion model. In contrast, hybrid implant decreases the pressure in the adjacent disc L2/3 about 79~86%.

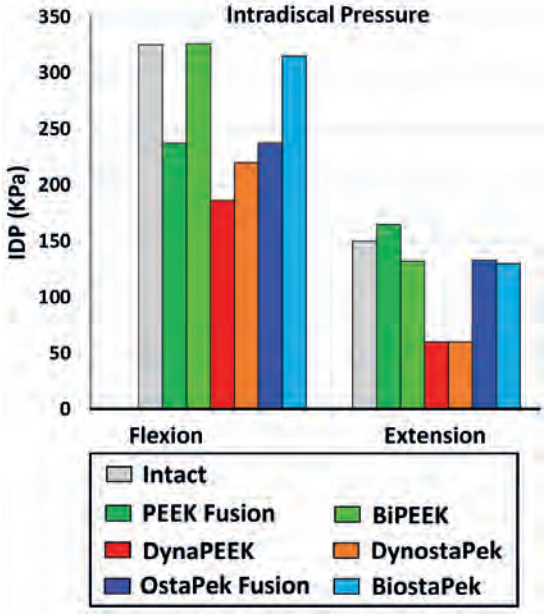

Fig.4. Intradiscal pressure IDP at the L2/L3 level for the intact, Polymeric and composites constructs under Flexion-Extension
4. ábra Intradiszkális nyomás az L2/L3 szinten – ép, polimer és kompozit szerkezet hajlítás és megnyúlás hatására

4.3. Stress results

As it is predicted; the hybrid systems are highly stressed, while the rest of the structure's motion is preserved (Fig. 5).

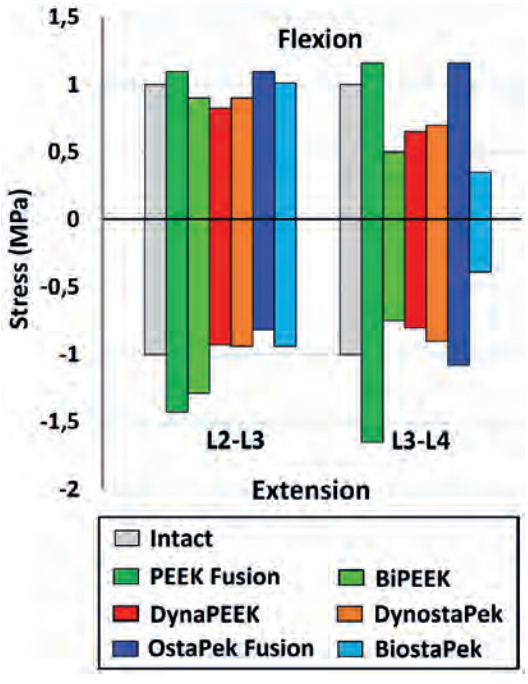

Fig 5. Von Mises Stress distribution in the Annulus of L3/L4 level for various scenarios under flexion and extension
5. ábra Von-Mises feszültségeloszlás az L3/L4 szint gyűrűjén eltérő hajlítás és megnyúlás hatására

Principal stresses in the intervertebral disc specify that, the nucleus pulposus is always induced in compression; with fusion the tensions were higher at the periphery of the Annulus for both flexion and extension, as predicted that the decrease of stresses was accompanied by an increase of shear strain.

5. Discussion

The treatment outcome using hybrid constructs was relatively satisfactory [2]. A PDS topping off semi-rigid fusion system was optimized with a stiffness equivalent to that of an intact spinal segment is sufficient to stabilize the spine while preserving 60% of its intact ROM, Consequently reducing the load on its structural element. Dynesys and ostaPek rods reduced most of segment ROM, as well as strengthening as fusion devices. Semi-rigid Fusion PEEK Fusion alters the kinematics in the adjacent segment by redistributing the range of motion and leads to increase tension in the disc's fibers. The fusion surgery of the spine is accomplished by stimulating bone to grow between two or more adjacent spinal segments to prevent future motion. The instrumentation used in flexible stabilization is designed to control the amount of motion between adjacent vertebrae, but it does not completely eliminate this movement, preventing degenerative changes in the adjacent segments, and reducing instrument failures such screw toggling and loosening. Flexible stabilization for fusion technology support for better physiological bony fusion without shielding the stress. As such, the system is adaptable to the various stages of disc degeneration from early degenerative stage of intervertebral disc to ultimate stage of disc degeneration requiring a fusion. This level of flexibility (PEEK~ostaPek) not only offers spine surgeons more options in the treatment of lumbar disc diseases.

The tensile strength, stiffness makes the constructs ideal as a metal replacement in spinal implants. It provides the high strength of conventional systems and at the same time increases the flexibility to allow load-sharing while still protecting against pathological displacements.By choosing a strength and stiffness closely matches that of cortical bone, PEEK Polymer and ostaPek composite are employed in spinal applications in order to avoid stress shielding and result a transition bridge from the fused to the unfused level

6. Significance

The current FE investigation suggested that substitution of the superior level fusion with the adjunct PDS devices in multi-level fusion procedures may be able to offer similar biomechanical outcome and stability while reducing likelihood of ASD and the feasibility of a PDS adjunct combined to fusion implant system that provides increased load sharing with the construct addressing the Lumbar stenosis, facet pain and the disc degeneration. This avoids the PDS material stress shielding compared to non-dynamic design iterations. Non fusion techniques are newly innovated compared to fusion, as an option in the surgical treatment for low back pain. As new techniques, long term prospective studies must be designed to achieve their effectiveness.

7. Limitations

Our FE study certain limitations. Firstly, The Nucleus was modeled with a fluid filled cavity without considering its continuum structure, muscle forces and loads were not simulated in the current study. The muscle contractions may carry complicated external forces that have significant influences on the biomechanical viewpoint [9]. The above factors will be considered in our further study. Although there were certain simplifications in our FE model, the FE model was well validated previously. Consequently, the L1/S1 model modified in this study is reasonable and can be used as an effective tool to assess the effects of three stabilization systems on the lumbosacral spine. In all the placement cases, there was no incidence of abnormal high stress concentration that could lead to the implant failure.

References:

[1] Chen, H. – Charles, Y. P. – Bogorin I. – Steib J. P. (2011): Influence of 2 different dynamic stabilization systems on sagittal spinopelvic alignment. *Journal of spinal disorders & techniques.*2011; 24(1):37-43.

[2] Denoziere, G. – Ku, D. N. (2006): Biomechanical comparison between fusion of two vertebrae and implantation of an artificial intervertebral disc, *Journal of Biomechanics*, 39(4), 766-775.

[3] Goel, V. K. – Monroe, B. T. – Gilbertson, L. G. – Brinckmann, P. (1995): Interlaminar shear stresses and laminae separation in the disc. Finite element analysis of the L3-L4 motion segment subjected to axial compressive loads. *Spine*, 20(6), 689-698.

[4] Kashkoush, A. – Agarwal, N. – Paschel, E. – Goldschmidt, E. – Gerszten P. C. (2016): Evaluation of a Hybrid Dynamic Stabilization and Fusion System in the Lumbar Spine: A 10 Year Experience. *Cureus*. 2016 Jun 10;8(6):e637. https://doi.org/10.7759/cureus.637

[5] Lee, S. E. – Jahng, T. A. – Kim, H. J. (2015): Hybrid surgery combined with dynamic stabilization system and fusion for the multilevel degenerative disease of the lumbosacral spine. *International Journal of Spine Surgery*. 2015, 9:45. https://doi.org/10.14444/2045

[6] Marion, P. H. – Barrios, C. – Rouch, P. – Charles, Y. P. – Steib, J. P. – Skalli, W. (2015): Clinical Outcomes and Complications After Pedicle-anchored Dynamic or Hybrid Lumbar Spine Stabilization: A Systematic Literature Review. *Journal of Spinal Disorders & Techniques* 2015 Oct;28(8):E439-48

[7] Maserati, M. B. – Tormenti, M. J. – Panczykowski, D. M. – Bonfield, C. M. – Gerszten, P. C. (2010): The use of a hybrid dynamic stabilization and fusion system in the lumbar spine: preliminary experience. *Neurosurgical focus*. 2010;28(6):E2.

[8] Moumene, M. – Geisler, F. H. (2007): Comparison of biomechanical function at ideal and varied surgical placement for two lumbar artificial disc implant designs: mobile-core versus fixed-core. *Spine*. 32:1840–1851. https://doi.org/10.1097/BRS.0b013e31811ec29c

[9] Paige, L. J. (2004): Finite element modeling of annular lesions in the lumbar intervertebral disc. (Doctoral Thesis).

[10] Patwardhan, A. G. (1999): A Follower Load Increases the Load-Carrying Capacity of the Lumbar Spine in Compression. *Spine*, 24(10), 1003 (1999).

[11] Prasath, M. – Fernando, T. – Robb, W. C. – Tara, F. B. – Robert, F. M. (2012): Hybrid dynamic stabilization: a biomechanical assessment of adjacent and supra adjacent levels of the lumbar spine Laboratory investigation, *Spine*, 2012. https://doi.org/10.3171/2012.6.SPINE111054

[12] Rahm, M. D. – Hall, B. B. (1996): Adjacent-segment degeneration after lumbar fusion with instrumentation: a retrospective study. *Journal of Spinal Disorders* 1996;9:392-400.

[13] Rohlmann, A. – Zander, T. – Schmidt, H. – Wilke, H-J. – Bergmann, G. (2006): Analysis of the influence of disc degeneration on the mechanical behaviour of a lumbar motion segment using the finite element method. *Journal of Biomechanics* 39:2484–2490. https://doi.org/10.1016/j.jbiomech.2005.07.026

[14] Schmidt, H. – Heuer, F. – Simon, U. – Kettler, A. – Rohlmann, A. – Claes, L. (2006): Application of a new calibration method for a three-dimensional finite element model of a human lumbar annulus fibrosus, *Clinical Biomechanics*, 2006, 21, 337–344.

[15] Sharma, M. – Langrana, N. A. – Rodríguez, J. (1995): Role of ligaments and facets in lumbar spinal stability. *Spine*. 1995; 20:887-900.

[16] Shih, S. L. – Liu, C. L. – Huang, L. Y. – Huang, C. H. – Chen, C. S. (2013): Effects of cord pretension and stiffness of the Dynesys system spacer on the biomechanics of spinal decompression- a finite element study. *BMC Musculoskeletal Disorders* 2013 19; 14:191. Epub 2013 Jun 19.

[17] Tsuang, Y. H. – Chiang, Y. F. – Hung, C. Y. – Wei, H. W. – Huang, C. H. – Cheng, C. K. (2009): Comparison of cage application modality in posterior lumbar interbody fusion with posterior instrumentation—A finite element study. *Medical Engineering & Physics* 31 (2009) 565–570

[18] Zhong, Z. C. – Wei, S. H. – Wang, J. P.. – Feng, C. K.. – Chen, C. S. – Yu, C. H. (2006): Finite element analysis of the lumbar spine with a new cage using a topology optimization method, *Medical Engineering and Physics,* 28(1), 90-98.

[19] Bendoukha, M. – Mosbah, M. (2017): Biomechanical Evaluation of Lumbosacral Segments Response under Physiological Functions: Finite Element Analysis, *Építőanyag – Journal of Silicate Based and Composite Materials*, Vol. 69, No. 3 (2017), 122–126. p. https://doi.org/10.14382/epitoanyag-jsbcm.2017.22

[20] Abaqus Analysis 6.10 User's Manual

[21] Benzel, E. (2001): Biomechanics of Spine Stabilization, *Stuttgart: Thieme* 2001; pp 19 - 221

Ref.:

Mosbah, Moustafa – **Bendoukha,** Mohammed: *Comparative Analysis of Flexible Stabilization Devices Based on Polymeric and Composite Materials for Degenerative Disorders: Finite Element Analysis*
Építőanyag – Journal of Silicate Based and Composite Materials, Vol. 70, No. 5 (2018), 146–150. p.
https://doi.org/10.14382/epitoanyag-jsbcm.2018.27

Characteristics of cement pastes incorporating different amounts of waste cellular concrete powder

Mohammed ABED ▪ Department of Construction Materials and Technologies Budapest University of Technology and Economics, Hungary ▪ abed.mohammed@epito.bme.hu
Rita NEMES ▪ Department of Construction Materials and Technologies Budapest University of Technology and Economics, Hungary ▪ nemes.rita@epito.bme.hu
Érkezett: 2018. 06. 01. ▪ Received: 01. 06. 2018. ▪ https://doi.org/10.14382/epitoanyag-jsbcm.2018.28

Abstract
In this study, different amounts of waste cellular concrete powder (WCCP) as replacement of cement have been investigated as an attempt to produce green binder, which is useful for sustainable construction applications. In previous studies for the authors, the compressive strength increased when very fine WCCP was added as a filler material to the concrete. In the present study, the cement has been replaced by different amounts of WCCP where the replacement has been conducted from zero to up to 60% of cement mass. Consistency, compressive strength, bending strength and the activity index of WCCP through seven to ninety days specimens' age have been examined. The optimum WCCP replacement was up to 30%, depending on which the activity index still increased to the end of the test period (90 days), and this could be an evidence for its continuity to increase for the longer ages. Despite replacing cement to up to 30% by WCCP increased the bending strength to be higher than the control one; it does the opposite for compressive strength. The main point in the present study is that there is a possibility of replacing cement by 30% of WCCP; however, it is preferable to be less than this amount.
Keywords: cellular concrete powder (WCCP), supplementary cementitious material (SCM), activity index, mechanical properties, waste material.
Kulcsszavak: pórusbeton por (WCCP) cementkiegészítő anyag (SCM), aktivitási index, mechanikai jellemzők, cementpép, hulladékok.

Mohammed ABED
civil engineer (MSc). PhD candidate at the Department of Construction Materials and Technologies, Budapest University of Technology and Economics. Main fields of interests: recycled concrete aggregate, non-destructive testing of concrete, high performance concrete, supplementary cementations materials, fire resistance, self-compacting concrete. Member of the Hungarian Group of fib and the Scientific Society of Silicate Industry.

Rita NEMES
civil engineer (MSc), postgraduate degree in concrete technology, PhD, associate professor at the Department of Construction Materials and Technologies, Budapest University of Technology and Economics. Main fields of interest: concrete technology, ceramics, non-destructive testing of concrete, supplementary cementing materials for concrete, bond in concrete, fiber reinforced concrete, lightweight concrete, shrinkage of concrete, durability measurement, waste materials as aggregates. Member of the Hungarian Group of fib and the Scientific Society of Silicate Industry.

1. Introduction

Concrete is the second highest used material in our plant after fresh water, and one of the most widely used construction materials; due to its durability, recycling potential, large range of performance and low materials cost, whereas the construction industry is one of the most industries that contribute to increased carbon emissions, especially production of Portland cement, which is the major source for the strength of concrete and the most expensive component as well, it is mandatory to minimize environmental impact and carbon footprint by incorporating the use of wastes materials as SCM in building construction. That is will be considered as a sustainable solution for enhancing the properties of concrete, decreasing the environmental impact of cement production and will also contribute to sustainable concrete [1-7].

Last decades witnessing discovering a big number of materials that prove its efficiency to use as supplementary materials for cement, where mainly used to improve the hydration of cement due to their physical characteristics and chemical compositions [8], but some of them full waste materials and also have the ability to improve various properties of concrete, which make them a suitable alternative of the traditional SCM [1, 9]. One of these waste materials is waste cellular concrete powder (WCCP) which exists as one of the modern alternatives of these materials. WCCP has the same chemical composition as concrete, and fine powder has become as a by-product when the masonry elements are manufactured [10].

In the previous study [11], which studied the effect of some waste materials that used as non-hydraulic supplementary materials on the compressive strength and durability of C25/30 concrete, WCCP was one of these waste materials, which proved its ability to increase the compressive strength and enhance the durability performance of concrete based on the freeze test. One of the main conclusions was that it could enhance the performance of concrete by the using up to 10% replacement of very fine WCCP, which is the result of the cutting of cellular concrete blocks, where it has minimal cost and it does not require any preparation or pulverization before mixing. However, the optimal dosage of cellular concrete powder still requires further investigation.

As a continue for the previous study, another attempt has been investigated to introduce the application of very fine WCCP as a supplementary material, aiming to increase the durability of normal strength concrete [9]. The main finding of this study is that a given amount of WCCP could increase the strength and durability of concrete however, too much of amount of WCCP could cause detrimental effects, especially in compressive strength. The correct amount of WCCP can have a better performance than metakaolin on the durability of concrete, despite that metakaolin increases the compressive strength more than WCCP. WCCP is a completely a waste raw material and it is not need any production and preparation process, which means a significant decrease in cost and in CO_2 emission as well.

According to the literature, the incorporating of WCCP in concrete is not discussed enough especially the part of activation behaviour of the binder itself with time. The present study investigated the effect of incorporation of different replacement amount WCCP on the binder paste. Which is through pozzolanic reactions an additional hydration products could be formed by using SCM, where the expected results of these process are: increase strength, decrease in permeability and improvement of other durability properties [12]. Thus the physical, fresh and hardened properties have been tested in different ages aiming to determine the maximum replacement amount could be applied for concrete mixtures.

2. Experimental work

This experimental work was examined as an initial phase to PhD work for producing green self-compacting high performance concrete (GSCHPC) using different waste materials and recycled concrete aggregate, one of these waste materials is WCCP. Whereas the response of mortar systems and concrete systems depend greatly on the properties of paste materials especially in case of self-compacting concrete [13, 14].

2.1 Materials

The performance of seven groups of paste mixtures with replacement amounts (0, 10, 20, 30, 40, 50, and 60% by mass) of cement by WCCP were examined with a w/b ratio of 0.35, where the finding of optimum dosage and substitution ratio is very important because the application of SCM over the optimum amount may reduce performance both in strength and durability parameters [12]. A plain cement paste without the addition of WCCP was prepared at the same w/b ratio as a reference. The composition of mixtures shown in *Table 1*. Paste mixtures were tested for their fresh and mechanical properties including consistency and compressive strength. The cement used throughout the experimental program was CEM I 42.5 N that complies with the requirements of EN 197-1:2000 to eliminate the effect of mineral admixtures on the test [15], however the WCCP used in this experimental work was a factory waste material that was collected from factory for cutting cellular concrete masonry in Hungary. The sieve curves for both WCCP and cement is shown in *Fig. 1*, which shows the large particles of WCC comparing to the cement.

Name of mixture	Binder amount						superplasticizer (cm³)
	Cement (g/mix)	WCCP (g/mix)	Cement (%)	WCCP (%)	Water (g)	w/b (%)	
G0	1500	0	100	0	525	35	0
G10	1350	150	90	10	525	35	0
G20	1200	300	80	20	525	35	0
G30	1050	450	70	30	525	35	0.5
G40	900	600	60	40	525	35	1
G50	750	750	50	50	525	35	2
G60	600	900	40	60	525	35	4

Table 1. Mixture proportions of cement pastes
1. táblázat A cementpépek összetétele

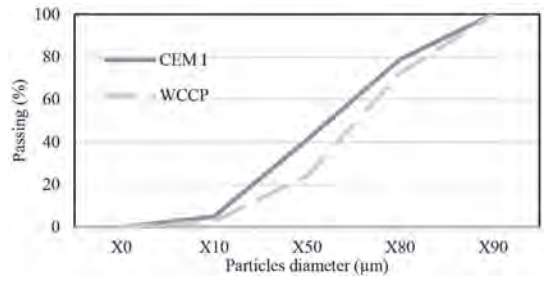

Fig. 1. Grading curves of cement and WCCP
1. ábra A cement és a pórusbeton por lézergranulometriás szemmegoszlása

The mixing water used for the reference was tap water that complies with the requirements of EN 1008:2002 [16]. To achieve the same flow-ability for the mixtures and produce a workable paste with the same w/b ratio, a considerable amount of high range water reducing admixture (HRWRA) "Sika ViscoCrete-5 Neu" has been used in the present study. This type of admixtures reduces the water dosage of a concrete mixture for the desired slump class.

2.2 Mixing and method

Mixing was carried out in accordance with EN 196-1 [17], for a total mixing time of four and a half minutes partitioned in three stages, using a KM250 Kenwood Chef Major mixer, between each stage the mixture manually homogenized to achieve the highest homogeneity. The pastes were casted and compacted to produce two kinds of specimens: cubes (40×40 mm) and prisms (160×40×40 mm), which vibrated using a vibrating table, to make nine cubes and nine prisms paste specimen for each mixture type. Casted specimens were covered with plastic sheets and placed in temperature room (20 ± 2 °C) for 24 hours until de-molding. Thereafter, specimens were cured for 7, 28, and 90 days by wrapping them using cling film. 18 samples in each group were tested; average values are reported. A total of 126 samples were prepared (6 samples × 3 ages × 7 mixtures). The consistency of fresh mixtures was obtained using the flow table, then for each testing age the bending and compressive strength have been examined.

3. Results and discussion

3.1 Consistency

Rheological behavior of fresh cement paste, mortar, and concrete is a key characteristic since it determines workability of the materials and greatly influence the final characteristics of the hardened properties [18]. For achieving the same range of flow-ability for all the groups of pastes it was necessary to use superplasticizer, whereas the workability decreased with increasing the WCCP amount, moreover decreased significantly when a high amount of WCCP. In the beginning, the flow-ability for G0 was determined and recorded 235 mm, then for other mixtures superplasticizer added to achieve flow-ability in the same range (+/- 5%) of the reference mixture. The reduction in flow-ability may be due to the high surface area and the availability of WCCP to absorb a high amount of water, which absorbs hydration water resulting in less workability. *Fig. 2* shows the increasing of superplasticizer demand with

increasing WCCP amount as a result of decreasing the flowability for the same w/b ratio.

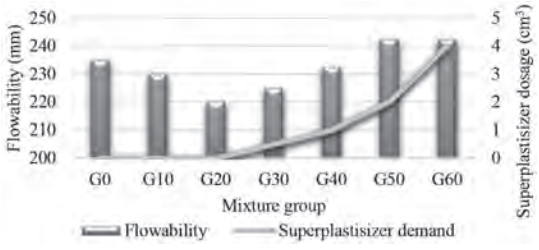

Fig. 2. Impact of WCCP on flow-ability & superplasticizer dosage
2. ábra Apórusbeton por hatása terülésre és a folyósítószer-igényre

3.2 Density

The density has been measured for all specimens during different ages and the average values reported in *Fig. 3*, which is illustrated the decreasing of density by increasing the dosage of WCCP. It goes without reason that the density will decrease by increasing the amount of WCCP due to its lower density comparing to cement. Where depending on the density values it could be produced lightweight concrete by incorporating WCCP.

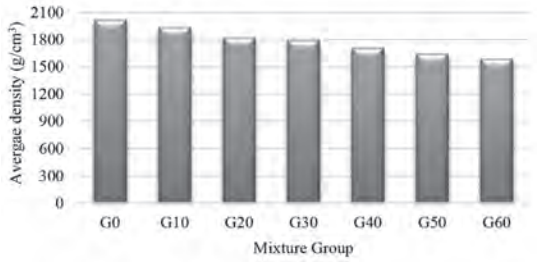

Fig. 3. Impact of WCCP on average density
3. ábra A pórusbeton por hatása a testsűrűségre

3.3 Compressive strength

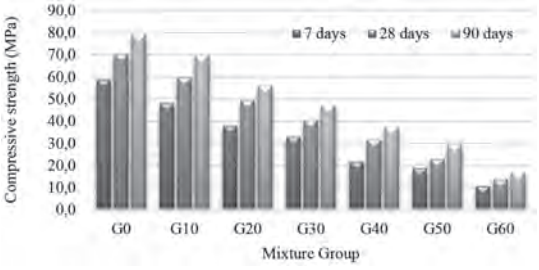

Fig. 4. Impact of WCCP on compressive strength
4. ábra A pórusbeton por adagolás hatása a nyomószilárdságra

Fig. 4 presents the compressive strength of the paste mixes at 7, 28 and 90 days the compressive strength generally decreased when WCCP was included, and the greatest compressive strength was achieved for the paste mix with 0% WCCP. The compressive strength decreased linearly with increasing the amount of WCCP replacement. Nevertheless, the increasing of strength with time for the paste groups incorporated WCCP is higher than reference one up to 30% replacement by WCCP, which is an indication for the possibility of increasing the long-term compressive strength for pastes incorporating up to 30% of WCCP to be higher than the reference.

3.4 Bending strength

Incorporating WCCP up to 30% shows enhancing in the bending strength of cement paste, the increasing of bending strength with time for the paste groups incorporated WCCP is indicated to the low w/b ratio and the ability of WCCP for filling the pours which is enhance the bending strength, and also due to the low strength of paste itself. *Fig. 5* presents the bending strength of the paste mixes at 7, 28, and 90 days.

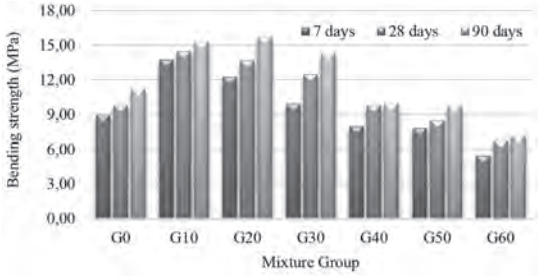

Fig. 5. Impact of WCCP on bending strength
5. ábra A pórusbeton por adagolás hatása a hajlító-húzószilárdságra

3.5 Activity index

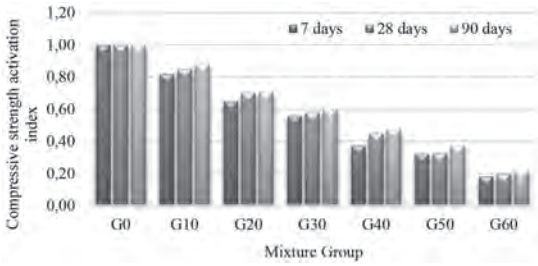

Fig. 6. Impact of WCCP on compressive strength activation index
6. ábra A pórusbeton por adagolás hatása az aktivitási index értékére nyomás esetén

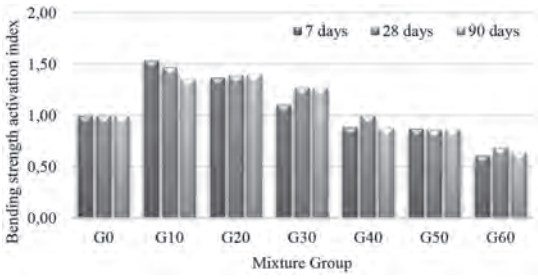

Fig. 7. Impact of WCCP on bending strength activation index
7. ábra A pórusbeton por adagolás hatása a aktivitási index értékére hajlítás esetén

Activity index is expressed by the ratio of both compressive and bending strength of cement paste mixture containing SCM replacement and strength of reference mixture with just cement, and it is express the hydration rate of the SCM [19]. The activity indices are presented in *Fig. 6* and *Fig. 7* for all mixtures groups in different ages. It shows that with increasing the age of specimens incorporating WCCP the activity index increase, thus the main reason for getting higher compressive and bending strength for WCCP specimens. It is clear that the most valuable replacement of cement by WCCP is up to 30% where the activity index increased up to 90 days. It is clear the positive effect of increasing WCCP replacement up 30% in the activity index since the activity index increase with age.

Whereas the behavior of activation for the pastes with more than 30% WCCP shows optimum activation index after 28 and the start to decrease.

4. Conclusions

Using unprocessed WCCP as a replacement of cement for specific amount will not just decrease the cement consumption and its energy needed for production, but also will eliminate a series of costly and energy consuming mechanical and physical applications generated to treat other supplementary cementitious materials (SCM). Based on the results of this paper for replacing cement by WCCP up to 60% by mass for different aged up to 90 days have been conducted and the following conclusion could be drawn:

- The density and consistency of paste decreased with increasing WCCP dosage while increasing the WCCP dosage by more than 60% significantly made worse consistency.
- The compressive strength at 7, 28, and 90 days decreased when WCCP included.
- The bending strength at 7, 28, and 90, days increased when WCCP included as a replacement of cement amount up to 30%.
- Moreover, the activity index for both compressive and bending strength values still increased up to 90 days when up to 30% of WCCP used, which indicate for higher strength for long ages. However, the activation behavior is changing when the WCCP dosage being more than 30%, where the relationship between the activation index and age turn from direct proportion to inverse proportion.
- In case of 40% or higher replacement, the long-time strength is unfavorable. The activation after 90 days was lower than the activation at 28 days of age.
- Although the present study justified using WCCP up to 30% replacement of cement amount, it should be less than this amount since the commonly used SCM amount is from 10% to 20%.
- WCCP used in the present study effect the compressive strength negatively in the short-term results due to its coarse particles.

These conclusions are calling for farther detailed investigation research to produce green self-compacting high performance concrete while using different waste materials and recycled concrete aggregate.

5. Acknowledgments

Authors are grateful to the Hungarian Scientific Research Fund (OTKA) for the financial support of the OTKA K 109233 research project. Special thanks to Duna-Dráva Cement Kft., SIKA Hungária Kft. for providing the materials used in the experiments.

References

[1] Abed, M. – Nemes, R. (2017): Possibility of Producing Green, Self-Compactin, High Performance Concrete (GSCHPC) – *Review. Concrete Structures*, 2017. 18: p. 21-29.

[2] Aydin, E. – Arel, H. Ş. (2017): Characterization of high-volume fly-ash cement pastes for sustainable construction applications. *Construction and Building Materials*, 2017. 157: p. 96-107. https://doi.org/10.1016/j.conbuildmat.2017.09.089

[3] Mueller, H. S. (2017): Design, Material Properties and Structural Performance of Sustainable Concrete. *Procedia Engineering,* 2017. 171: p. 22-32. https://doi.org/10.1016/j.proeng.2017.01.306

[4] Dolado, J. S. – van Breugel, K. (2011): Recent advances in modeling for cementitious materials. *Cement and Concrete Research*, 2011. 41(7): p. 711-726. https://doi.org/10.1016/j.cemconres.2011.03.014

[5] Borosnyói, A. – Szijártó, A. (2015): Metakaolin vizsgálata cement kiegészítő anyagként a k-érték elve szerint, *Építőanyag - Journal of Silicate Based and Composite Materials*, Vol. 68, No. 2, pp. 40-44. https://doi.org/10.14382/epitoanyag-jsbcm.2016.7

[6] Borosnyói, A. (2015): Development of compressive strength of HPC with the use of supplementary cementing material (SCM) combination, *Építőanyag - Journal of Silicate Based and Composite Materials*, Vol. 67, No. 3, pp. 110-115. https://doi.org/10.14382/epitoanyag-jsbcm.2015.18

[7] Nemes, R. – Török, B. (2014): Bond of steel reinforcement in different lightweight aggregate concretes, *Építőanyag - Journal of Silicate Based and Composite Materials*, Vol. 66, No. 2, pp. 7-12. https://doi.org/10.14382/epitoanyag-jsbcm.2014.2

[8] El Mir, A. – Nehme, S. G. (2017): Long term mechanical properties of self-compacting concrete made with slag cement and supplementary cementitious materials, *Építőanyag - Journal of Silicate Based and Composite Materials*, Vol. 69, No. 2, pp. 59-65. https://doi.org/10.14382/epitoanyag-jsbcm.2017.11

[9] Nehme, S. G. (2015): Infuence of supplementary cemneting materials on conventionel and self compacting concrete Part 1. –Literature review. *Építőanyag - Journal of Silicate Based and Composite Materials*, 2015. 67: p. 28-33. https://doi.org/10.14382/epitoanyag-jsbcm.2015.6

[10] Gyurkó, Z. (2017): Effect Of Cellular Concrete Powder On Durability Of Normal Strength Concrete, *Proceeding 12th Central European Congress on Concrete Engineering 2017*, Tokaj p. 179-186.

[11] Gyurkó, Z. – Szijártó, A. – Nemes, R. (2017): Increasing freeze-thaw resistance of concrete by additions of powdered cellular concrete and clay bricks. *International Conference on Analytical Models and New Concepts in Concrete and Masonry Structures AMCM*. 2017, Procedia Engineering p. 11–18. https://doi.org/10.1016/j.proeng.2017.06.180

[12] Mlinárik, L. – Kopecskó, K. – Borosnyói, A. (2016): Properties of cement mortars in fresh and hardened condition influenced by combined application of SCMs, *Építőanyag - Journal of Silicate Based and Composite Materials*, Vol. 68, No. 2, pp. 62-65. https://doi.org/10.14382/epitoanyag-jsbcm.2016.11

[13] Rizwan, S. A. – Bier, T. A. (2008): Self-Compacting Paste Systems using Secondary Raw Materials. *Pakistan Journal of Engineering & Applied Sciences*, 2008. 3: p. 1-7.

[14] Rizwan, S. A. – Latif, W. – Bier, T. A. (2016): Response of self-consolidating cement paste systems containing Acacia Nilotica Gum as an organic admixture. *Construction and Building Materials*, 2016. 126: p. 768-776. https://doi.org/10.1016/j.conbuildmat.2016.09.097

[15] EN 197-1: Cement - Part 1: Composition, specifications and conformity criteria for common cements 2000.

[16] EN 1008: Mixing water for concrete-Specification for sampling, testing and assessing the suitability of water, including water recovered from processes in the concrete industry, as mixing water for concrete 2002.

[17] EN 196-1: Methods of testing cement. Determination of strength. 2016.

[18] Kara, P. (2015): Performance of lamp glass waste powder (LGWP) as supplementary cementitious material (SCM) – viscosity and electrical conductivity, *Építőanyag - Journal of Silicate Based and Composite Materials*, Vol. 67, No. 1, pp. 12-18. https://doi.org/10.14382/epitoanyag-jsbcm.2015.3

[19] Mucsi, G. – Csőke, B. (2012): Power Plant Fly Ash as a Valuable Raw Material. *Geosciences and Engineering*, 2012. 1(1): p. 223–236.

Ref.:
Abed, Mohammed – **Nemes,** Rita: *Characteristics of cement pastes incorporating different amounts of waste cellular concrete powder*
Építőanyag – Journal of Silicate Based and Composite Materials, Vol. 70, No. 5 (2018), 151–154. p.
https://doi.org/10.14382/epitoanyag-jsbcm.2018.28

Effect of combined use of crushed sand and Algerian desert dune sand on fresh properties and strength of self-compacting concrete

Benchaa BENABED
Associate professor at the Department of Civil Engineering, University of Laghouat, Algeria. His research interests include, self-compacting concrete, reuse of local materials, rheology and durability of cement-based materials

Benchaa BENABED ▪ Civil Engineering Laboratory, University of Laghouat ▪ b_benchaa@yahoo.fr
Érkezett: 2018. 06. 14. ▪ Received: 14. 06. 2018. ▪ https://doi.org/10.14382/epitoanyag-jsbcm.2018.29

Abstract
The main objective of this research work is to examine the influence of combined use of various types of sand on the fresh and hardened properties of SCC. The types of sand used are crushed sand (CS), river sand (RS) and dune sand (DS). In addition, binary or ternary system mixture of these sands were also used. SCC mixes were made with constant content of cement and marble powder waste. In this investigation, the flow ability was evaluated by slump flow, L-Box, J-ring V-funnel tests for SCC. The resistance to segregation was measured by GTM sieve stability test. Compressive strength was also determined at age of 28 days. The experimental results indicate that, there is an improvement in the fresh and strength properties of SCC when using binary mixtures of CS and RS. However, there is a decrease in workability and strength using binary system of CS+DS and RS+DS especially for higher DS content up to 50%. This effect was also observed with SCC containing ternary system (CS+RS+DS). Based on the results obtained of this investigation, CS and DS may provide a readily available alternative material to ordinary fine aggregates in concrete applications with competitive cost.
Keywords: crushed sand, river sand, dune sand, binary system, ternary system, SCC, fresh properties, strength
Kulcsszavak: zúzott homok, folyami homok, dűne homok, kétkomponensű rendszer, háromkomponensű rendszer, öntömörödő beton, frissbeton, szilárdság

1. Introduction

Self-compacting concrete (SCC) is a new generation of concrete that fits well with the current state of development of the structures facing a labor less qualified. This range of concrete is characterized by a high workability and a high deformability, while being stable and ensures durable structures. For achieving these contradictory properties, the formulation of SCC needs the use of high Portland cement content and superplasticizer (SP). However, using high volume of Portland cement causes many problems such as: increase in the consumption of cement; environmental impacts due to CO_2 emissions; consumption of energy and natural resources; high production cost since the cement is the most expensive element in the concrete; risk of cracking associate to the high heat of cement hydration. The SCC can be implemented without vibration, through confined areas only under the effect of gravity, while developing good compactness without requiring skilled labor during the consolidation. These properties contribute to a sustainable concrete quality. Depending on the density and complexity of the reinforcement of structural elements, the need for vibration can decrease significantly and even be eliminated, which is a labor-intensive economy [1, 2]. SCC is characterized, in general, by a formulation containing various chemical and mineral additives in precise proportions to meet the requirements of the specifications for workability and stability. The incorporation of supplementary cementitious materials improves the rheological, physical, mechanical and durability properties of SCC [3, 4]. For example, the limestone fillers are generally used to increase the amount of powder in the composition of SCC [5]. Recycling waste powders of marble and granite in the production of SCC was proved to be useful because the marble powder acts as filler, and granite powder acts as pozzolanic material despite its small pozzolanic activity [6].

The demand for natural sand is quite high in developing countries owing to rapid infrastructural growth which results supply scarcity. Therefore, construction industries of developing countries are in stress to identify alternative materials to replace the demand for natural sand. On the other hand, the advantages of utilization of by-products or aggregates obtained as waste materials are pronounced in the aspects of reduction in environmental load and waste management cost, reduction of production cost as well as enhancing the quality of concrete. Quarry dust has been used for different activities in the construction industry such as road construction and manufacture of building materials. Crushed rock aggregates are more suitable for production of high strength concrete compared to natural gravel and sand. High percentage of dust in the aggregate increases the fineness and the total surface area of aggregate particles. In the production of crushed sand, there is a significant proportion of fines in the sand; this proportion of fines is approximately 10-15% of the total weight of crushed sand. The use of sands rich in fines may be regarded as an alternative source of fillers. These sands enhance the cost of SCC by reduction of the high demand for fillers on the one hand. On the other hand obtaining a SCC with good physical and mechanical properties such as permeability, absorption and strength [7-18].

Attempts have been made to investigate some property of quarry dust and the suitability of those properties to enable quarry dust to be used as partial replacement material for sand in concrete [19, 20]. The use of quarry dust in concrete is desirable because of its benefits such as useful disposal of by products, reduction of river sand consumption as well as increasing the strength parameters and increasing the workability of concrete [21, 22]. The overall workability value of quarry dust concrete in terms of slump as well as compaction factor was less in comparison to conventional concrete. The workability of the concrete mixes decreased with an increase in percentage of stone dust. It indicates that water requirement is higher in such concrete to maintain the desired workability [23-31]. *Celik* et al. [19] studied the effects of various proportions of crushed dust content on properties of fresh concrete and hardened concrete. Test results indicate that slump of concrete decreased as the percentage of dust content increased, and air content of fresh concrete decreased as the percentage of dust content increased. Saeed and Shahid [28] have found that workability of various mix ratios decreased from 11% to 67%, whereas compressive strength increased from 7% to 33% with increasing proportion of manufactured sand. *Akrout* et al. [29] investigated an experimental study on the effect of crushed limestone sand proportioning to the workability and the compressive strength of concrete. The performance of the crushed limestone sand concretes was compared with those of siliceous sand concretes. It was observed that, the properties of crushed limestone sand concretes, although lower than those of siliceous sand concretes, remain completely comparable.

Shi-Cong and *Chi-Sun* [32] showed that the workability of crushed fine stone CFS concrete mixes was decreased with an increase in CFS content probably due to the angular shape of the CFS when compared to river sand. Also, *Donza* et al. [33] found that when crushed sand was incorporated in concrete, the increase of water demand due to the shape and texture of the crushed sand can be mitigated by using a water reducing admixture [34]. *Rao* et al. [35] reported an increasing compressive strength by use of rock flour as fine aggregate instead of river sand. The idea of using quarry sand as an alternative aggregate was developed because granite, which is the parent material, is hard and dense and therefore can serve as an excellent aggregate material. Its use as a fine aggregate in concrete is expected to improve certain properties, such as the compressive strength, durability, strength development, workability and economy. The importance of the compressive strength in concrete is such that for structural design purposes, the compressive strength is the criterion for quality.

Menadi et al. [11] showed the influence of fines in crushed sand on the physical and mechanical properties of concrete. Four different cement types were used while maintaining a constant water/cement ratio, and examined the influence of limestone fines in crushed sand on concrete strength. The test results showed that up to 15% of fines content in crushed sand could be used without adversely affecting concrete strength. It was tried experimentally to explore the use of crusher dust, stone chips and fly ash in self-compacting concrete. Test results indicated that for SCC, sufficiently low water to powder ratio can be attained even with the use of crusher dust, leading to high compressive strength [36].

Shanmugapriya and *Uma* [37] concluded from experimental researchers that compressive and flexural strength of concrete can be improved by partial replacement of cement by silica fume and manufactured sand for natural fine aggregates. They suggested that optimum replacement of natural sand by manufactured sand is 50%. *Raman* et al. [38] studied the effect of quarry dust and found that the partial replacement of river sand with quarry dust without resulted in a reduction in the compressive strength of concrete. *Reddy* and *Reddy* [39] reported an increasing compressive strength by use of rock flour as fine aggregate instead of river sand. *Ilangovana* et al. [30] reported strength of quarry rock dust concrete was comparably more than that of similar mix of conventional concrete. *Hameed* and *Sekar* [31] studied effect of crushed stone dust as fine sand and found the flexural strength increases than the concrete with natural sand but the values decreases as percentage of crusher dust increases.

Ilangovana et al. [30] found that the natural river sand, if replaced by hundred percent quarry rock dust from quarries, may sometimes give equal or better than the reference concrete made with Natural Sand, in terms of compressive and flexural strength studies. Also, they concluded that the replacement of fine aggregate with 50% marble powder and 50% quarry rock dust gives an excellent result in tensile strength. Poon et al. [34] reported that the hardened properties of concrete mixes with partial proportions of manufactured and natural sand achieved a higher compressive strength at all test ages for normal strength, intermediate strength and high strength concrete.

In many desert regions, there is an abundance of fine sand dunes, particularly in Sahara desert of Algeria, which covers more than 60% of its area. The idea of promoting its value in the manufacturing of concrete represents a great economic importance. With the depletion of aggregate resources in Algeria and the high cost of transportation, it becomes economic and environmental interests that could present the valorization of abundant local sands such as the dune sand for manufacturing of concretes. *Bederina* et al. [40] have studied the possibility of using local sand available in large quantities in sandcrete. This study showed that the correction of the granular distribution by means of mixing two local sands in predetermined proportions has allowed obtaining a more workable, more compact, and more resistant sandcrete. In concrete design, the dosage and fineness of aggregates have an important influence on quality of fresh and hardened properties of concrete. *Brouwers* and *Radix* [41] have found that the fine sand is useful component in optimizing the particle size distribution and thereby increasing the flowability, stability and mechanical properties of concrete mixes. *Kay* et al. [42] investigated the potential of using DS as fine aggregates in concrete. Results indicated that DS could be used as fine aggregate in concrete production. *Banfill* et al. [43] have also studied the effect of very fine sand dredged from river estuaries on concrete mixtures. It was found that as the sand content increases, the water required for a given workability increases and the strength development is not different than conventional concrete. *Laquerbe* et al. [44] studied the effect of using laterite gravel and DS as aggregates for concrete. The authors showed that, the laterite gravels can be used instead of basalt or limestone, and DS can serve as a substitute for seashore sand.

Bouziani et al. [45-49] have studied the properties of flowable concrete (FSC) made with DS. Test results show that an optimal content of dune sand, which makes satisfied fresh and hardened properties of FSC, is obtained. *Bouziani* [47] used a mixture design modelling approach to highlight the effects of river sand (RS), crushed sand (CS) and dune sand (DS) on flowability, passing ability, segregation and mechanical strength of SCC. The derived mathematical models make it possible to illustrate the variation of different responses in with respect to the proportions of RS, CS and DS. Results indicate that when flowability requirements are combined, proportions of DS and CS with RS must be below 0.24 and 0.6 respectively. Moreover, it is shown that passing ability can be satisfied by using a CS proportion above 0.3 in RS–CS system and above 0.65 in CS–DS system. On the other hand, proportions above 0.5 of CS in RS–CS system and above 0.2 of DS in RS–DS system are recommended to meet stability limits. Results also indicate that compressive strength days increased with the increase of CS proportion and decreased with the increase of DS proportion. Another experimental research on fresh and hardened properties of flowable sand concrete (FSC) reinforced by polypropylene fibers (PF) has been carried out by *Bouziani* et al. [48]. Results indicate that all studied mixtures have a pseudo-plastic behavior in fresh state. Results also confirmed that PF incorporation increases the viscosity and reduces free shrinkage of FSC. In terms of mechanical strength, results show that incorporating PF would enhance flexural strength. However, a reduction in compressive strength is observed.

R'mili et al. [50, 51] studied the incorporation of roller sand, crushed sand and desert sand in the composition the self-compacting concretes (SCC). Desert dune sand, which has a fine extra granulometry, and the crushed sand, which contains an important content of fines, can constitute interesting components for SCC. These sands, with different sizes, consist of several combinations of rolled sand (RS), crushed sand (CS) and desert sand (DS). The study examines the influence of the granular combination of sands on the characteristics in the fresh and the hardened state of SCC. The results of the experimental tests showed an improvement of the workability of the fresh SCC by combining the different sands. The addition of the DS to CS or to RS allowed to increasing the mixture viscosity, but decreased the mechanical strengths. Furthermore, the CS-RS combinations increased the compressive and the tensile strengths of the studied SCC. The optimized formulations of sands gave the highest performances of the SCC.

It should be noted that, no detailed investigation has been done to study the effect of combining different sand in binary and ternary system on some properties of self-compacting concrete. It is in this context that, the present work aims to study the effect of different types of sand fresh and hardened properties of SCC made with marble powder as cement replacement in one hand. In the other hand, recycling this waste powder, which is not used and can cause a very serious environmental problem.

In this regard, three types of sand with different origin and morphology are used; crushed sand (CS), dune sand (DS) and river sand (RS). Binary (CS+DS; CS+RS; RS+DS) and ternary (CS+DS+RS) system mixtures of proportions of these sands were also used in this study. Tests used to evaluate the filling ability are slump flow and V-funnel tests. The passing ability was measured by L-Box and J-ring tests. The resistance to segregation was checked by GTM sieve stability test. Compressive strength were also determined at age of 28 days.

2. Materials and tests

2.1. Materials

The cement used in the present study was a CEM I 42.5. The chemical and physical properties of cement are given in *Table 1.* The waste marble powder (WMP) used in this study as cement supplementary material is a waste powder resulting from cutting, shaping and lustrating of the marble stones as shown in *Fig 1.* The chemical composition and physical properties of WMP are also given in *Table 1.* From this table, the WMP is mainly consisted of calcite about 56.01% with some traces of the quartz and dolomite as confirmed shown by of X-ray diffraction analysis presented in *Fig. 2.* Scanning electron microscopy (SEM) was performed to determine the surface characteristics of the WMP and typical image is presented in *Fig. 3.* As it can be seen, WMP presents angular shapes with rough surface texture. In order to determine particle size distribution of WMP and cement, laser distribution analysis was realized and the results are illustrated in *Fig. 4.* The results indicate that WMP is relatively finer than the cement, and about 70% of particles of WMP have a size less than 10 μm, and about of 40% of these particles are lower than 63 μm. A polycarboxlic-ether type superplasticizer (SP) with a specific gravity of 1.07 and a solid content of 30% was used.

Chemical composition (%)	Cement	Waste marble powder
SiO_2	21.7	0.42
CaO	65.7	56.01
MgO	0.7	0.12
Al_2O_3	5.2	0.13
Fe_2O_3	2.7	0.06
SO_3	0.6	0.01
K_2O	0.4	0.01
TiO_2	0.21	0.01
Na_2O	0.7	0.43
Cl	0.01	0.03
Loss of Ignition	0.3	42.78
Physical properties		
Specific density	3.15	2.7
Fineness (m^2/kg)	300	360
Compressive strength at 28 days (MPa)	44	-

Table 1. Chemical composition and physical properties of cement and waste marble powder
1. táblázat Cement és márvány hulladék por kémiai összetétele és fizikai jellemzői

Fig. 1. Disposal of waste marble to the ground
1. ábra Hulladék márvány ártalmatlanítása

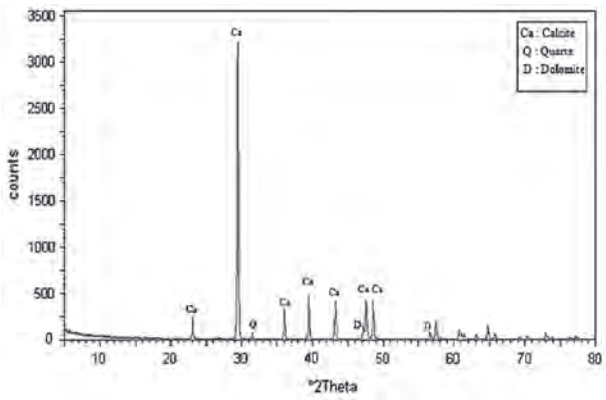

Fig. 2. X-ray diffraction of waste marble powder (WMP)
2. ábra Márvány hulladék por röntgendiffraktogramja

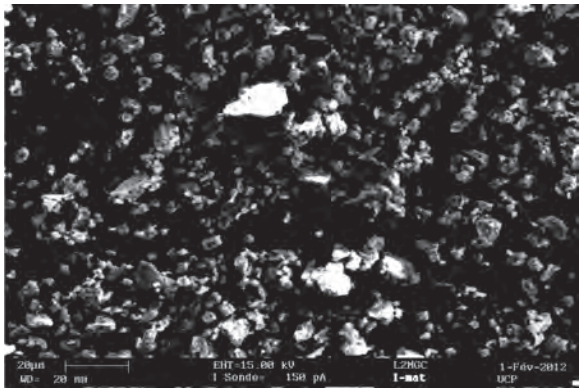

Fig. 3. SEM view of waste marble powder (WMP)
3. ábra Márvány hulladék por elektronmikroszkópos felvétele

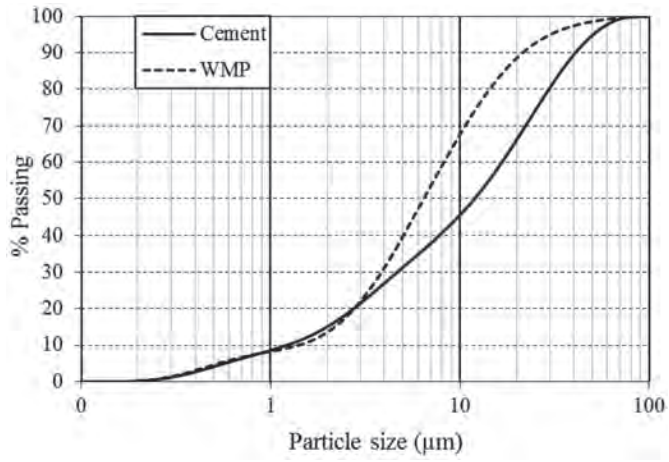

Fig. 4. Particle size distribution of cement and waste marble powder (WMP)
4. ábra Márvány hulladék por és cement szemeloszlása

Continuously graded coarse aggregates (CA) (3/8 and 8/15 mm) were used in this study with a specific gravity and water absorption of 2.7 and 2.5% respectively. Various types of sand are used: river sand (RS) which is available natural source as shown in *Fig. 5,* crushed sand (CS) which is a waste of quarry stone crushing as seen in *Fig. 6*, and dune sand (DS) very available in the desert of Algeria as shown in *Fig. 7*. Mixtures of these sands in binary and ternary system are also used. The physical properties and sieve analysis results of these sands are given in *Table 2* and *Fig. 8* respectively. The maximum (D) dimension of RS, CS and DS sands were respectively 5, 4 and 0.63 mm. in order to determine the surface characteristics of the different sands, scanning electron microscope (SEM) was carried out and images of RS, CS and DS grains are given in *Fig. 9*. SEM investigations reveal the rounded shape of the RS and DS grains, and angular shape of CS grains. They show also the fineness and cleanness of DS compared to RS and CS, and the high filler content of CS. Moreover, X-ray diffraction analysis was performed; results are represented in *Fig. 10*. The X-ray diffraction analysis shows that RS and DS contain mainly the quartz (SiO_2) with some traces of calcite. However, CS contains the calcite ($CaCO_3$).

Fig. 5. Huge use of river natural sand (RS)
5. ábra Természetes folyami homok kitermelése

Fig. 6. Disposal of quarry crushed sand to the ground (CS)
6. ábra Zúzott bányahomok deponálása

Fig. 7. Large quantities of dune sand in the desert of Algeria (DS)
7. ábra Algériai sivatagi dűne homok

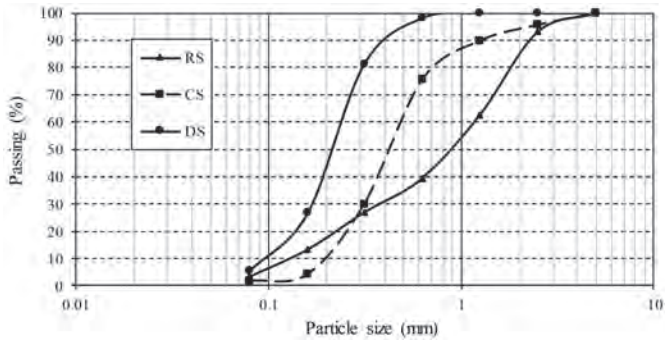

Fig. 8. Particle size distributions of different types of sand (RS, CS, DS)
8. ábra A felhasznált homokok szemeloszlása

Properties	Sand type		
	CS	RS	DS
Specific gravity	2.68	2.67	2.65
Unit weight (kg/m³)	1541	1758	1520
Fineness modulus	2.21	2.45	0.78
Sand equivalent (%)	71	87	83

Table 2. Physical properties of the used sands
2. táblázat A felhasznált homokok fizikai jellemzői

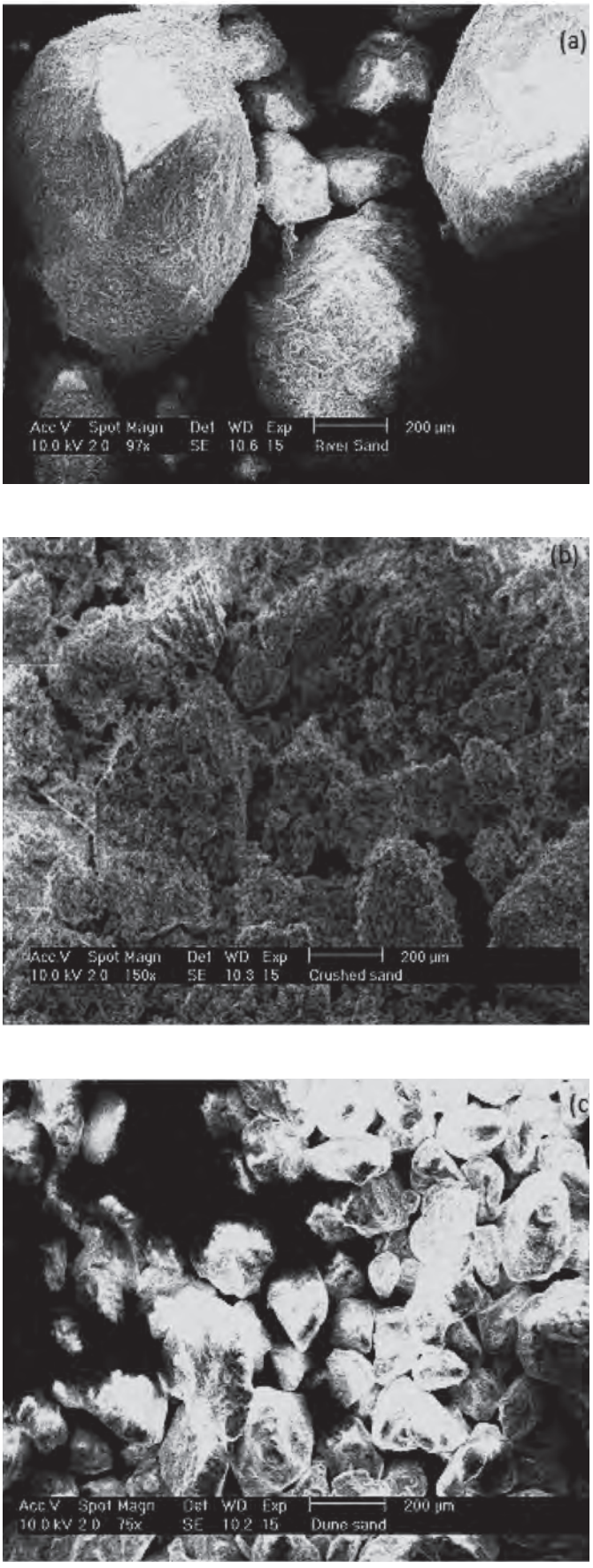

Fig. 9. SEM views of different types of sand: (a) RS; (b) CS; (c) DS
9. ábra A felhasznált homokok elektronmikroszkópos felvételei

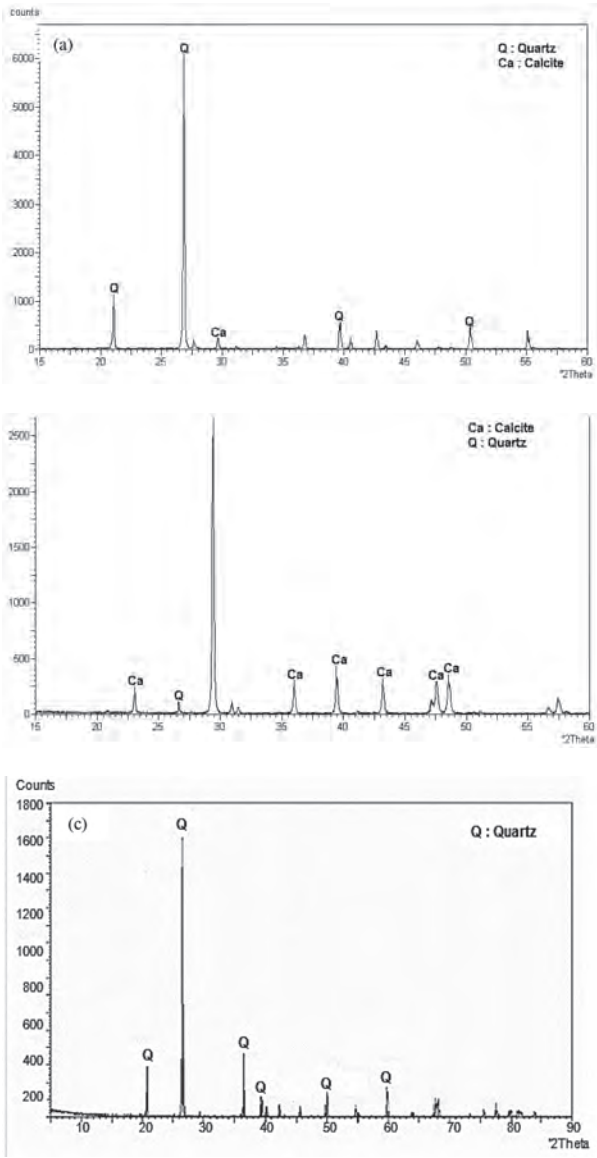

Fig. 10. X-ray diffraction of different types of sand: (a) RS; (b) CS; (c) DS
10. ábra A felhasznált homokok röntgendiffraktogramjai

2.2. Mixture proportions

SCC mixes were made, which had total powder binder (cement + marble powder) content of 475 kg/m^3. The coarse aggregates content was maintained at 31% by volume of cement for concrete and fine aggregates content at 50% by volume of mortar in concrete. The water to powder ratio (W/P) was fixed at 0.4 by weight with air-content being assumed to be 1%. SCC mixes were prepared with different types of sand: crushed sand, river sand, dune sand and binary or ternary sands. The SCC mixture proportions are summarized in *Table 3.*

2.3. Mixing procedure

The mixing procedure and time are very important, thus the mixing process was kept constant for all concrete mixtures. The batching sequence consisted of homogenizing the powder and aggregates for 30 sec in a rotary planetary mixer, then adding 70% of water and mixed for 1 min. Thereafter remaining water (30%) with SP was introduced, and the concrete was mixed for 5 min, then the mixing was stopped for 2 min and again the concrete was further mixed for 30 sec before it was discharged from the mixer.

2.4. Concrete testing

In this investigation, the slump flow test was used to evaluate the flow ability of self-compacting concrete in terms of mean spread diameter. The minimum value of self-compacting concrete to be 650 mm and a maximum of 800 mm for a fresh self-compacting concrete [52]. During the slump flow test, the time required to reach 50 cm diameter of slump flow is measured (T_{50}). The V-funnel test is used to determine the filling ability of the concrete. The time taken for the concrete to flow down is noted in seconds [53]. The maximum time that can be taken by a self-compacting concrete mix in V-funnel is 10 seconds. The passing ability was measured by L-Box test. The test was started by removing the control gate at once to allow the flow of self-compacting concrete through the horizontal obstruction in the box and then the ratio of H_2/H_1 were determined, if the concrete flows freely as water, at rest it will be horizontal and therefore the

Mix. N°	Mix. code	*(C+WMP) (kg/m^3)	CS (%)	CS (kg/m^3)	RS (%)	RS (kg/m^3)	DS (%)	DS (kg/m^3)	CA (kg/m^3)	SP (kg/m^3)	Water (kg/m^3)
SCC1	100CS	475	100	886	0	0	0	0	830	2.9	190
SCC2	100RS	475	0	0	100	886	0	0	830	4.2	190
SCC3	100DS	475	0	0	0	0	100	886	830	7.1	190
SCC4	75CS+25RS	475	75	665	25	222	0	0	830	2.9	190
SCC5	50CS+50RS	475	50	443	50	443	0	0	830	2.9	190
SCC6	25CS+75RS	475	25	222	75	665	0	0	830	2.9	190
SCC7	75CS+25DS	475	75	665	0	0	25	222	830	2.9	190
SCC8	50CS+50DS	475	50	443	0	0	50	443	830	2.9	190
SCC9	25CS+75DS	475	25	222	0	0	75	665	830	2.9	190
SCC10	75RS+25DS	475	0	0	75	665	25	222	830	4.2	190
SCC11	50RS+50DS	475	0	0	50	443	50	443	830	4.2	190
SCC12	25RS+75DS	475	0	0	25	222	75	665	830	4.2	190
SCC13	50CS+25RS+25DS	475	50	443	25	222	25	222	830	2.9	190
SCC14	25CS+50RS+25DS	475	25	222	50	443	25	222	830	2.9	190
SCC15	25CS+25RS+50DS	475	25	222	25	222	50	443	830	2.9	190

*(C+WMP): 90%Cement (C)+10% waste marble powder (WMP) CS: crushed sand; RS: river sand; DS: dune sand; CA: coarse aggregate; SP: superplasticizer

Table 3. SCC mixture proportions with different types of sand
3. táblázat Öntömörödő betonok összetételei különböző homokok felhasználásával

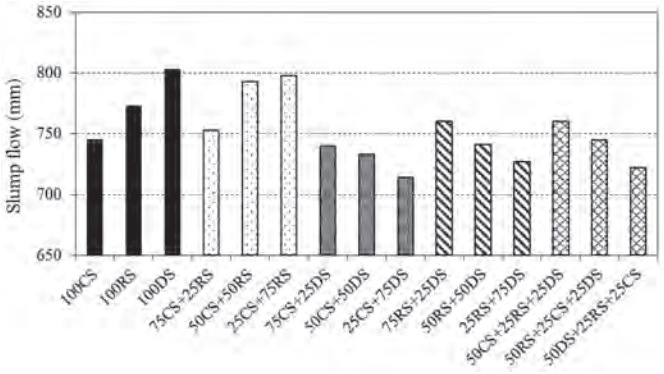

Fig. 11. Slump flow of SCC with different types of sand
11. ábra Öntömörödő beton roskadási terülése különböző homokok felhasználásával

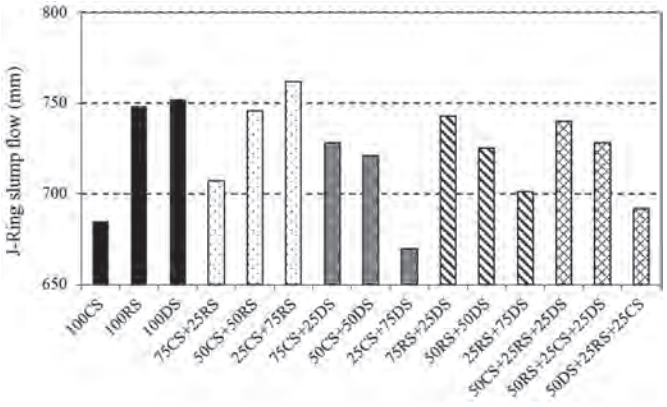

Fig. 12. J-Ring Slump flow of SCC with different types of sand
12. ábra Öntömörödő beton blokkológyűrűs roskadási terülése különböző homokok felhasználásával

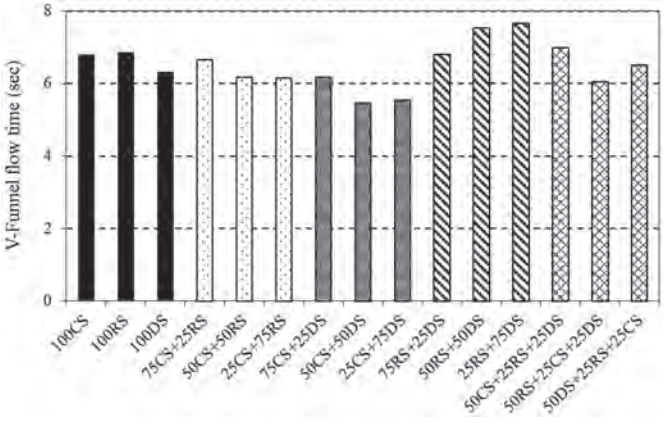

Fig. 13. V-Funnel flow time of SCC with different types of sand
13. ábra Öntömörödő beton kifolyási ideje különböző homokok felhasználásával

ration will be equal to unity. The minimum acceptable value is to be 0.8 [52]. J-Ring slump test was also used to evaluate the passing ability. The resistance to segregation was assessed by GTM sieve stability test. The minimum acceptable value is to be 15% [52].

For compressive strength tests, from each concrete mixture three prisms of 70×70×280 mm were cast. After removal from moulds, at 24 h of age, concrete specimens were immersed in water saturated with lime at 20 °C until the age of testing. The compressive test was conducted at the age of 28 and 90 days for the different mix proportions according to NFP 15-451 on the half samples obtained after the flexural test.

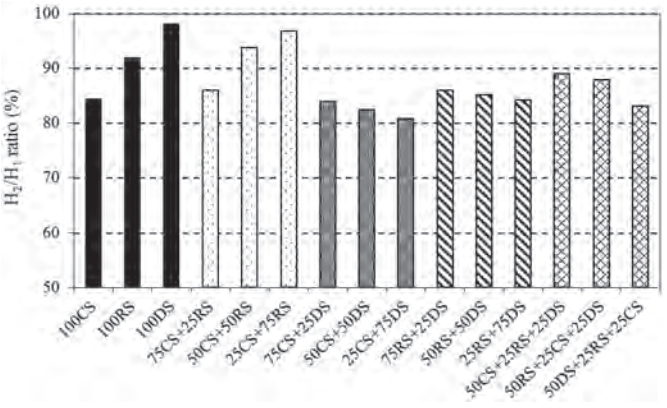

Fig. 14. L-Box filling high H_2/H_1 ratio of SCC with different types of sand
14. ábra Öntömörödő beton L-doboz H2/H1 feltöltési hányadosa különböző homokok felhasználásával

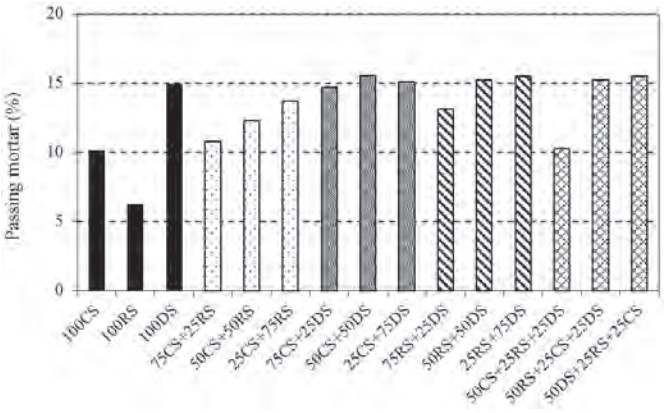

Fig. 15. Passing mortar using sieve stability test (GTM) of SCC with different types of sand
15. ábra Öntömörödő beton szitastabilitási (GTM) vizsgálata különböző homokok felhasználásával

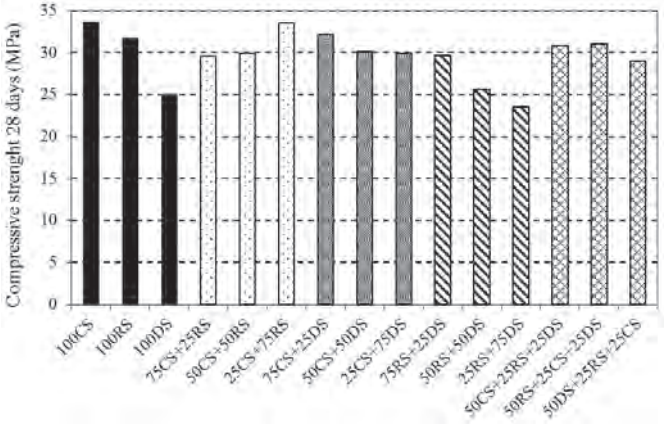

Fig. 16. Compressive strength at 28 days of SCC with different types of sand
16. ábra Öntömörödő beton nyomószilárdsága különböző homokok felhasználásával 28 napos korban

3. Results and discussion

3.1. Slump flow test

The results of slump flow are presented in *Fig. 11*. It is noted, that the slump flow values of all SCC mixtures are in the range slump flow values defined by the AFGC recommendations [53]. It is remarked an increase in the slump flow of SCC with mixture sand of RS+CS, this increase becomes very important

when the percentage of RS exceeds 50%. A decrease in slump flow was observed in SCC with binary mixture sand of CS+DS and RS+DS, this decrease also becomes very important when the DS percentage is very high. Therefore, the addition of dune sand up to 25% improves the slump flow of SCC. Beyond this content of dune sand, the slump spread decreases and does not meet the criteria for self-compacting concrete, and behaves like an ordinary concrete. R'mili et al. [50, 51] studied the effect of the incorporation of crushed sand and desert sand on the properties of self-compacting concretes. The results show that the workability parameters are improved when the crushed sand is partially replaced by desert sand (dune sand). A substitution rate of 15% gives good workability in terms of flow spreading and T_{50} flow time. Beyond this sand dune content these parameters decrease and do not meet the criteria of a self-compacting concrete.

From this, it can be concluded that the river sand has a beneficial effect on the slump spread, unlike the dune sand, which reduces remarkably the slump spread of SCC. The SCC highly proportioned in DS required at the same time important proportioning in SP and in water. This is due to the large finesses of these sands and to their need for water causing an increase in the viscosity. A demand for additional water is then necessary to improve the workability behavior of these SCC. Omar et al. [54] studied the influence of crushed sand substitution with different percentages of 25, 50 and 75% on the properties of concretes. They noticed that the use of crushed sand as fine aggregates improves the flow spreading of concrete due to the existence of fines. Gristsada and Natt [55] used calcareous sand to improve the properties of self-compacting concretes. They noticed an increase in flow spreading with increasing dosage in calcareous sand. A substitution rate of 60% gave the best flow spreading of the used concretes.

3.2. J-Ring slump flow

The J-Ring spread results are shown in *Fig. 12*. It is noticed an increase in the J-Ring spreading in SCC with binary system mixture sand of CS+RS. On the other hand, a decrease in the spreading with the increase of the percentage of DS in SCC with binary sand and ternary system mixture of CS+RS+DS. This means that the high dosage of DS remarkably decreases the spread of SCC, hence the flowability of SCC. *Nanthagopalan* and *Santhanam* [57] studied the fresh properties of SCC prepared with crushed sand. They noted that the spread of SCC increases with the use of crushed sand compared to SCC made with natural sand. This is due to the increase in paste volume due to the existence of fines in the crushed sand [7].

3.3. V-funnel flow time

The results of the flow time using the V-Funnel test are shown in *Fig. 13*. This test indicates the filling capacity of mixture. The test of the flow through the funnel in V is a way to evaluate the viscosity and resistance to segregation of concrete. From *Fig. 13*, it can be noted that the values of the flow time through V- funnel are included in the interval (6-12 sec) proposed by *Domone* [48]. The addition of DS increases the flow time of SCC compared to that with RS, but the recorded values of the flow time meet the recommendations of SCC production. *R'mili* et al. [50] have noted that the substitution of crushed sand by a sand dune in the composition of self-compacting concretes, allows to increasing the flow time to the V-funnel. This is explained by the increasing the viscosity up to a rate of 30%. Beyond this content, the SCC required an addition of water and superplasticizer to have self-placing properties [51]. One can say even with moderate dosages of DS that the measured flow time shows that incorporation of DS increases the viscosity of SCC and this is due to the increase of the specific surface area of fine aggregate of binary or ternary mixture. *Gristsada* and *Natt* [55] have studied the properties of SCC with calcareous sand. They noticed that the flow time increases with the increase of the sand content. This is explained by the increase of the compactness of the mixture and consequently the increase of the viscosity.

3.4. L-box test

The results of variation of H2 / H1 using L-box test are shown in *Fig. 14*. It is seen that all results comply with the requirements of AFGC recommendations (H_2 / H_1> 0.8) [53]. It is also noted a decrease in H_2 / H_1 in SCC with binary and ternary mixtures sands when the sand dune percentage is above 50%. The partial incorporation of DS in the mixtures increases the filling capacity of SCC, and therefore the mobility of SCC in confined areas. *R'mili* et al. [50] studied the effect of the incorporation of crushed sand and desert sand on the properties of self-compacting concretes. The results show that the L-box filling capacity is improved when the crushed sand is partially replaced by desert sand (dune sand). The H_2/H_1 ratio increases to a substitution rate of 15%. Beyond this sand dune content, this ratio decreases. For high amounts of DS, SCC behave like ordinary concrete. The use of binary and ternary mixtures sands improves the rheological properties of SCC. *R'mili* et al [50] have studied the effect of the incorporation of crushed sand and desert sand on properties of self-compacting concrete. The results show that the ability to fill in L-box is improved when the crushed sand is partially replaced by the desert sand. Kou and Poon [59] prepared a SCC with natural and recycled sand. The replacement rate of natural sand by recycled sand is 0, 25, 50, 75 and 100%. They noticed an increase in H_2 / H_1 ratio with increases in percentage of recycled sand.

3.5. Sieve stability test

Sieve stability test (GTM) results are shown in *Fig. 15*. It is noted that the percentages of mortar passing through the sieve are between 6 and 15% according to recommendations ENFRAC [52], except for SCC with DS as partial replacement of RS or CS in binary and ternary system mixtures, which are slightly over than the recommended values for SCC, but remain acceptable values. This is due to high percentage of DS used in blends, since the latter has a fine particle size that passes through the sieve with the amount of milt. Generally, the results obtained show that all SCC have good resistance to segregation and bleeding. Further, visual examination of SCC reveals that they are homogeneous and stable. The use of CS with RS or DS increases the volume of the paste and therefore improves the stability of the SCC.

3.6. Compressive strength

Fig. 16 shows the variation of the compressive strength of different SCC at 28 days. It can be noted that, the best strengths achieved after 28 days are obtained with SCC made with mixture sand of river and crushed sand. It is shown that the river sand has a beneficial effect on the compressive strength of SCC due to its continuous particle size. However, the strength gain for SCC containing crushed sand appears to be linked to the existence of limestone fines in sand in one hand, and in other hand the large size of the crushed sand. *Abdulghani* [60] studied the effect of sand size on the properties of self-compacting concretes. He noticed that, the resistance is not significantly affected by the size of fine aggregates. The sharp edges of the particles in crushed sand provide better bond with cement than rounded particles of river sand. Shaik and *Diami* [61] carried out a study on the mechanical properties of concretes made with industrial sand (crushed sand) and natural sand (river sand). They have demonstrated that industrial sand used as fine aggregates can significantly improve the mechanical properties of concrete. The crushed aggregates with angular shape confer a good bond granulate-cement compared to rolled aggregates. *Kothai* and *Malthy* [62] carried out a study on the influence of replacing natural sand with crushed sand on the mechanical strength of self-compacting concrete. They found that a substitution rate of natural sand by industrial sand or crushed of 30% gives good mechanical strength in terms of compressive, tensile and flexural strength. A reduction in the compressive strength was observed in SCC with binary and ternary mixtures of crushed- dune sand, river - dune sand and crushing- river -dune sand. This means that the dune sand decreases compressive strength of SCC due to its very fine particle size, high surface area and high porosity, which gives less compactness of SCC than those made with river and crushed sand [63, 64]. *R'mili* et al. [50] found that the partial substitution (30%) of crushed sand by desert sand (dune sand) in the composition of self-compacting concretes, contributed to the improvement of mechanical resistance. Beyond 30% substitution of dune sand resistances decrease, but they reach acceptable values compared to ordinary concrete.

3.7. Microstructure

Since the siliceous sand is inert, the increase in strength is obtained by densification of the matrix and the matrix-aggregate interface. In the case of sand limestone and silico-limestone, adds to the densification an interaction between the matrix and the aggregates, which gives good adhesion sand-cement paste and increases the strength. This is verified by the SEM examination of the samples, which shows crack propagation through the cement paste and aggregates. *Fig. 17* represents SEM examinations of SCC with 100% RS, 100% CS and 100% DS respectively. The crack propagation is observed through the cement paste.

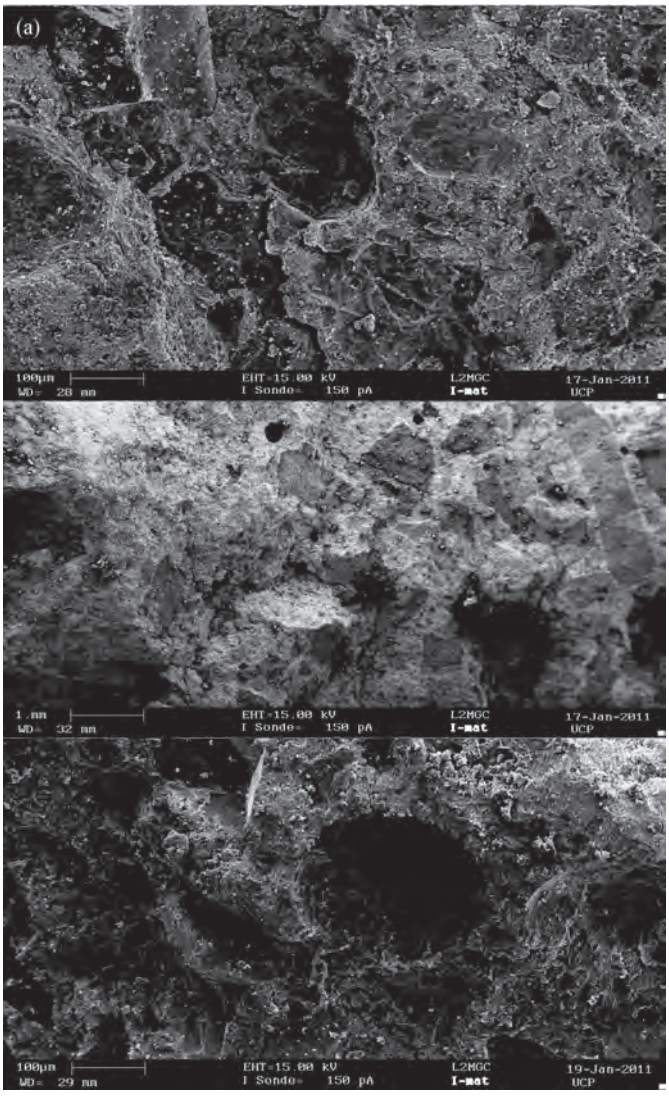

Fig. 17. SEM views of SCC with different types of sand: (a) 100% RS; (b) 100% CS; (c) 100% DS

17. ábra Öntömörödő beton elektronmikroszkópos felvételei különböző homokok felhasználásával, (a) 100% RS; (b) 100% CS; (c) 100% DS

Bellanger et al. [68] observed in this connection that the character of the fracture, in mortar or concrete, differed according to the type of a: it is always intergranular in a siliceous concrete, it is intergranular in the case of hard limestone aggregates, and intragranular when the paste is less deformable than the aggregate. *Bachiorrini* [69] has also observed changes in the mode of crack propagation in aluminous calcareous sand mortars. Different authors have studied the properties of calcareous aggregates in a cement matrix. *Husson* [70] has shown that limestone fines were active within a cement matrix and that they participated in hydration reactions by forming between others carboaluminates. To highlight this phenomenon, *Husson* [70] worked on calcite (98.6% $CaCO_3$) with a particle size slightly smaller than that of the binder. Other authors [70] have shown that the composition of the interfacial zone could be modified when the aggregate is reactive (e.g. calcite) by the formation of carboaluminates, calcium carbonate complexes, calcium hydroxide. Therefore, the surface of the aggregates was attacked by the formation of these compounds. Interface resistance tests

have shown that for these reactive aggregates, the fracture was farther away than at the surface of the aggregate. The further the breaking zone is from the aggregate, the higher the resistance at the interface [71].

Bellanger et al. [72] have demonstrated the contribution of these chemical interactions on the mechanical strength, both in flexural and compressive strength, on mortars or concretes based on calcareous aggregates compared to the same materials with siliceous aggregate. They have also shown, with a succession of charge-discharge cycles, that calcareous sand mortar and concrete have an almost perfect elastic character, that is to say that the deformations are quasi-reversible up to 80% maximum stress. Under the same conditions, siliceous concrete has shown irreversible deformations for much lower stresses.

4. Conclusions

The assessment of the behavior of SCC at fresh and hardened state leads to the followings:

- The use of binary and ternary mixtures sands improves the rheological and mechanical properties of SCC.
- At different contents of river and crushed sand, the rheological and mechanical characteristics are met and comply with recommendations of the manufacturing of SCC. However, the use of high dosages of sand dunes reduces the rheological parameters of SCC. Therefore, to meet the self-compacting properties, additional amounts of water and superplasticizer are strongly required.
- The best strengths are obtained for SCC made with crushed and river sand. This is due to the good size distribution of these sands. The mechanical strengths decreased by adding a high content of dune sand but they reach acceptable values.

Based on the obtained results, it can be argued that the use of locally available materials in the manufacturing of concrete can be an economic and technological important alternative in some developing countries. The partial incorporation of the sand dune in the composition of self-compacting concrete can provide a solution for some work in the southern regions of the country where this material is very abundant. Moreover, crushed limestone sands are interesting alternative source to replace the river sand (rolled) for making any kind of concrete.

References

[1] Okamura, H. – Ouchi, M. (1999): Self-compacting concrete, development, present use and future, in: *A. Skarendahl, O. Petersson (Eds.), Self-Compacting Concrete, RILEM Symposium Stockholm*, RILEM Publications, 3-14, 1999.

[2] Okamura, H. – Ouchi, M. (2003). Self-compacting concrete, *Journal of Advanced Concrete Technology*, 1: 5-15, 2003. https://doi.org/10.3151/jact.1.5

[3] Sonebi, M. (2004): Medium strength self-compacting concrete containing fly ash: modeling using factorial experimental plans, *Cement and Concrete Research*, 34:1199-208, 2004. https://doi.org/10.1016/j.cemconres.2003.12.022

[4] Sonebi, M. – Bartos P. J. (1999): Hardened SCC and its bond with reinforcement, *Proceedings of First International RILEM Symposium on Self-Compating Concrete* (PRO 7), Stockholm, Sweden, 1999.

[5] Uysal, M. – Yilmaz, K. – Ipek, M. (2011): The effect of mineral admixtures on mechanical properties, chloride ion permeability and impermeability of self-compacting concrete, *Construction and Building Materials*, 27: 263-70, 2011. https://doi.org/10.1016/j.conbuildmat.2011.07.049

[6] Sadek, D. M. – El-Attar, M. M. – Haitham, A. A. (2016): Reusing of marble and granite powders in self-compacting concrete for sustainable development. *Clean Production*, 121: 19-32, 2016. https://doi.org/10.1016/j.jclepro.2016.02.044

[7] Felekoglu, B. (2008): A comparative study on the performance of sands rich and poor in fines in self-compacting concrete, *Construction and Building Materials*, 22: 646-654, 2008. https://doi.org/10.1016/j.conbuildmat.2006.10.007

[8] Bosiljkov, V. B. (2003): SCC mixes with poorly graded aggregate and high volume of limestone filler, *Cement and Concrete Research*, 33:1279–1286, 2003. https://doi.org/10.1016/S0008-8846(03)00013-9

[9] Ho, D. W. S. – Sheinn, A. M. M. – Ng, C. C. – Tam, C. T. (2002): The use of quarry dust for SCC application, Cement and Concrete Research, 32: 505–511, 2002. https://doi.org/10.1016/S0008-8846(01)00726-8

[10] Felekoglu, B. (2007): Utilisation of high volumes of limestone quarry waste in concrete industry (SCC case), *Resources Conservation and Recycling*, 51: 770–791, 2007. https://doi.org/10.1016/j.resconrec.2006.12.004

[11] Menadi, B. – Kenai, S. – Khatib, J. – Ait, Mokhtar A. (2009): Strength and durability of concrete incorporating crushed limestone sand, *Construction and Building Materials*, 23: 625–33, 2009. https://doi.org/10.1016/j.conbuildmat.2008.02.005

[12] Guimaraes, M. S. – Valdeo, J. R. – Palomino, A. M. – Santamarina, J. C. (2007): Aggregate production: fines generation during rock crushing, *International Journal of Mineral Process*, 81: 237–47, 2007. https://doi.org/10.1016/j.minpro.2006.08.004

[13] Johansen, K. – Mortsell, E. – Lindgard, J. (2000): Effect of adding natural fine sand rich in fines on the fresh concrete properties, *Nordic concrete Research Publications*, 22, 2000.

[14] Donza, H. – Cabrera, O. – Irrassar, E. F. (2002): High strength with different fine aggregate, *Cement and Concrete Research*, 32: 1755–1761, 2002. https://doi.org/10.1016/S0008-8846(02)00860-8

[15] Johansen, K. – Busterud, L. (2001): Low grade SCC with secondary natural sand rich in fine. *In: Ozawa K, Ouchi M, editors, Second International RILEM Symposium on SCC*, Japan, 2001.

[16] Topoçu, I. B. – Ugurlu, A. (2003): Effect of the use of mineral filler on the properties of concrete, *Cement and Concrete Research*, 33: 1071–1075, 2003. https://doi.org/10.1016/S0008-8846(03)00015-2

[17] Topoçu, I. B. (1999): Effects of using crushed stone dust on concrete properties. In: *Tenth engineering symposium, Civil Engineering'99, Suleyman Demirel University*, Isparta, Turkey, 1999.

[18] Okamura, H. – Maekawa, K. – Ozawa, K. (1993): High performance concrete, 1st edition: *Gihoudou Publication*, Tokyo, 1993.

[19] Celik, T. – Marar, K. (1996): Effects of crushed stone dust on some properties of concrete, *Cement and Concrete Research*, 26: 1121-1130, 1996. https://doi.org/10.1016/0008-8846(96)00078-6

[20] Dehwah, H. A. F. (2012): Mechanical properties of self-compacting concrete incorporating quarry dust powder, silica fume or fly ash, *Construction and Building Materials*, 26: 547-551, 2012. https://doi.org/10.1016/j.conbuildmat.2011.06.056

[21] Jain, M. E. M. – Safiuddin, M. – Yousuf, K. M. (1999): A study on the properties of freshly mixed high performance concrete, *Cement and Concrete Research*, 29(9), 1427-1432, 1999. https://doi.org/10.1016/S0008-8846(99)00108-8

[22] Lohani, T. K.. – Padhi, M. – Jena, S. (2012): Optimum utilization of quarry dust as partial replacement of sand in concrete, *International Journal of Applied Science and Engineering Research*, Vol.1, No.2, 391-404, 2012.

[23] Hudson, B. P. (1997): Manufactured sand for concrete. *The Indian Concrete Journal*. 71(5): 237-240, 1997.

[24] Sahu, A. K. – Kumar Sunil, Sachin A. K. (2003): Crushed stone waste as fine aggregate for concrete. *The Indian Concrete Journal*. 77(1): 845-847, 2003.

[25] Chitlange, M. R.. – Pajgade, P. S.. – Nagarnaik, P. B. (2008): Artificial sand as fine aggregate for concrete. *Civil Engineering and Construction Review*. 21 (12): 64-67, 2008.

[26] Kode, V. R. – Murty, D. S. R. – Swarna, Kumar P. (2007): Appraisal of crushed stone dust, as fine aggregate in structural concrete. *Civil Engineering and Construction Review*. 20(7): 52-58, 2007.

[27] Ahmed, A. E. – El-Kourd, A. A. (1989): Properties of concrete incorporating natural and crushed stone very fine sand. *ACI Materials Journal*. 86(4): 417-424, 1989.

[28] Ahmad, S. – Mahmood, S. (2008): Effects of crushed and natural sand on the properties of fresh and hardened concrete, *33rd Conference on Our World In Concrete & Structures, Singapore*, pp. 25-27, 2008.

[29] Akrout, K. – Mounanga, P. – Ltifi, M. – Jamaa, N. (2010): Rheological, mechanical and structural performances of crushed limestone sand concrete, *International Journal of Concrete Structures and Materials*, Vol. 4, No. 2: 97-104, 2010. DOI 10.4334/IJCSM.2010.4.2.97

[30] Ilangovana, R. – Mahendrana, N. – Nagamanib, K. (2008): Strength and durability properties of concrete containing quarry rock dust as fine aggregates, *ARPN Journal of Engineering and Applied Science*, Vol.3(5), pp 20-26, 2008.

[31] Hameed, M. S. – Sekar, A. S. S. (2009): Properties of green concrete containing quarry rock dust and Marble sludge powder as fine aggregates, *ARPN journal of Engineering and applied Science*, Vol.4(4), pp 83-89, 2009.

[32] Shi-Cong, K. – Chi-Sun, P. (2009): Properties of concrete prepared with crushed fine stone, furnace bottom ash and fine recycled aggregate as fine aggregates. *Construction and Building Materials* 23: 2877–2886, 2009. https://doi.org/10.1016/j.conbuildmat.2009.02.009

[33] Donza, H. – Cabrera, O. – Irassar, E. F. (2002): High-strength concrete with different fine aggregate. Argentina, *Cement and Concrete Research*. 32, 1755–1761, 2002. https://doi.org/10.1016/S0008-8846(02)00860-8

[34] Poon, C. S. – Shui, Z. H. – Lam, L. – Fok, H. – Kou, S. C. (2004): Influence of moisture states of natural and recycled aggregates on the slump and compressive strength of concrete, *Cement and Concrete Research*, Vol.34, Iss.1, 31-36, 2004. https://doi.org/10.1016/S0008-8846(03)00186-8

[35] Rao, K. B. – Desai, V. B. – Mohan, D. J. (2011): Experimental investigation on mode II fracture of concrete with crushed granite stone fine aggregate replacing sand, *Material Research*, Vol.15, No.1, 41-50, 2011.

[36] Kumar, P. – Kaushik, S. K. (2005): SCC with crusher dust, fly ash and micro silica. *The Indian Concrete Journal*. 79(8): 32-37, 2005.

[37] Shanmugapriya, T. – Uma, R. N. (2012): Optimization of partial replacement of m-sand by natural sand in high performance concrete with silica fume, *International Journal of Engineering Sciences & Emerging Technologies*, Vol. 2, pp. 73-80, 2012.

[38] Raman, S. N. M. – Zain, F. M. – Mahmud, H. B. – Tan, K. S. (2005): Influence of quarry dust & fly ash on the concrete compressive strength development. *Proc. AEESEAP Int. Conf.* 2005. Kuala Lumpur, Malaysia, 78, 2005.

[39] Reddy, M. V. – Reddy, C. N. V. S. (2007): An experimental study of rock flour and insulator ceramic scrap in concrete, *Journal of Institute of Engineer* (India), Vol. 88, pp 47-50, 2007.

[40] Bederina, M. – Khenfer, M. M. – Dheilly, R. M. – Quéneudec, M. (2005): Reuse of local sand: effect of limestone filler proportion on the rheological and mechanical properties of different sand concretes. *Cement and Concrete Research*, 35: 1172–1179, 2005. https://doi.org/10.1016/j.cemconres.2004.07.006

[41] Brouwers, H. J. H. – Radix, H. J. (2005): Self-compacting concrete: the role of the particle size distribution. In: *First International Symposium on Design*, Performance and Use of SCC. Hunan, China; 109–118, 2005.

[42] Kay, A. – Freason, J. (1994): An investigation into the use of dune sand in concrete. In: *Fookes, Party*, editor. In Proceeding of the 1st International Symposium on Engineering Characteristics of Arid Soils. Rotterdam: Balkema, 261–672, 1994.

[43] Banfill, P. F. G. – Carr, M. P. (1987): The properties of concrete made with very fine sand. *Concrete*; 21: 11–16, 1987.

[44] Laquerbe, M. – Cisse. I. – Ahouansou, G. (1995): For a rational use of lateritic gravel and dune sand as aggregates in concrete: application to the case of Senegal. *Materials and Structures*, 28: 604–610, 1995.

[45] Tayeb, B. – Abdelbaki, B. – Madani, B. – Mohamed, L. (2011): Effect of Marble Powder on the Properties of Self-Compacting Sand Concrete, *The Open Construction and Building Technology Journal*, 5, 25-29, 2011

[46] Bouziani, T. – Bederina, M. – Hadjoudja, M. (2012): Effect of dune sand on the properties of flowing sand-concrete (FSC). *International Journal of Concrete Structures and Materials*, 6: 59–64, 2012. https://doi.org/10.1007/s40069-012-0006-z

[47] Bouziani, T. (2013): Assessment of fresh properties and compressive strength of self-compacting concrete made with different sand types by mixture design modelling approach. *Construction and Building Materials,* 49: 308–314, 2013. https://doi.org/10.1016/j.conbuildmat.2013.08.039

[48] Bouziani, T. – Bédérina, M. – Makhloufi, Z. – Hadjoudja, M. (2014): Mixture design approach to evaluate fresh properties of SCC made with various sands. *Journal of Building Materials and Structures*, 1: 1–9, 2014.

[49] Bouziani, T. – Benmounah, A. – Makhloufi, Z. – Bédérina, M. – Queneudec, M. (2014): Properties of flowable sand concretes reinforced by polypropylene fibers. *Journal of Adhesion Science and Technology*, 28: 1823– 1834, 2014. https://doi.org/10.1080/01694243.2014.924176

[50] R'mili, A. – Ben Ouezdou, M. – Added, M. – Ghorbel, I. (2009): Incorporation of crushed sands and Tunisian desert sands in the composition of self-compacting concrete, Part II: SCC fresh and hardened states characteristics, *International Journal of Concrete Structures and Materials*, 3: 11 – 14, 2009.

[51] R'mili, A. – Ben Ouezdou, M. (2011): Incorporation of crushed sand and desert sand in the composition of Self-Compacting Concrete, *International conference, Innovation and Valorization in civil engineering and construction materials*, N10-271, Rabat, Morocco, 2011. https://doi.org/10.4334/IJCSM.2009.3.1.011

[52] EFNARC (2005): The European guidelines for self-compacting concrete, *The European Federation of Specialist Construction Chemicals and Concrete Systems*, p. 68, 2005

[53] AFGC (2002): French Association of Civil Engineering, *Guidelines for self-compacting concrete: scientific and technique documents*, 2002.

[54] Omar, O. M. – Abd El-hameed, G. D. – Sherif, M. A. – Mohamadien, H. A. (2012): Influence of limestone waste as partial replacement material for sand and marble powder in concrete properties, *Journal of Housing and Building National Research Center*, 8: 193 – 203, 2012.

[55] Gritsada, Sua-iam – Natt, Makul (2013): Utilization of limestone powder to improve the properties of SCC incorporating high volumes of untreated rice husk ash as fine aggregate, *Construction and Building Materials* 38: 455 – 464, 2013. https://doi.org/10.1016/j.conbuildmat.2012.08.016

[56] Domone, P. L. – Jin, J. – Chai, H. W. (1999): Optimum mix proportioning of self-compacting concrete, *Innovation in Concrete Structures: Design and Construction, Proceeding of creating with concrete*, University of Dundee, September 1999, 277 – 285

[57] Nanthagopalan, P. – Santhanam, M. (2011): Fresh and hardened properties of self-compacting concrete produced with manufactured sand, *Cement and Concrete Composites*, 33: 353 – 358, 2011. https://doi.org/10.1016/j.cemconcomp.2010.11.005

[58] Domone, P. L. – Jin, J. (1999): Properties of mortar for Self-Compacting Concrete, *Proceedings of the 1st International Symposium on SCC,* RILEM Proceedings PRO 7, Sweden, 1999.

[59] Kou, S.C. – Poon, C. S. (2009): Properties of SCC prepared with coarse and fine recycled aggregates, *Cement and Concrete Composites*, 31: 622 – 627, 2009. https://doi.org/10.1016/j.cemconcomp.2009.06.005

[60] Abdul Ghani Zghair Luma (2010): Influence of fine aggregate grading on some properties of SCC, *Journal of Engineering and Development*, 14: 18 – 37, 2010,

[61] Shaikh, M. G.. – Daimi S. A. (2011): Durability studies of concrete made by using artificial sand with dust and natural sand, *International Journal of Earth Sciences and Engineering*, 04: 823 – 825, 2011,

[62] Kothai, L. – Malathy, R. (2012): Strength studies on self-compacting concrete with manufactured sand as partial replacement of natural sand, *European Journal of Scientific Research*, Vol. 89, N° 3: 490 – 496, 2012,

[63] Elyamany, H. E. – Abd Elmoaty, M. A. E. – Mohamed, B. (2014): Effect of filler types on physical, mechanical and microstructure of self-compacting concrete and Flow-able concrete, *Alexandria Engineering Journal*, 53: 295–307, 2014. https://doi.org/10.1016/j.aej.2014.03.010

[64] Lasintha, E. D. L. – Prabath, R. M. T. – Sooriaarachchi, H. P. (2012): Influence of fine aggregate types on the performance self-flowing concrete, *Proceedings of International Symposium on Advances in Civil and Environmental Engineering Practices for Sustainable Development ACEPS*: 251- 259, Sri Lanka, 2012.

[65] Li, B. – Ke, G. – Zhou, M. (2011): Influence of manufactured sand characteristics on strength and abrasion resistance of pavement cement concrete, *Construction and Building Materials*, 25: 3849 – 3853 , 2011. https://doi.org/10.1016/j.conbuildmat.2011.04.004

[66] Wakchaure, M. R. – Shaikh, A. P. – Gite, B. E. (2012): Effect of types of fine aggregate on mechanical properties of cement concrete, *International Journal of Modern Engineering Research*, Vol. 2 (5): 3723 – 3726, 2012,

[67] Luo, F. J. – He, L. – Duan, W. H. – Zhao, X. L. – Collins, F. (2013): Effect of very fines particles on workability and strength of concrete made with dune sand, *Construction and Building Materials*, 47: 131 – 137, 2013. https://doi.org/10.1016/j.conbuildmat.2013.05.005

[68] Bellanger, M. – Chaouch, M. (1996): Interaction of binder-aggregate, Influence on mechanical properties of mortars and concretes, *Mines and quarries*, Mineral industry, 81-83, 1996. (in French)

[69] Bachiorrini, A. (1985): Physical and chemical interaction of monocalcic aluminate and carbonates during the hydration reaction, PhD thesis, University of Lyon I, p. 215, 1985 (in French)

[70] Husson, S. (1991): Physical-chemical and mechanical study of cement-fillers interactions, application on mortars, PhD thesis, *INP Grenoble and ENS of Mines Saint-Etienne*, p. 139, 1991 (in French)

[71] Bentur, A. – Odler, I. (1996): Development and nature of interfacial microstructure. *Interfacial transition zone in concrete*, Ed. by Maso, J.C., RILEM Report 11, E & FN Spon, London, 19 – 44, 1996.

[72] Bellanger, M. – Chaouch, M. – Homand, F. (1996): Mechanical behavior of mortars and concrete based limestone, *Mines and quarries, Mineral industry*, 57 – 61, 1996 (in French)

Ref.:
Benabed, Benchaa: *Effect of combined use of crushed sand and Algerian desert dune sand on fresh properties and strength of self-compacting concrete*
Építőanyag – Journal of Silicate Based and Composite Materials, Vol. 70, No. 5 (2018), 155–167. p.
https://doi.org/10.14382/epitoanyag-jsbcm.2018.29

Expanded clay is a well-proven, high quality, efficient and durable lightweight aggregate suitable for a wide range of applicants in the construction sector. It is a sustainable construction material packed with properties that improve the economic, social and environmental performance of a building or infrastructure over its whole lifetime.

EXCA is the European expanded clay association and represents the interests of all major expanded clay producers throughout Europe. With its 12 member companies in 11 countries operating some 20 plants throughout Europe EXCA represents more than 90% of the European industry.

EXCA
EUROPEAN EXPANDED CLAY ASSOCIATION

EXCA, European Expanded Clay Association
info@exca.eu | www.exca.eu

The localization of plastic deformation in bimetal

Yulia V. Li ▪ Institute of Strength Physics and Materials Science ▪ jul2207@mail.ru
Svetlana A. Barannikova ▪ Institute of Strength Physics and Materials Science ▪ bsa@ispms.tsc.ru
Lev B. Zuev ▪ Institute of Strength Physics and Materials Science ▪ lbz@ispms.tsc.ru
Érkezett: 2018. 06. 22. ▪ Received: 22. 06. 2018. ▪ https://doi.org/10.14382/epitoanyag-jsbcm.2018.30

Li Yulya VLADIMIROVNA
post-graduate student of the Laboratory of Strength Physics in the Institute of Strength Physics and Materials Science SB RAS (ISPMS).

Barannikova Svetlana ALEKSANDROVNA
Doctor of Physical and Mathematical Sciences, leading Scientific worker of the Laboratory of Strength Physics in the Institute of Strength Physics and Materials Science SB RAS (ISPMS).

Zuev Lev BORISOVICH
Doctor of Physical and Mathematical Sciences, Head of the Laboratory of Strength Physics in the Institute of Strength Physics and Materials Science SB RAS (ISPMS).

Abstract
Plastic flow localization patterns in bimetal laminates at the macroscale level have been researched. It has been found that plastic deformation proceeds during the whole process of deformation and localized in base, transition and cladding layer of bimetal. Kinetics of proliferation of plastic deformation localization fronts has been traced at different stages of the curve demonstrating plastic flow in A 283 Grade +301 AISI bimetal composed of 301 AISI austenitic stainless steel and A 283 Grade low-carbon steel. Staging of deformation curves has been analyzed.
Keywords: bimetal, localization of the plastic deformation, DESP, plastic flow, autowaves
Kulcsszavak: bimetál, képlékeny alakváltozás lokalizálása, DESP, képlékeny folyás, autohullámok

1. Introduction

In recent decades, studies of the plastic deformation localization at the macroscale level have been one of the most complex problems related to the plastic flow of materials. Experimental studies of plastic deformation localization [1,2] conducted using the double-exposure speckle photography (DESP) method [3,4] and digital image correlation (DIC) method [5] showed that plastic deformation is localized within the whole deformation process for different types of materials with FCC, BCC and HCP lattice.

Different forms of plastic deformation localization at the macroscale level can be considered as different types of autowaves depending on applicable strain hardening law [6,7].

There are lots of examples of plastic deformation localization at the macroscale level. First of all, well-known studies of localized deformation fronts by *Chernov* and *Lüders* [8 - 10] should be recalled. They initiated the modern approach to study of plastic flow. Such a band typical for deformation of several alloys [11] in the yield plateau is a front of plastic deformation moving from on machine grip to another. These bands are often visible to the unaided eye on the preliminary polished surface of a metal specimen. Fronts separate from each other areas of elastic (more exactly, microflow) and plastic deformation.

At present, there is growing interest in studies of deformation behaviour of multilayer materials in the course of severe plastic deformation. These materials can be made by combining dissimilar metals into a solid composite, which preserves reliable bonding of components during further processing and under operation conditions. These materials include two-layer metal composites, namely, bimetals, including corrosion resistant bimetals, which are quite resistant to exposure of corrosive media and have excellent mechanical properties [12-16].

It is known that diffusion processes occur during manufacturing of bimetals in the course of joint hot rolling of dissimilar layers and further process heating. These processes are found in the interface area of materials, and they form transition areas, which are chemically and structurally inhomogeneous. Nature of occurrence and propagation of plastic deformation localization fronts in base, transition and cladding layers of bimetal differs from the nature of front propagation in a single-layer material. In this connection, it is necessary to improve knowledge on the processes of joining dissimilar metals and their joint deformation on micro-, meso- and macroscale levels.

2. Materials and methods

Bimetal samples, cut from the strip, produced according to the following procedure, were studied: A 283 Grade steel (backing metal) was poured between the sheets of 301 AISI cladding metal put into the mold box –(T=1500°C) followed by hot rolling of a produced three-layer sheet at T=1200÷1400 °C. Along the outer edge of the specimen, on both sides, a cladding layer approximately 750 μm thick made of 301 AISI steel is provided, and in the center - a base metal layer approximately 6.7 mm thick made of A 283 Grade steel is provided.

Mechanical uniaxial tensile tests were conducted at T=300 K at deformation velocity of 6.67×10^{-5} s^{-1} using testing machine LFM-125.

Detailed research of plastic flow localization patterns at the microscale level was conducted using multipurpose measuring complex ALMEC-tv designed for digital registration of fields of displacement vectors and tensor component of plastic distortion [3]. Using this complex, the tensile sample was illuminated with coherent light of a semiconductor laser with a wavelength of 635 nm and a power of 15 mW. Obtained images of the deformed sample superimposed with speckle patterns were recorded with PixelLink PL-B781 digital video camera. A count sequence for each image point was formed characterizing the time course of its brightness; dispersion and expectation for speckle flicker brightness were calculated, which were used for mapping plastic deformation localizations. This method allowed in situ recording of areas, where deformation of material is localized at the specified growth of sample length.

Material	$\sigma_{0.2}$, MPa	σ_B, MPa	δ, %	Stage of linear hardening			Parabolic stage			Predegradation stage		
				n	ε_n	ε_k	n	ε_n	ε_k	n	ε_n	ε_k
Bimetal	250	421	27.2	1	-	-	0.5	0.09	0.20	0.3	-	-
A 283 Grade	262.7	391.92	28	1	-	-	0.5	0.15	0.23	0.3	-	-
301 AISI	247	812	73	1	0.04	0.13	0.5	-	-	0.3	-	-
				1	0.14	0.68						

Table 1. Mechanical properties of materials
1. táblázat Az anyagok mechanikai jellemzői

3. Result and discussion

Tensile diagrams of flat bimetal sample as well as diagrams of similar samples made of A 283 Grade and 301 AISI steel are shown in *Fig. 1*. They cover the area of elastic and plastic deformations and degradation.

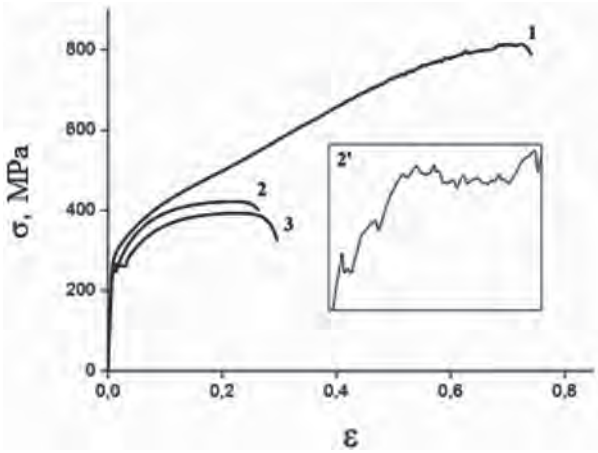

Fig. 1. Stress-strain diagrams: 1 – 301 AISI; 2 – bimetal; 3 – A 283 Grade; 2' –yield plateau of curve 2 for bimetal
1. ábra Feszültség-alakváltozás diagramok: 1 – 301 AISI; 2 – bimetál; 3 – A 283 acél; 2' –folyási határ a 2 – bimetál görbéhez

Bimetal curve downstream of the yield plateau in the area of plastic deformation is located between curves for its components (20 samples of each metal were tested). Loading diagrams of A 283 Grade steel and bimetal show clearly marked yield drop and yield plateau, where oscillations of stress are visible (*Fig. 1*). Cladding layer of stainless steel provides reduction of yield plateau propagation, improvement of tensile strength and reduction of plasticity of base metal (A 283 Grade steel). For complete coverage of occurrence and propagation of Chernov-Lüders bands (CLBs) in bimetal, registration of speckle image during experiments started when stress was lower that the value of yield strength and stopped when the yield plateau was ended and during transition to the stage of strain hardening.

Analysis of plastic yielding curves of materials (*Fig. 1*) showed that diagrams are related to the general type diagrams. Bonding between deformations and stress is reasonable to demonstrate using Ludwick equation

$$\sigma(\varepsilon) = \sigma_y + \theta\varepsilon^n \quad (1)$$

where ε and σ – current stress and deformation, σ_y – yield strength, θ – deformation hardening factor; n≤1– deformation hardening index. Application of Ludwick equation and presentation of loading curve in coordinates $\ln(s - s_0) = f(\ln e)$ allow for defining stages in deformation curves, where index n is constant and changes discretely from section to section, where *s* - true stress disregarding changes in cross section of an operating part during uniaxial tension, MPa; *e* - true strain.

Analysis of loading curve staging revealed the following stages of plastic flow:

1. In A 283 Grade steel, downstream of the transition section from the elastic part to plastic flow at total deformation ε_{tot} = 0.008 – 0.03 a yield plateau is observed; then, at total deformation ε_{tot} = 0.15 – 0. 23 the stage of parabolic deformation hardening is found with total length ε_{tot} = 0. 08. Stages of linear deformation hardening and predegradation are not found for this material.
2. In 301 AISI austenitic stainless steel at total deformation ε_{tot} = 0.04 - 0.13 and ε_{tot} = 0.14 - 0.68, two long sections are found, which correspond to the stage of linear deformation. Stages of parabolic (Taylor) deformation hardening and predegradation are not found for this material.
3. For bimetal, the similar situation as for A 283 Grade low-carbon steel is observed sharp yield point and yield plateau with duration of 0.006 can be defined in the curve. In case of total deformation ε_{tot} = 0.09 - 0,20 it is possible to define the stage of parabolic (Taylor) deformation hardening with total duration of ε_{tot} = 0.11. Stage of linear deformation hardening and predegradation is not found for this material.

As a result of mechanical tensile tests, the following mechanical properties were obtained: $\sigma_{0,2}$ – conventional yield strength, MPa; σ_B – tensile strength, MPa; δ – specific tensile elongation, % (*Table 1*).

According to the analysis of load deformations, plastic deformation in a bimetal sample is localized in the area of base material of A 283 Grade in the form of Chernov-Lüders band.

Chernov-Lüders band formed near the mobile grip is limited by a pair of fronts moved in opposite directions along the axis of the sample (*Fig. 2*) at different velocities $\pm V_f$. Front (1) moves in the direction of mobile grip and disappears after passing by a short section while front (2) continues moving in the ditection of fixed grip. If total deformation is ε_{tot} = 0.012, another front of Chernov-Lüders band (front (3)) is formed in the area of fixed grip. Fronts (2) and (3) move towards each other, and when total deformation becomes equal to ε_{tot} = 0.015, they meet and disappear.

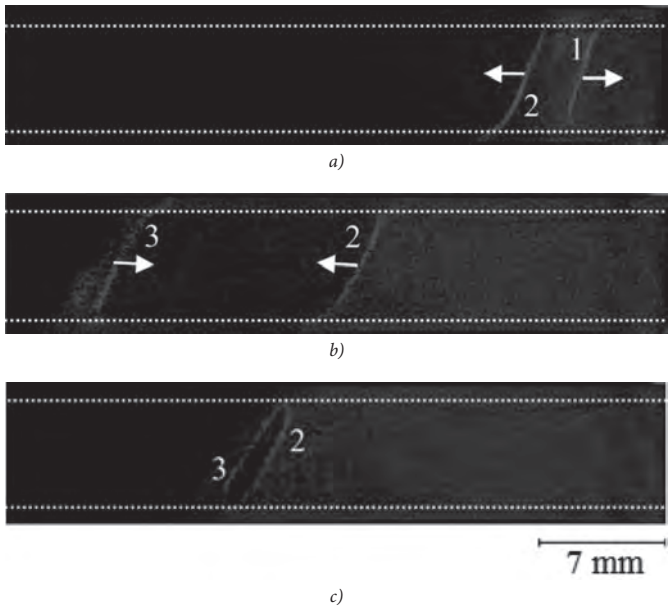

a)

b)

c)

Fig. 2. Propagation of Chernov-Lüders band at total deformation: a) 0.006, b) 0.013, c) 0.014
2. ábra A Chernov-Lüders szakasz előrehaladása képlékeny alakváltozás során: a) 0.006, b) 0.013, c) 0.014

To study kinetics of macrolocalization pattern development, presentation of positions X of local elongation centers ε_{xx} in a sample was used as a function of total deformation time. Authors of [17] demonstrate that this approach allows determining the velocity of deformation centers movement V = dX/dt using kinetic diagrams (*Fig. 3*).

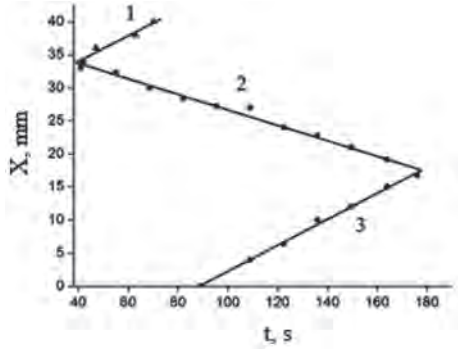

Fig. 3. Kinetic diagram of Chernov-Lüders band on the base layer of A 283 Grade material
3. ábra A Chernov-Lüders szakasz kinetikus diagramja A 283 minőségű anyag alaprétegében

Thus, velocities of Chernov-Lüders band propagation were measured in the base layer of A 283 Grade material. Propagation velocity of first two centers of Chernov-Lüders band occurred at the early stage of plastic deformation process is $V_1 = -1.9 \cdot 10^{-4}$ m/s, $V_2 = 1.2 \cdot 10^{-4}$ m/s. Velocity of the third center of Chernov-Lüders band is $V_3 = -1.9 \cdot 10^{-4}$ m/s (*Fig. 3*).

Since deformation is caused by complex resistance of bimetal to loading in comparison with its components, plastic flow is implemented by propagation of the front of Chernov-Lüders band in base soft metal at the initial stage. At the same time, solid cladding layer of stainless steel is elastically deformed. As a result only one front of Chernov-Lüders band is propagated in the upper cladding layer of 301 AISI material at the velocity of $V_2 = 2.4 \cdot 10^{-4}$ m/s. Two fronts of Chernov-Lüders band propagate in the lower cladding layer of 301 AISI material in the opposite directions at the velocities of $V_1 = 0.7 \cdot 10^{-4}$ m/s, $V_2 = 2.3 \cdot 10^{-4}$ m/s.

For comparison, the following was revealed during analysis of plastic deformation localization patterns for samples of A 283 Grade low-carbon steel and 301 AISI austenitic stainless steel during tension.

Occurrence of fronts of Chernov-Lüders band corresponds to stress of the upper sharp yield point in the diagram (*Fig. 1*). As a result, within the yield plateau, two fronts of Chernov-Lüders band are propagated towards each other at the velocity of $V_1 = 0.6 \cdot 10^{-4}$ m/s, $V_2 = 1.1 \cdot 10^{-4}$ m/s (*Fig. 4*).

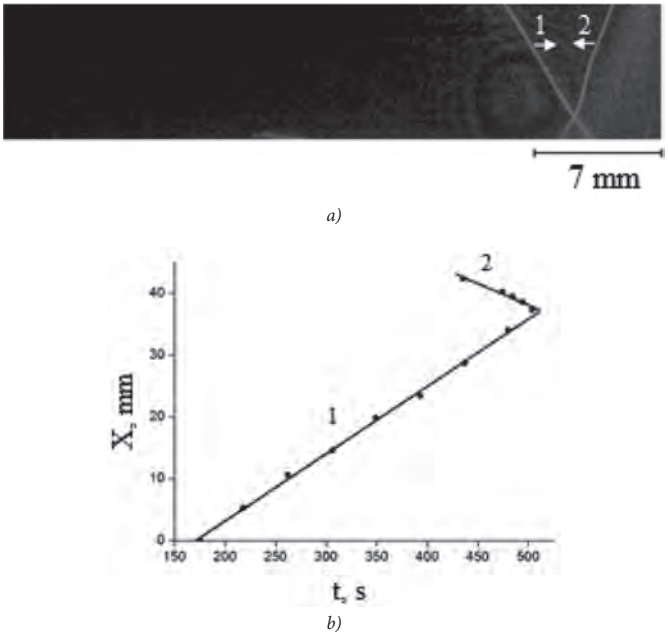

a)

b)

Fig. 4. Propagation of Chernov-Lüders band in 301 AISI material: a) visualization of Chernov-Lüders band propagation, b) kinetic diagram
4. ábra Chernov-Lüders szakasz előrehaladása 301 AISI anyagban: a) A Chernov-Lüders szakasz előrehaladásának megjelenítése, b) kinetikus diagram

At early stages of plastic deformation, the fronts of localized plastic deformation do not occur in austenitic stainless steel. At further stages of deformation, if total deformation is ε = 0.52, ε = 0.58, ε = 0.62, ε = 0.68, four fronts, which move one after the other at velocities of $V_1 = 2.1 \cdot 10^{-4}$ m/s, $V_2 = 2.1 \cdot 10^{-4}$ m/s, $V_3 = 1.7 \cdot 10^{-4}$ m/s, $V_4 = 1.3 \cdot 10^{-4}$ m/s correspondingly, were revealed (*Fig. 5*).

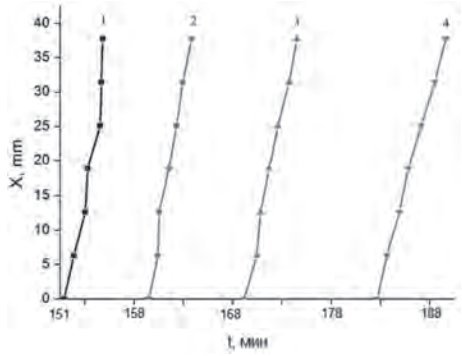

Fig. 5. Kinetic diagram of plastic deformation localization fronts propagation in 301 AISI austenitic stainless steel
5. ábra Képlékeny deformáció lokalizációs frontok kinetikus diagramja 301 AISI ausztenites rozsdamentes acél anyagban

Process of material degradation starts with the localization of plastic deformation near structural heterogeneity and stress raisers [17] in the area of bonding of two dissimilar metals. At early stages of plastic deformation when total deformation is ε = 0.24, micro stress raisers are formed in the area of material bonding. These raisers contribute to formation of a localized area (*Fig. 6*), which is a prerequisite for neck formation in a sample and further degradation of material.

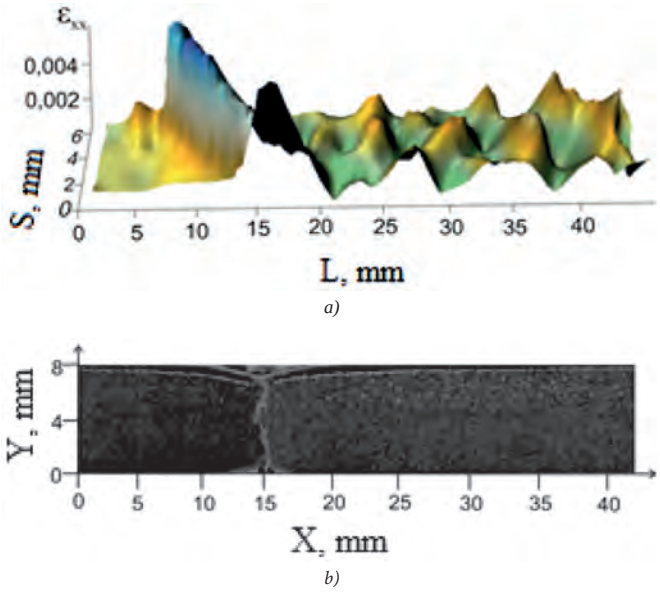

Fig. 6. The picture of localized zones evolution deformation when total deformation is ε = 0.24 (a); bimetal fracture (b)
6. ábra Lokalizációs frontok fejlődése ε = 0.24 teljes deformáció esetén (a); bimetál törése (b)

4. Conclusions

The research conducted allowed formulation of the main laws of propagation of plastic deformation localization in a bimetal material and its component metals.

Analysis of localization patterns of plastic deformation showed that Chernov-Lüders band in the base A 283 Grade layer is limited with a pair of fronts moving in the opposite directions along the axis of bimetal at different velocities. Cladding layer of stainless steel 750 μm thick: (1) causes the reduction of the yield plateau of bimetal; (2) does not suppress the occurrence of Chernov-Lüders band; (3) leads to increase in rates of propagation of Chernov-Lüders band fronts in the base layer and (4) decreases propagation of Chernov-Lüders band in all layers of bimetal.

Area of occurrence and development of a crack can be detected at early stages of strain hardening 8% prior to formation of a neck.

5. Acknowledgements

The work was supported by the Russian Science Foundation (project No. 16-19-10025).

References

[1] Zuev, L. B. – Barannikova, S. A. (2010): Plastic flow macrolocalization: autowaves and quasi-particles. *Journal of Modern Physics*. Vol. 1, pp.1-8. https://doi.org/10.4236/jmp.2010.11001

[2] Danilov, V. – Shlyakhova, G. – Semukhin, B. (2014): Plastic deformation macrolocalization. Local stresses and fracture in ultrafine grain titanium. *Applied Mechanics and Materials*. Vol. 682, pp. 351-356. https://doi.org/10.4028/www.scientific.net/AMM.682.351

[3] Zuev, L. B. – Danilov, V. I. – Barannikova, S. A. – Gorbatenko, V. V. (2009): Autowave model of localized plastic flow of solids. *Physics of Wave Phenomena*. Vol. 17, pp.66-75. https://doi.org/10.3103/S1541308X09010117

[4] Zuev, L. – Polyakov, S. – Gorbatenko, V. (2002): Instrumentation for speckle interferometry and techniques for investigating deformation and fracture. *Proceedings of SPIE - The International Society for Optical Engineering*. Vol. 4900, pp. 1197-1208. https://doi.org/10.1117/12.484526

[5] Barannikova, S. – Zuev, L. – Li, Y. (2018): Plastic flow heterogeneity and failure of bimetal material. *International Journal of GEOMATE*. Vol. 14, no. 43. pp. 112-117. https://doi.org/10.21660/2018.43.3578

[6] Zuev, L. (2017): Autowave processes of the localization of plastic flow in active media subjected to deformation. *Physics of Metals and Metallography*. Vol. 118, no. 8, pp. 810–819. https://doi.org/10.1134/S0031918X17060114

[7] Zuev, L. B. (2014): Using a crystal as universal generator of localized plastic flow autowaves. *Bulletin of the Russian Academy of Sciences: Physics,* Vol. 78, pp. 957–964. https://doi.org/10.3103/S1062873814100256

[8] Bell, J. F. (1973): Mechanics of Solids. The Experimental Foundations of Solid Mechanics, *Springer*. Berlin.

[9] Pelleg J. (2013): Mechanical Properties of Materials, *Springer*. Dordrecht.

[10] Hähner, P. (1994) Theory of solitary plastic waves. *Journal of Applied Physics*. Vol. A 58, pp. 41–58 (1994). https://doi.org/10.1007/BF00331515

[11] Srinivasan, N. – Raghu, N. – Venkatraman, B. (2012): Study on Lüders deformation in welded mild steel using infrared thermography and digital image correlation. *Advanced Materials Research*, Vol. 585, pp. 82-86. https://doi.org/10.4028/www.scientific.net/AMR.585.82

[12] Jiang, W. – Li, G. – Wu, Y. – Liu, X. – Fan, Z. (2018): Effect of heat treatment on bonding strength of aluminum/steel bimetal produced by a compound casting. *Journal of Materials Processing Technology*. Vol. 258, pp. 239-250. https://doi.org/10.1016/j.jmatprotec.2018.04.006

[13] Fu, B. – Qin, G. – Li, F. – Meng, X. – Zhang, J. – Wu, C. (2015): Friction stir welding process of dissimilar metals of 6061-T6aluminum alloy to AZ31B magnesium alloy. *Journal of Materials Processing Technology.* Vol. 218, pp. 38-47. https://doi.org/10.1016/j.jmatprotec.2014.11.039

[14] Jiang, Z. – Fan, Z. – Jiang, W. – Li, G. – Wu, Y. – Guan, F. – Jiang, H. (2018): Interfacial microstructures and mechanical properties of Mg/Al bimetal produced by a novel liquid-liquid compound casting process. *Journal of Materials Processing Technology*. Vol. 261, pp. 149–158. https://doi.org/10.1016/j.jmatprotec.2018.06.013

[15] Xiao, X. F. – Ye, S. P. – Yin, W. X. – Xue, Q. (2012): HCWCI/Carbon steel bimetal liner by liquid-liquid compound lost foam casting. *Journal of Iron and Steel Research*. Vol. 19, pp. 13–19. https://doi.org/10.1016/S1006-706X(12)60145-9

[16] Li, Y. – Gong, M. – Wang, K. – Li, P. – Yang, X. – Tong, W. (2018): Diffusion behavior and mechanical properties of high chromium cast iron/low carbon steel bimetal. *Materials Science and Engineering*. Vol. 718, pp. 260-266. https://doi.org/10.1016/j.msea.2018.01.111

[17] Li, Yu. – Barannikova, S. – Shlyakhova, G. – Zuev, L. (2017): Investigation of structure and heterogeneity of the plastic deformation in bimetal exposed to uniaxial tension. *AIP Conference Proceedings*. Vol.1800, P. https://doi.org/10.1063/1.4973037

Ref.:
Li, Yulia V. – **Barannikova,** Svetlana A. – **Zuev,** Lev B.: *The localization of plastic deformation in bimetal*
Építőanyag – Journal of Silicate Based and Composite Materials, Vol. 70, No. 5 (2018), 168–171. p.
https://doi.org/10.14382/epitoanyag-jsbcm.2018.30

GUIDELINE FOR AUTHORS

The manuscript must contain the followings: title; author's name, workplace, e-mail address; abstract, keywords; main text; acknowledgement (optional)**; references; figures, photos with notes; tables with notes; short biography** (information on the scientific works of the authors).

The full manuscript should not be more than 6 pages including figures, photos and tables. Settings of the word document are: 3 cm margin up and down, 2,5 cm margin left and right. Paper size: A4. Letter size 10 pt, type: Times New Roman. Lines: simple, justified.

TITLE, AUTHOR

The title of the article should be short and objective.

Under the title the name of the author(s), workplace, e-mail address.

If the text originally was a presentation or poster at a conference, it should be marked.

ABSTRACT, KEYWORDS

The abstract is a short summary of the manuscript, about a half page size. The author should give keywords to the text, which are the most important elements of the article.

MAIN TEXT

Contains: materials and experimental procedure (or something similar), results and discussion (or something similar), conclusions.

REFERENCES

References are marked with numbers, e.g. [6], and a bibliography is made by the reference's order. References should be provided together with the DOI if available.

Examples:

Journals:

[6] Mohamed, K. R. – El-Rashidy, Z. M. – Salama, A. A.: In vitro properties of nano-hydroxyapatite/chitosan biocomposites. *Ceramics International.* 37(8), December 2011, pp. 3265–3271, http://doi.org/10.1016/j.ceramint.2011.05.121

Books:

[6] Mehta, P. K. – Monteiro, P. J. M.: Concrete. Microstructure, properties, and materials. *McGraw-Hill*, 2006, 659 p.

FIGURES, TABLES

All drawings, diagrams and photos are figures. The **text should contain references to all figures and tables**. This shows the place of the figure in the text. Please send all the figures in attached files, and not as a part of the text. **All figures and tables should have a title**.

Authors are asked to submit color figures by submission. Black and white figures are suggested to be avoided, however, acceptable.

The figures should be: tiff, jpg or eps files, 300 dpi at least, photos are 600 dpi at least.

BIOGRAPHY

Max. 500 character size professional biography of the author(s).

CHECKING

The editing board checks the articles and informs the authors about suggested modifications. Since the author is responsible for the content of the article, the author is not liable to accept them.

CONTACT

Please send the manuscript in electronic format to the following e-mail address: femgomze@uni-miskolc.hu and epitoanyag@szte.org.hu or by post: Scientific Society of the Silicate Industry, Budapest, Bécsi út 122–124., H-1034, HUNGARY

We kindly ask the authors to give their e-mail address and phone number on behalf of the quick conciliation.

Építőanyag – *Journal of Silicate Based and Composite Materials*, Quarterly peer-reviewed periodical of the Hungarian Scientific Society of the Silicate Industry, SZTE.
http://epitoanyag.org.hu

ICCX

INTERNATIONAL CONCRETE CONFERENCE & EXHIBITION

Central Europe 2019

13 - 15 February 2019, Warsaw, Poland

For over 20 years CPI has been providing concrete professionals worldwide with up-to-date technical information and news - from around the world.
CPI was founded out of the need to address the opportunities and challenges of the globalization in the concrete industry.

As the demand for information and technology grew, CPI introduced ICCX conference into developing areas of the world in 2005. Today CPI hosts ICCX conferences around the world. The trademark of ICCX is a unique combination of conference and trade exhibition, covering all aspects of modern concrete production and technology. This format gives suppliers to the concrete industry the opportunity to meet face-to-face with decision makers in a technical setting.

Over the past several years industry decision makers have made ICCX conferences a must attend event!

WWW.ICCX.ORG

sampe

Conference 19 Nantes

DATE 17 - 19 September 2019

LOCATION La Cité des Congres de Nantes

THEME Challenging Applications in Composites

SAMPE Europe: Where industry meets science!

www.sampe-europe.org